Study On All-Optical Signal Processing by Semiconductor Optical Amplifiers for Ultra-High-Speed Optical Fiber Communications

半導体光増幅器を用いた超高速光ファイバ通信用全光信号処理技術に関する研究

February 2011

Munefumi TSURUSAWA

鶴澤　宗文

TABLE OF CONTENTS

Abbreviations

Abbreviation	*Definition*
ADSL	Asymmetric Digital Subscriber Line
ASE	Amplified Spontaneous Emission
B-B	Back-to-Back
BER	Bit Error Rate
CW	Continuous Wave
DCF	Dispersion Compensation Fiber
DGD	Differential Group Delay
DSF	Dispersion Shifted Fiber
EAM	Electro Absorption Modulator
EDFA	Erbium Doped Fiber Amplifier
FEC	Forward Error Correction
FRML	Fiber Ring Mode locked Laser
FTTx	Fiber To The x (home, building, premise and so on)
HiBi	Highly Bi-refringent
HWP	Half Wave Plate
IP	Internet Protocol
LAN	Local Area Network
LD	Laser Diode
MAN	Metro Area Network

MMI	Multi Mode Interference
MQW	Multiple Quantum Well
MZI	Mach-Zehnder Interferometer
NNR	Noise Reduction Ratio
NRZ	Non Return to Zero
O/E	Optical-Electrical
O/E/O	Optical-Electrical-Optical
OPM	Optical Power Meter
ORD	Optical Reshaping Device
OSA	Optical Spectrum Analizer
OSNR	Optical Signal to Noise Ratio
OTDM	Optical Time Domain Multiplex
OXC	Optical Cross Connect
PBS	Polarization Beam Splitter
PD	Photo Detector
PMD	Polarization Mode Dispersion
PMF	Polarization Maintaining Fiber
PRBS	Pseudo Random Bit Sequence
RZ	Return to Zero
SA	Saturable Absorber
SCH	Separate Confinement Hetero
SNR	Signal to Noise Ratio

SOA	Semiconductor Optical Amplifier
TDM	Time Domain Multiplex
UNI	Ultrafast Nonlinear Interferometer
VPN	Virtual Private Network
WAN	Wide Area Network
WDM	Wavelength Division Multiplex
XGM	Cross Gain Modulation
XPM	Cross Phase Modulation

CHAPTER 1 INTRODUCTION

1.1. Introductory Remarks

1.1.1 Background

An optical fiber communication system has been playing an important central role in all segments of networks in tier-one carriers as well as the Internet service providers. The domain of applicability is no longer limited to point-to-point long haul core networks and is also applied to wide area networks (WAN), metropolitan area networks (MAN) and access networks and local area networks (LAN). Transmission speed per one wavelength of the optical communication technology has steadily improved by development of semiconductor optical devices and technologies of system construction. Even in the commercial optical communication systems, 10 Giga-bits per second (Gbit/s) is regular speed not only in the aggregated core network but also in the MAN to aggregate both traffic of enterprise users and residential customers. Furthermore, the interface of 40 Gbit/s (SONET OC-768) has been appeared not only for long distance transmission equipment but also for a tributary port of high-end core routers. In the background of the emerging hardware, there is sure demand for supporting a continuous increase of packet-based data traffic driven by the demand of rapid increase of the Internet traffic, such as a video streaming, search based Web surfing and so forth. An asymmetric digital subscriber line (ADSL) and a fiber to the home/building (FTTx) have so far been expanded as the Internet access methodologies for residential customers. The maximum bandwidth of the ADSL and FTTx are up to several tens of Mega bits per seconds (Mbit/s) and one Gbit/s for one customer, respectively. On the other hand, there is also an obvious migration trend of the WAN connection service for enterprise customers from a time domain multiplex (TDM) based “assured narrow band” to a the packet based “best-effort broadband” due to the cost effective manner.

The main reason is that the TDM based network constructed by the carrier's specified dedicated devices is migrating to the packet centric network built by the commoditized equipment such as layer two switches and routers. Consequently, The Internet protocol (IP) virtual private network (VPN) service and Ethernet based VPN service can be allowed to use the bandwidth up to 1 Gbit/s per customer. Furthermore, the Internet access services via the third generation cell phone, for instance, namely a code division multiple access (CDMA) 2000 1x evolution data only (EV-DO), has commercially deployed in 2003. It enables one customer to use the bandwidth up to 2.4 Mbit/s for data communication services, such as a web browsing, an email and a short messaging. Consequently, a large capacity network has been realistically required using both a high-speed TDM technology and a wavelength division multiplex (WDM) technology as a backbone network.

Optical fiber communication technology is able to provide the capability of telecommunicating huge amounts of data exceeding 10 Tbit/s on a single fiber with WDM technology. To establish the future ultra-high speed and large capacity optical network, an all-optical signal processing as well as the all-optical regeneration will be an essential technology. An all-optical signal processing means that the optical data signal is not converted to an electrical signal when the logical or the physical operation is given to the optical data signal in the transmission line that includes nodes, repeaters and branching devices. The same functionalities can be realized by the optical-electrical-optical (O/E/O) conversion. However, there will be limitations of a repetition rate for the signal processing due to the response time of the device, radio frequency parts in the system such as an RF amplifier, coaxial cables and so on. The primitive methodology for the regeneration of the optical data signal is the O/E/O type one by using the combination of the photodiode (PD), electrical decision circuit and laser diode (LD). Although this scheme is sure-footed and reliable technology for the regeneration of the optical data signal, the limitation of the conversion speed is

around 40 Gbit/s due to the response time of both the PD and the LD. Therefore, the O/E/O type regeneration does not suit for the future ultra-high speed optical communication up to 100 Gbit/s per one wavelength.

1.1.2 Issues of All-Optical Networks

To realize the all-optical networks, there are a lot of issues to be solved by "all-optical" functionalities that are able to be replaced a transponder based O/E/O conversion at each network node or repeater. The required functions that are able to operate and maintain scalability of the all-optical network are summarized in the following.

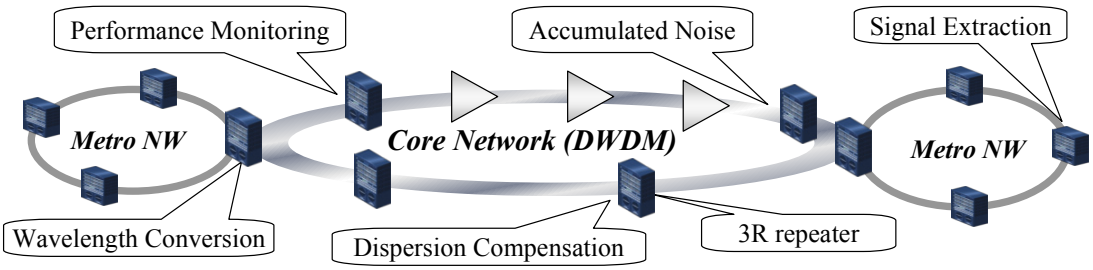

	Requirements and current solutions	Issues for the all-optical NWs
Wavelength Conversion	C-band <-> C-band, C-band <->L-band	*All-optical wavelength conversion*
3R Regeneration	No wavelength change, clock extraction	*All-optical 3R regeneration*
Signal Extraction	Channel recognition	*All-optical demultiplexing*
Dispersion Compensation	Dispersion compensation fiber or devices, O/E/O regeneration	*All-optical 2R/3R regeneration,* Variable dispersion compensation
Performance Monitoring	Measurement in the electrical domain; Signal degradation (SD), signal failure (SF), packet counter	All-optical performance monitoring 1. "bit-by-bit" inspection 2. Quality of optical signal 3. Optical signal or cw light 4. Presence of light
	Measurement in the optical domain; Optical power in transmitter / receiver, flexible optical power adjustment in each wavelength	

Figure 1-1: (upper) Schematic viewgraph of incumbent carrier's network. (lower) Summarized table of requirements and current solutions and Issues for the all-optical networks of each function in actual networks.

Figure 1-1 shows a schematic viewgraph of incumbent carrier's network which consists of a metro area network and DWDM based optical core network and summarized table of requirements and current solutions and Issues for the all-optical networks of each function in actual networks. The transponder of network nodes in ADM system and WDM system roles three important functions that are wavelength conversion, 3R regeneration and performance monitoring. The wavelength conversion at the transponder is to maintain scalability of network as well as flexibility of design and construction. The wavelength of 1550 nm is utilized for middle and long distance transmission using an EDFA. As for the interconnecting metro network and core network, the wavelength range of 1550nm, which is called C-band, is dominant for construction of the network. To remove the transponders from each hub node for realizing the all-optical networks, the all-optical wavelength converter is essential functional device. Quality of optical signals is degraded by an accumulated ASE noise from concatenated EDFAs. Also chromatic dispersion and nonlinear effects of an optical fiber impair the performance of the transmission signals. Current optical networks deploy dispersion compensation fibers in front of the network nodes. The transponders with O/E/O conversion realize re-shaping, re-amplifying and re-timing of the degraded optical signals. Therefore the all-optical network needs to deploy optical 3R regenerators that can be replaced with the transponders in the hub node. Operation, administration and maintenance (OAM) of network is essential work of network operators. It is important to figure out the failure point in the network not only in the case of disconnection but also in the case of performance degradation. It is not difficult to detect the disconnection of fiber or the lost of optical signal. However, monitoring the performance of the optical signal is the issue to be solved for the actual network operation.

The objective of this thesis work is to realize elemental technologies, such as a wavelength conversion, 3R regeneration and demultiplexing functionalities by utilizing the all-optical signal

processing of an SOA. The following sections describe the methodologies for the each functionality.

1.2 All-Optical Signal Processing

1.2.1 All-optical regeneration

An all-optical regeneration means so far the two kinds of regeneration functionalities that are optical 2R regeneration and optical 3R regeneration. The optical 2R regeneration represents the "re-amplification" and the "re-shaping" of the optical data signals. The optical 3R regeneration realizes the "re-timing" functionality for the optical data signals in addition to the optical 2R regeneration functionality. Both functionalities are the technology for the improvement of the transmission performance for extending the transmission distance. A lot of researchers have been making an effort to solve the articles by the optical 2R regeneration [1-3] and the 3R regeneration including the clock recovery technique [4-18] for realization of the next-generation ultra-high speed and the large capacity optical networks.

The effective functionality of the all-optical 2R regeneration is the re-shaping of the optical data signal, which means to reduce the optical noise that is mainly an amplified spontaneous emission (ASE) generated by concatenated erbium-doped fiber amplifier (EDFA) deployed along the transmission line as well as the reformation of the optical pulse by the passive compensation device for the chromatic dispersion or the polarization mode dispersion. The optical noise reduction functionality is also realized by the O/E/O conversion in the current optical communication system. However, when the electric processing is employed in the terminal nodes or the repeaters, a lot of articles for consideration, such as the limitation of the processing speed, the consumption power and so on, have been pointed out by the system architects. Therefore, the all-optical noise reduction

device that has features such as the smallness and the low consumption power is expected to realize for the ultra-high speed optical communication systems.

The all-optical 3R regeneration is the technology basically for the improvement of the transmission performance. It enables to reduce an optical noise of both the mark level (logically "1") and space level (logically "0"), and to correct the timing of the optical data signals. To realize the all-optical 3R regeneration in the most case, wavelength conversion functionality has been deployed in the optical regeneration schemes. It is represented as the "regenerative wavelength conversion" due to the following reason. All-optical 3R regeneration is realized by the combination of the clock extraction functionality from the optical data signal, the optical clock pulse generator and the optical gate switch in the one system. When the original optical data signal comes into the optical regeneration device/system, the well-ordered optical / electrical clock pulse is generated by the clock extraction system and the optical clock generator using the accurately extracted clock. The gating functionality that is operated by the original data signal enables to pass the well-ordered clock pulse when the original signal equals to the logical "1". Therefore, the impaired original data pulses are converted to the high-quality optical pulses. If the wavelength of the well-ordered clock pulse is different from the original one, this conversion process is all-optical 3R regeneration as well as the wavelength conversion at the same time. The all-optical regeneration technology had been started by the direct optical amplification, which was realized by the EDFA. The optical fiber communication system had been drastically changed by the EDFA, which does not convert the optical data signal into the electric data signal. However, there was intrinsic problem that was an ASE noise, which degraded the signal to noise ratio of the optical data signal passing through the EDFA. The optical noise due to the EDFA that was deployed to improve the system performance limited the performance of the optical fiber communication system. Consequently, the all-optical 2R regeneration functionality, which includes the

optical noise reduction in addition to the amplification, was required to improve the performance of the EDFA-based optical fiber communication system. The following sections describe the all-optical 2R and 3R regeneration functionalities.

1.2.1.1 Optical 2R Regeneration

All-optical 2R regeneration is an enhanced functionality that realizes the re-amplification and re-shaping of an optical data signal. The effective functionality of the all-optical 2R regeneration is the re-shaping of the optical data signal, which means to reduce the optical noise that is mainly an ASE generated by concatenated erbium-doped fiber amplifier EDFA deployed along the transmission line. Moreover, the functionality is important for the long-haul transmission system to correct the other impairment factors of the optical pulse transmit in the concatenated optical fibers, such as the chromatic dispersion and the polarization mode dispersion. The optical noise reduction functionality is also realized by O/E/O conversion as mentioned in the previous section. However, when the electric processing is employed in the terminal nodes or the repeaters, a lot of problems, such as the limitation of the processing speed, the consumption power and so on, have been pointed out by the system architects. Therefore, the all-optical noise reduction device that has features such as the

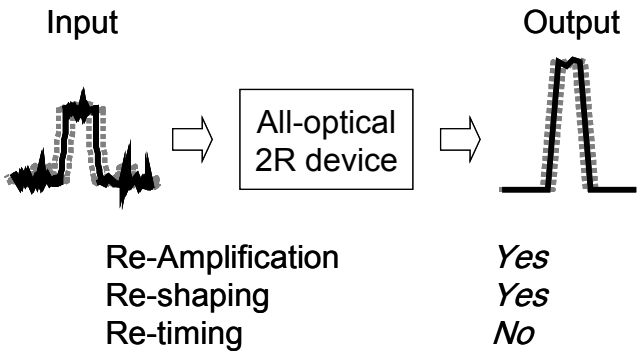

Figure 1-2: Schematic diagram of an all-optical 2R regeneration device.

smallness and low consumption power is expected to realize for the ultra-high speed optical communications.

Figure 1-2 shows the schematic diagram of the all-optical 2R regeneration functionality. It enables to correct the signal degradation except the re-timing of the optical data signal by itself. The remained timing jitter due to the ASE was accumulated along the transmission line, hence the transmission performance is impaired by the mismatch of the timing in the signal decision circuit at the receiver. The all-optical noise reduction is realized by the several methodologies that are the semiconductor optical device and the optical fibers. The fiber-based optical 2R regeneration device has the features that are the low loss for the connection to the transmission line and extremely low polarization-dependent properties by nature. However, it requires being induced large optical power to obtain the 2R regeneration effect due to the smallness of the optical nonlinearity. On the other hand, the semiconductor-based 2R regeneration device has the advantages with regard to the large nonlinearity against the optical pulse as well as the smallness and the possibility of the integration with the optical waveguide. An SOA or a saturable absorber (SA) is an attractive candidate as optical functional devices, because they have large optical nonlinearity against the optical pulse intensity. Several semiconductor-based 2R devices have been so far reported in various bit rate applications. In this dissertation, the semiconductor waveguide device is selectively investigated with novel scheme for the high-speed repetition rate.

1.2.2.2 Optical 3R regeneration

In addition to the 2R regeneration functionality, the re-timing mechanism is essential technology for further improvement of the transmission performance. All-optical 3R regenerator is expected to enhance flexibility, scalability and cost-down in future high-speed all-optical photonic

network. Major interests in the all-optical 3R regenerators are "in-line optical regeneration functions" employed in repeaters and/or network nodes to extend the transmission distance.

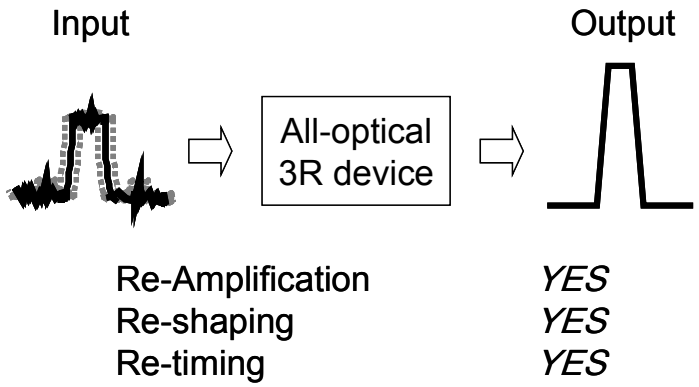

Figure 1-3: Schematic diagram of an all-optical 3R regeneration device.

Figure 1-3 shows the schematic diagram of the all-optical 3R functionality. It enables to correct the timing of the signal while maintaining the 2R functionality. There are several approaches to realize the all-optical 3R regeneration functionality, that are utilizing the fiber-based functional device or the semiconductor-based one as remarked in the previous section. In the both methodologies, the optical gating function that is operated by the optical data pulse passes the locally prepared optical clock pulses for regenerated optical data signal. The all-optical 3R regeneration by the fiber-based device also need to incident large optical power to obtain the expected effect. Therefore, the all-optical 3R regeneration is investigated by introducing the SOA-based functional device with proposed novel scheme for the high-speed repetition rate. It is also important to shorten the response time of the device for the all-optical high-speed 3R regeneration functionality.

Moreover, the low power operation of the device is an essential issue for the high-speed application. Because the intensity of the optical pulse for operating the gate function become small with compared to the low repetition rate in the case of the same average optical power.

Although the development during these ten years has born a lot of variations of all-optical regenerators and has verified their potential high bit-rate operability, there exists another hurdle to be passed before employing them in practical use. Nevertheless, there are few reports on how much the signal quality can be recovered from seriously impaired input signal by the reshaping function as well as the retiming function of the 3R regenerator. In the actual transmission line, many impairment factors, such as ASE noise in EDFA, chromatic dispersion, PMD and nonlinear effect in fibers, distort the optical waveform both in amplitude and in phase of timing. In that sense, quantitative investigations of the reshaping and retiming capability of the regeneration from highly impaired transmitted signals are intensively required. Although the complete 3R regeneration functionality in the transmission line is important issue, it is useful for the cost-effective system design to improve the transmission performance by the 3R regeneration device just in front of the receiver from operational point of view. The all-optical 3R regeneration functionality is expected to expand the receiver sensitivity or the eye-diagram of the received signal owing to the sinusoidal transfer function. In this dissertation, the feasibility of the all-optical 3R regeneration functionality is experimentally investigated by utilizing the SOA-based functional device for both in line application and in front of the receiver.

1.2.2 Applications of the ultra-high-speed all-optical signal processing

All-optical signal processing can be applied for many applications that are not only the optical communication but also the logical processing such as an AND/OR circuit. In the future high-speed photonic networks, the several application of the all-optical signal processing will be important for the flexibility of the network designing. The pulse width tunable wavelength conversion functionality is important function at the front of the optical receiver in the ultra-high speed

optical communications since it enables to optimize the pulse width for the receiver, especially for the photo diode. The optical parallel-to-serial conversion enables to realize not only the WDM-TDM conversion but also the optical code recognition in the optical burst switching functionality. The bit rate tunable wavelength conversion is useful for the optical cross connect (OXC) node for processing the several kinds of bit rate by one system. For example, forward error correction (FEC) functionality requires several percentile higher bit rate against the original one. The all-optical demultiplexing functionality enables to reduce the repetition rate of the TDM optical data signal at the end of the transmission systems. The following sections express the importance of the ultra high-speed all-optical signal processing. A lot of devices and sub-systems for the ultra-high speed optical communication, such as the all-optical wavelength conversion [19-28], the all-optical demultiplexing as well as the optical gating function [29-60] and the optical performance monitoring function [61-71], have so far been proposed by the various schemes. The all-optical demultiplexing functionality, at the end of the transmission systems, enables to reduce the repetition rate of the TDM optical data signal enough for the optical-to-electrical (O/E) converter of the receiver. Even though the bit rate of the ultra-high speed optical communication is more than 100 Gbit/s, the electric decision circuit should be operated at less than several tens of Gbit/s due to the response time of the semiconductor device as previously mentioned. One of the features of the optical signal processing is an ultra-high repetition rate that cannot be realized by an electrical signal processing as mentioned above. Therefore, the all-optical signal processing should be operated more than 50 Gbit/s.

1.2.2.1 Bit rate tunable wavelength conversion

Expansion of optical communication system, which was triggered by innovation of optical amplification technique using EDFA, is evolving from point-to-point long-haul system to metro or

regional network system in which a large number of wavelengths are multiplexed in one fiber while a bit-rate per channel is increased up to 40 Gbit/s or more. It is presupposed that such a network would suffer from confliction among intricate wavelength channels at the nodes as well as degradation in signal quality due to roundabout routing when the number of nodes and/or wavelengths increase rapidly. In the photonic cross connect node, for instance, the wavelength conversion functionality is able to reconfigure the optical lambda path for routing capability. In the case of the wavelength routing, the bit rate transparency is the great advantage of the scheme. However, if the bit rate of the wavelength converter is fixed, the flexibility of the wavelength routing will be small. Consequently, the bit rate tunability is an important requirement for the practical use not only for bit-rate transparent photonic network but also for upgrading a FEC coding with increasing bit-rate.

1.2.2.2 All-optical simultaneous demultiplexing

High capacity future all-optical networks based on OTDM and WDM will require compact and high speed demultiplexing devices. There have been already reported all-optical demultiplexing of 80-160 Gbit/s optical signal using SOA-based interferometric devices, but they have demonstrated only one channel extraction [43-46, 56-58]. As suggested in Ref. 43, an SOA-based Mach-Zehnder interferometric (MZI) device with multimode interference (MMI) coupler can extract both the switched and the un-switched states simultaneously into the two output ports. The input signal can be fully utilized without any waste in power if both the output signals have signal qualities well enough for further processing. However, it is difficult to attain equal signal qualities for both the switched and un-switched signals, since a fine balance in phase-shift between the two arms is not easy to realize. On the other hand, a one-arm MZI polarization switch, which is called "UNI (ultrafast nonlinear interferometer)", has an assured balance in phase-shift because it consists of only one SOA, therefore

it may provide two output signals having equal signal qualities with much less difficulty. The bit rate of the future photonic network will be faster than 40 Gbit/s or beyond. The bit rate of the optical data signal at the transmitter can be upgraded by the optical time domain multiplex technique up to more than 100 Gbit/s. However, there is no device that is able to detect and make decision the signal at such a fast repetition rate. The limitation of the detectable bit rate will be several tens of Giga bit per second. Therefore, the demultiplexing device is essential for the receiver. An electro-absorption modulator-based optical demultiplexer is used in the previous experimental work by many researchers. The intrinsic optical loss of the EAM, however, is as large as 10 dB. It must be compensated by EDFA in the actual usage. When the channels that should be demultiplexed from high-speed data signal, the total power and the complexity of the system will be not negligible in the actual deployment. Therefore, the power effective demultiplexing scheme will be an attractive candidate for the future ultra high-speed networks.

1.3 Outline of chapters

This dissertation describes the investigation about an ultra-high-speed all-optical signal processing by using a semiconductor waveguide device and a composition device of the semiconductor optical amplifier (SOA) and passive optical components. Although the all-optical signal processing is being investigated by the two categories that are an optical fiber-based system and a semiconductor waveguide-based system, this investigation focuses on the semiconductor waveguide-based one because of its advantages, such as large nonlinearity for optical data signals and the minimum size of the devices. The organization of this dissertation consists of six chapters including conluding remarks in chapter 6.

Chapter 2 proposes a new methodology of an ultra-high speed saturable absorber (SA) for

all-optical 2R regeneration by using a nonlinear absorption phenomena in a forward-biased SOA with continuous wave (CW) light, so-called CW assist light, for reducing an absorption recovery time. The device parameters of the SA for effective noise reduction are considered by both numerical calculation and experimental evaluation. To shorten the absorption recovery time of SA, the CW assist light that is basically transparent for a gain curve of an active layer in the SOA is introduced. The fundamental properties of the SA with the CW assist light are experimentally investigated by changing conditions such as a wavelength of the CW assist light and injection current for the SOA. The effectiveness of the optical noise reduction by the SA with the CW assist light is experimentally investigated using 5 Gbit/s NRZ signals and 10 Gbit/s RZ signals.

Chapter 3 describes the investigation of all-optical 3R regeneration that includes a wavelength conversion by an ultrafast nonlinear interferometer (UNI) switch with the CW assist light for reducing a gain recovery time of the SOA. The effectiveness of the CW assist light is experimentally investigated by measurement of the gain recovery time. A gain clamping effect due to the CW assist light at the transparent wavelength on the gain profile is compared to a gain saturation effect by a clock pulse in the active layer of the SOA. In this chapter, the investigation for the fundamental properties of the UNI switch with regard to the wavelength conversion functionality is described for the capability of the all-optical 3R regeneration. The experimental evaluations are carried out at 10 Gbit/s, 40 Gbit/s and 80 Gbit/s repetition rate by using almost the same configuration of the UNI switch excepting the birefringent (HiBi) medium that is a key component of a polarization-discriminated interferometric switching operation.

Chapter 4 describes a regeneration capability of the all-optical 3R regeneration functionalities and an operational margin of the all-optical regeneration scheme by using the UNI switch with the CW assist light at the repetition rate of 40 Gbit/s. The operational margin of the UNI

switch is described by changing the device parameters and the system parameters that are the pulse width of the optical data signal, the pulse width of the optical clock pulse and the differential group delay of the HiBi media. The distinct regeneration capability is demonstrated by changing the condition of optical signal degradation. An ASE noise generated by an EDFA and a timing jitter of the optical data signal emulated by the combination of HiBi device and the polarization scrambler are intentionally lapped over the optical data signal.

Chapter 5 proposes a novel scheme for the bit rate tunable all-optical wavelength conversion by utilizing the combination of the SOA and a variable DGD generator, which is re-configurable optics that are movable mirrors and polarization beam splitter. This scheme realizes a flexible design of ultra-high-speed all-optical networks since the optical nodes such as an OXC node with the wavelength conversion functionality can be configured to the input optical data signal with and without the FEC. A bit rate tunable wavelength conversion functionality is demonstrated at 10 Gbit/s, 40 Gbit/s and 80 Gbit/s using the almost same configuration of the devices excepting the bit rate of the local optical clock pulses. Also all-optical demultiplexing functionalities by using the combination of the UNI switch and the polarization beam splitter are proposed in this chapter. In the ultra-high-speed optical communication, the all-optical demultiplexing functionality is essential technology that enables to reduce the bit rate of the optical data signals down to the repetition rate that can be recognized by the electrical decision circuit of the receiver. The specialty of this scheme is to be able to divide the optical data signal into halves simultaneously. In this chapter, the all-optical simultaneous demultiplexing into the half bit rate is demonstrated from 20 Gbit/s, 40 Gbit/s and 80 Gbit/s, respectively.

Finally, chapter 6 represents concluding remarks that summaries all the investigations regarding the ultra-high-speed all-optical signal processing described in the all chapters of this

dissertation.

CHAPTER 2 ALL-OPTICAL 2R REGENERATION

2.1 Introduction

An SOA and an SA are attractive candidates as optical functional devices, because they have large optical nonlinearity against optical pulse intensity and their characteristics can be controlled electrically or optically. By using its optical nonlinearity, various optical functional devices, such as an optical gate, an optical processing, and an optical regenerator, are proposed as expressed in the chapter 2. All-optical signal processing, such as gating, pulse reshaping and retiming, is important technology for the realization of ultra-high-speed optical communication systems in the near future. However, the operating speed is usually limited by the recovery time (~1 ns) to the steady state governed by the carrier lifetime or carrier transport time in the semiconductor device from the electrodes to the active layer via the optical confinement layers. Therefore, it is essential to reduce the carrier lifetime for optical processing with an ultra-high repetition rate. Although there have been several reports on the reducing of the recovery time in SAs or SOAs [72-74], these devices were not sufficient in respect to in ultra-high repetition rate and in nonlinearity.

In this chapter, a novel way to use of an SOA driven under the loss condition as an SA is proposed for realizing the ultrafast all-optical 2R regeneration device. For reducing the absorption recovery time in an SOA, a stimulated recombination due to CW assist light is utilized. Since the stimulated recombination is an ultrafast process, it is expected that excess carriers will disappear in an instant. In addition, the process generates only little heat since it does not involve carrier transport. Therefore, this method will be a promising technique for achieving ultra-high repetition rate operation.

Section 2.2 proposes a new technique that is the way of use an absorption region of an SOA as an SA to obtain both the nonlinear absorption effect and the ultrafast recovery time. The device

parameters of an SOA are investigated by both the experimental evaluation and the numerical calculation in section 2.3. Section 3.4 describes the proposed methodology of using CW light for reducing the absorption recovery time and experimental evaluation by using the SOA. The all-optical 2R regeneration evaluation is demonstrated by using 5 Gbit/s NRZ signal and 10 Gbit/s RZ signal in section 2.5 and 2.6, respectively.

2.2 Saturable absorption in semiconductor optical amplifier

An SA has fundamentally absorption functionality by using its band gap for the optical signals. The physical and the logical investigations have so far been reported regarding nonlinearity by using semiconductor material [75-88]. An SOA reacts with three states, which are gain, transparency, and absorption media by changing the wavelength of an input optical signal even if under current injection. Figure 2-1 shows the simplified gain curve of the SOA with the current injection. The light with a wavelength between λ2 and λ3, so-called the gain region, can be amplified by the positive gain of the active layer. The light with a wavelength that is longer than the λ3 is transparent for the active layer. The light with a wavelength that is shorter than the λ2 is absorbed by the active layer of the SOA. Therefore, the SOA can be used as an SA by when the wavelength of input light is set at the λ1 that is shorter than and close to the λ2.

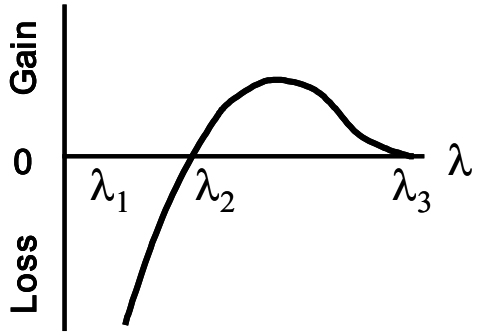

Figure 2-1: Schematic image of the gain curve of the SOA.

The nonlinear absorption effect, which is realized in the semiconductor active layer, in the shorter wavelength region may apply for a noise reduction function as shown in Fig. 2-2.

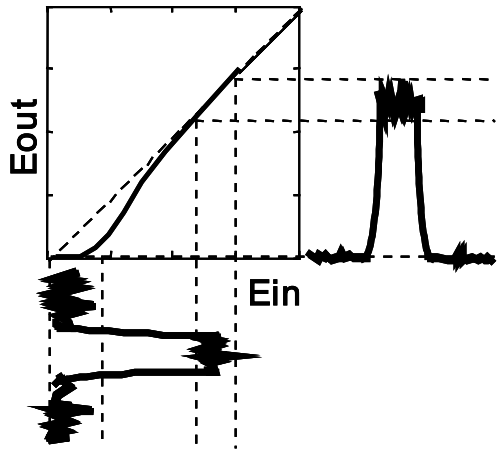

Figure 2-2: Transfer function of the nonlinear absorption and the noise reduction scheme

The transfer function curve of a nonlinear absorption effect that is called a saturable absorption effect versus input pulse energy E_{in} as shown in Fig. 2-2 is written as follows,

$$E_{out} = E_{in} \exp\left\{-\alpha_0 \exp\left(-\frac{E_{in}}{E_S}\right)L\right\} \qquad (1)$$

where α_0 is the unsaturated absorption coefficient, E_s is the saturation intensity and L is the length of the active layer of SOA. This nonlinear absorption effect has been mainly utilized for the optical re-shaping that means the narrowing the optical pulse in the solid-state mode-locked laser. The output energy E_{out} increases nonlinearly due to absorption in the active layer below the absorption saturation as the input energy increases. While the output energy is proportional to the input energy fairly linearly above the absorption saturation, therefore, the low intensity noise at a space level of optical signals can be suppressed by using a nonlinear absorption effect.

2.3 Consideration for the device parameters

In order to investigate the device parameter, the input and output (I/O) characteristics were evaluated under the various operational conditions. Figure 2-3 shows the schematic image of the experimental setup for the measurement of the I/O characteristics. The optical pulse source of 100 fs width in the 1.5-μm range was generated by an optical parametric oscillator pumped by a mode-locked Ti:Al_2O_3 laser with a repetition rate of 80 MHz.

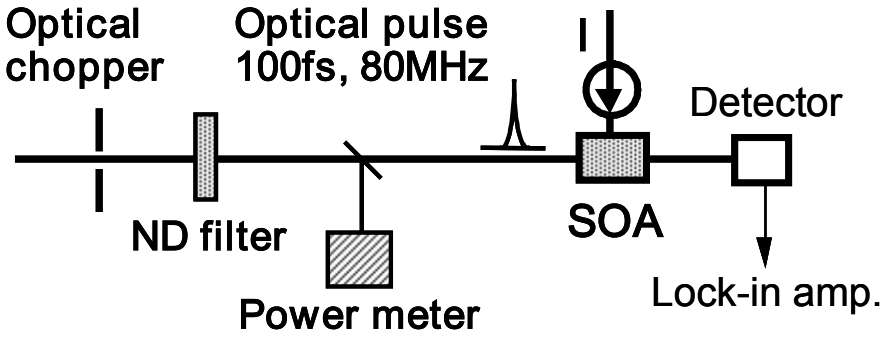

Figure 2-3: Experimental setup for the measurement of the input/output characteristics

The optical chopper and the lock-in amplifier were used to eliminate the optical background, which improve the signal to noise ratio of the measurement. The half mirror plate and the optical power meter were set in front of the SOA to monitor the optical input power when the variable neutral density filter was changed. The actual optical input and output powers of the SOA were measured by replacing the SOA to the IR detector in the back of the objective lens for focusing the optical input pulse and the SOA, respectively.

The tested SOA was a ridge waveguide SOA with an anti-reflection coating on both facets, as shown in Fig. 2-4. The lattice-matched multiple quantum well (MQW) active layer with a photo-luminescence peak of 1.56 μm consisted of five InGaAs (10 nm, λg=1.67 μm) wells and InGaAsP (8 nm, λg=1.2 μm) barriers.

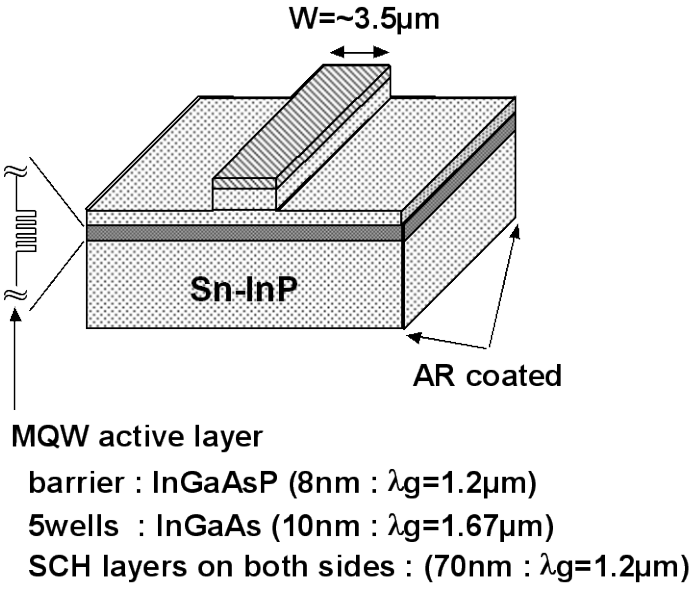

Figure 2-4: Schematic image of the ridge-waveguide SOA.

The MQW and the optical confinement layers that include the InGaAsP separate confinement hetero structure (SCH) layer (70 nm, λg=1.2 μm) and the InP cladding layer were grown on the InP substrate by the semiconductor crystal growth using the metal organic vapor phase epitaxy methodology. The gold electrodes on both p and n sides were evaporated in the vacuum chamber. The striped electrode on the p-side was made by the photolithography and the wet etching technique. The ridge-waveguide was also formed by the wet chemical etching using the gold electrode as a mask. The device length was decided according to the evaluation. After cleaving the device, the anti-reflection coating was carried out by spattering evaporation of the dielectric film

Figure 2-5(a) shows the I/O characteristics of the SOA with the parameters of the injection current. The device length and the wavelength of the input optical pulse were 100 μm and 1.55 μm, respectively. The input and the output optical pulse energy were estimated by the average power of the 100 fs pulse and the repetition rate of 80 MHz. The open marks and the dashed lines were the

measured results and the theoretical curves that were derived by the least-square method with the formula (1), respectively.

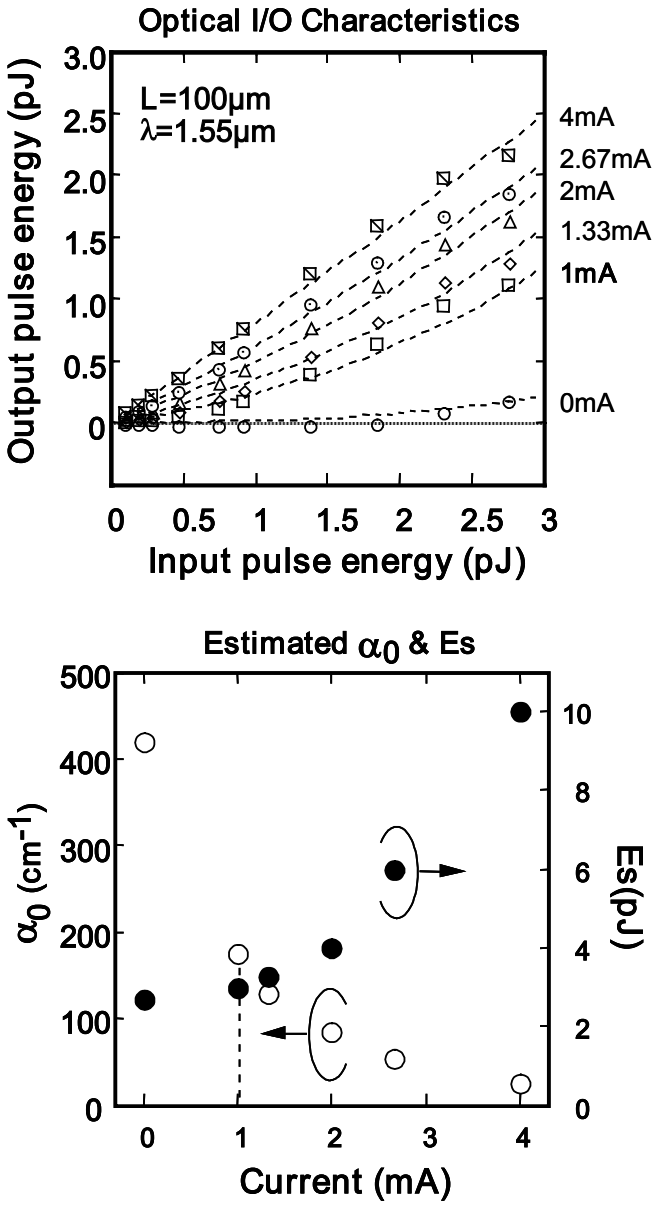

Figure 2-5: (a: upper graph) I/O characteristics of the SOA with the parameter of the injection current. (b: lower graph) Estimated unsaturated absorption coefficient α_0 and the saturation intensity E_s as a function of the injection current.

The nonlinearity of the fitting curve and the optical loss are decreasing as increasing the injection

current as shown in Fig. 2-5(a). Figure 2-5(b) shows the estimated device parameters that are the unsaturated absorption coefficient α_0 and the saturation pulse energy E_s derived by the fitting curves of the Fig. 2-5(a). Unsaturated absorption coefficient means the opacity of the medium against the optical pulse. Its budget is equivalent to the optical nonlinearity. Saturation pulse energy is the optical pulse energy to make medium transparent for the optical pulse. Therefore, the large unsaturated absorption coefficient and the small saturation pulse energy are desired for the optical noise reduction device. These characteristics are realized in the small injection current. Although the large nonlinearity is required to realize an optical noise reduction device, the optical loss of the device has to be small for the actual deployment of the optical noise reduction device.

In order to reconcile those requirements, optimal condition must be decided by the actual performance of the optical noise reduction. To investigate the optimal condition of the optical noise reduction device, the Q-factor calculation is introduced as shown in Fig. 2-6. Although the Q-factor is basically supposed by the Gaussian noise distribution both the mark level ("1" state of the digital signal) and the space level ("0" state of the digital signal), it can be useful for the approximate calculation. Ep1, Ep0, $\sigma 1$ and $\sigma 0$ depict the mean of the mark level, the mean of the space level, the standard deviation of the mark level and the standard deviation of the space level for the input optical pulse, respectively.

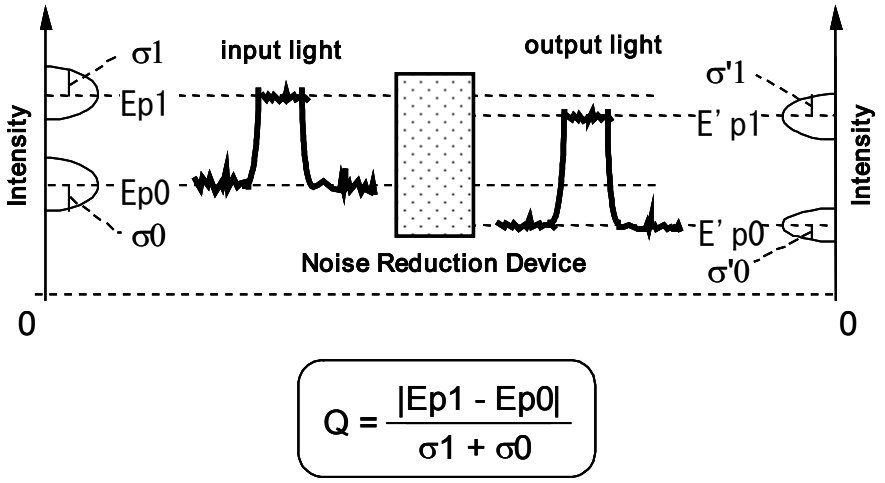

Figure 2-6: Definition of the Q-factor and the parameters. Schematic image shows the relation of the parameters and the Q-factor.

The apostrophized characters indicate the parameters of the output optical pulse. The Q-factor is expressed by the formula depicted in the inset of the Fig. 2-6. It means that the signal to noise ratio of the optical pulse and the budget of the noise both on the mark level and the space level. Several formulas are defined for the evaluation as follows. The loss at mark level and the loss at space level mean the difference of the optical power between the input and the output pulse. The noise reduction ratio (NRR) expresses the quantity that subtracted the loss at space level from the loss at mark level. It means that the one where the loss at space level is larger than the loss at mark level is meaningful. Figure 2-7 shows the calculation results of the loss at mark level and the NRR as a function of the injection current by using the estimated device parameters in Fig. 2-5. The loss at mark level is decreased as increasing the injection current. On the other hand, the NRR is deteriorated as increasing the injection current due to the decreasing the nonlinearity relevant to the $\alpha 0$.

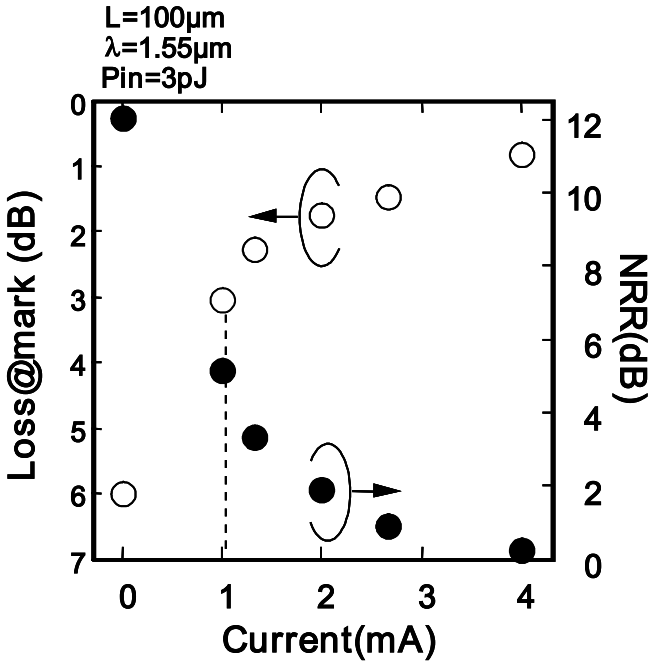

I (mA)	α_0 (cm^{-1})	Es (pJ)	loss@mark (dB)	NRR (dB)
0.0	420	2.7	6.00	12.03
1.0	*175*	*3.0*	*3.04*	*5.13*
1.33	130	3.3	2.27	3.32
2.00	85	4.0	1.74	1.92
2.67	55	6.0	1.45	0.93
4.0	25	10	0.80	0.28

Figure 2-7: Calculated results of the loss at mark level and the noise reduction ratio

The Q-factor that is defined in Fig. 2-6 can be calculated for both the input pulse and the output pulse. The improvement of performance can be evaluated by comparing the Q-factors. To generalize the Q-factor expression, the decibel indication is introduced by using the formula as follows.

SN = 20 log (Q-factor)

The delta-SN (d-SN) is defined as the improvement of performance after passing through the noise reduction device. It is defined as follows,

$$\text{d-SN} = \text{SN'} - \text{SN}$$

where SN' is the calculated Q-factor of the output pulse. There is a relationship among the Q-factor, the calculated SN and the bit error rate (BER) of the data signal supposing the Gaussian noise distribution. Here, the BER of 10^{-9} is equivalent to Q-factor of 6, which equals to SN of 15.56 dB. Figure 2-8(a) shows the calculated results of d-SN with the parameters of the injection current. The fixed parameters were the device length of 100 μm and the wavelength of the input optical pulse of 1.55 μm.

The parameters that have become the requisite for calculation were $\alpha 0$ of 175 cm^{-1} and Es of 3 pJ. When the injection current was 0mA, since the optical loss of a noise reduction device was large, the improvement of the performance could not be obtained until the input pulse energy equaled to 6 pJ. On the other hand, when the injection current was 4 mA, the improvement of the performance was very small due to the lack of the nonlinearity, as also shown in Fig. 2-7.

As seeing in the Fig. 2-8(a), the optimal conditions are between 1 mA and 2 mA with regard to the optical loss and the performance improvement. Figure 2-8(b) shows the calculated results of d-SN with the parameters of the device length. The fixed parameters were also $\alpha 0$ of 175 cm^{-1} and Es of 3 pJ. When the device length was 20 μm, the total improvement of the performance was about 1 dB because the waveguide lost the nonlinearity against the optical pulse. When the device length was 100 μm, the improvement for the small input pulse energy was negative. However, in the case of the input pulse energy beyond 2.5 pJ, the improvement of performance could be obtained. These results prove that the characteristics of the noise reduction device can be controlled by the injection current when the device length and the wavelength of the optical data signal are decided.

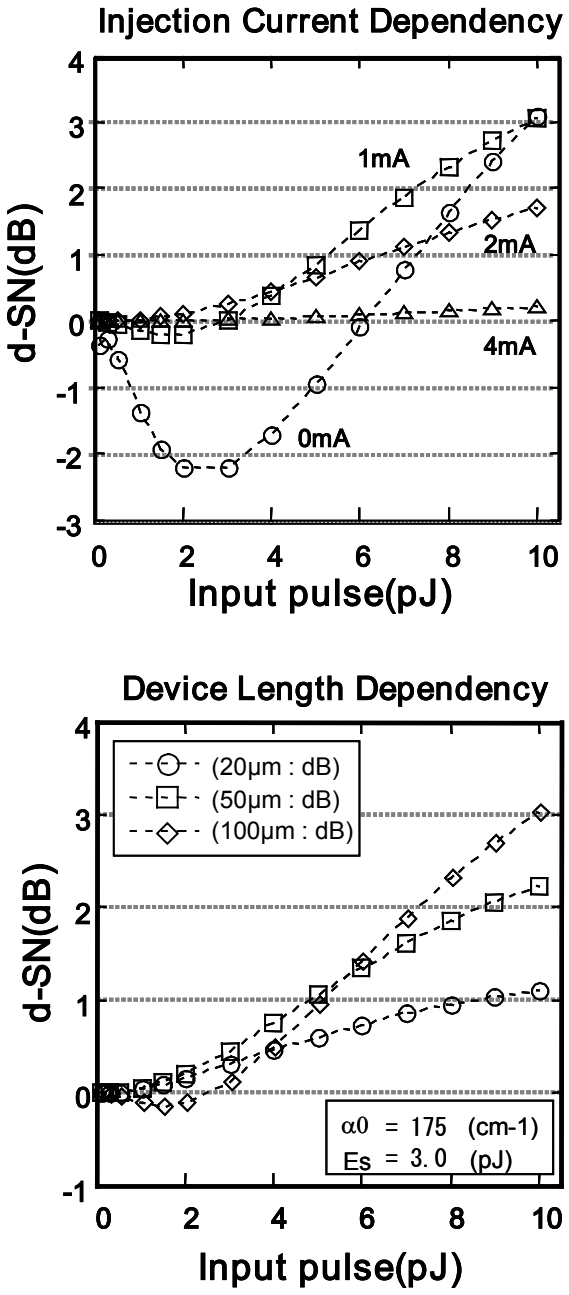

Figure 2-8: (a: upper graph) Calculated d-SN with parameters of the injection current.(b: lower graph) Calculated d-SN with parameters of the device length.

2.4 Reducing an absorption recovery time by external CW light

An SOA as an SA for a noise reduction device can be expected to improve the transmission performance as investigated in the previous section. However, if the absorption recovery time is

longer than the repetition rate of the optical data signal, the nonlinear absorption is not efficient for the improvement of performance. The absorption recovery time in the semiconductor absorption layer is limited by the carrier lifetime that is governed by a spontaneous emission. A lifetime in the active/absorption layer is usually around 1 ns that is almost equivalent to the repetition rate of 1 Gbit/s. If the noise reduction device is needed to apply for the several tens of Giga bit per second system, the absorption recovery time of less than 100 ps is an essential factor for the actual deployment.

In this section, a novel method for reducing the absorption recovery time in a semiconductor optical amplifier is proposed. The reduction of the absorption recovery time is realized by stimulated recombination due to continuous wave (CW) additional light, so-called assist light, whose wavelength is longer than that of the optical data signal. The stimulated recombination process is ultrafast and generates little heat since the process does not involve carrier transport in the device. This technique can be applied to ultra high repetition rate optical processing.

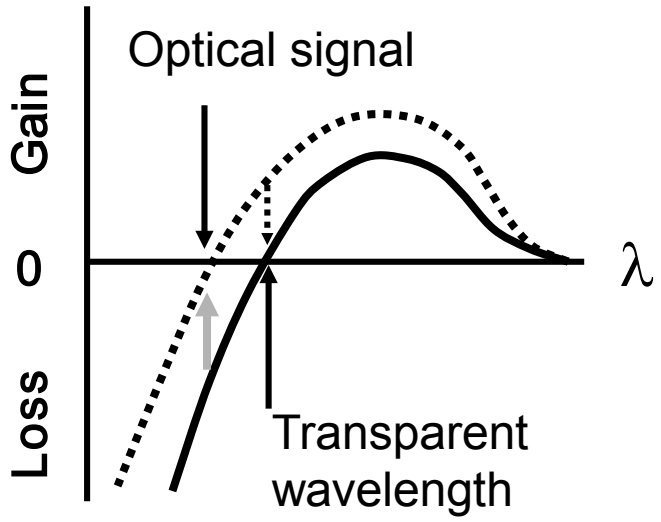

Figure 2-9: Simplified gain profile of an SOA. The solid line and the dashed line indicate the steady state of an SOA and the redistributed state of the excess carriers due to the absorption.

Figure 2-9 shows the simplified gain profiles to explain the principle, in which the steady-state profile is shown by a solid line. The wavelength of the assist light is set exactly at the transparent point on the curve. After the optical data signal passes through the SOA, the gain curve changes due to the absorption indicated by gray arrow in Fig. 2-9, hence, a positive gain for the assist light is generated as shown by a dashed line. The excess carriers change into photons by means of the stimulated recombination due to the assist light, and the gain curve quickly goes back to the steady state. A much shorter recovery time is expected using this method, because the stimulated recombination process is considered to happen in several pico seconds. When the wavelength of the assist light is set at the transparent point, the assist light does not change the electronic state of the SOA. On the other hand, when the wavelength of the assist light is set in the gain region the assist light is amplified in the SOA. Therefore, it is expected that the absorption recovery time may be shorter than the case of the assist light set at the transparent point. Two ways to create different gain conditions for the assist light was investigated. One is realized by changing the injection current, and the other is realized by changing the wavelength of the assist light from the transparent point to a longer wavelength.

Figure 2-10 shows an experimental configuration based on a conventional cross-polarized pump-probe technique [89-91] to measure the absorption recovery time. Pump and probe pulses of 100 fs width in the 1.5 μm range were generated by an optical parametric oscillator pumped by a mode-locked Ti:Al_2O_3 laser with a repetition rate of 80 MHz. CW assist light was coupled to the pump & probe beams and irradiated to the front facet of the SOA via the objective lens.

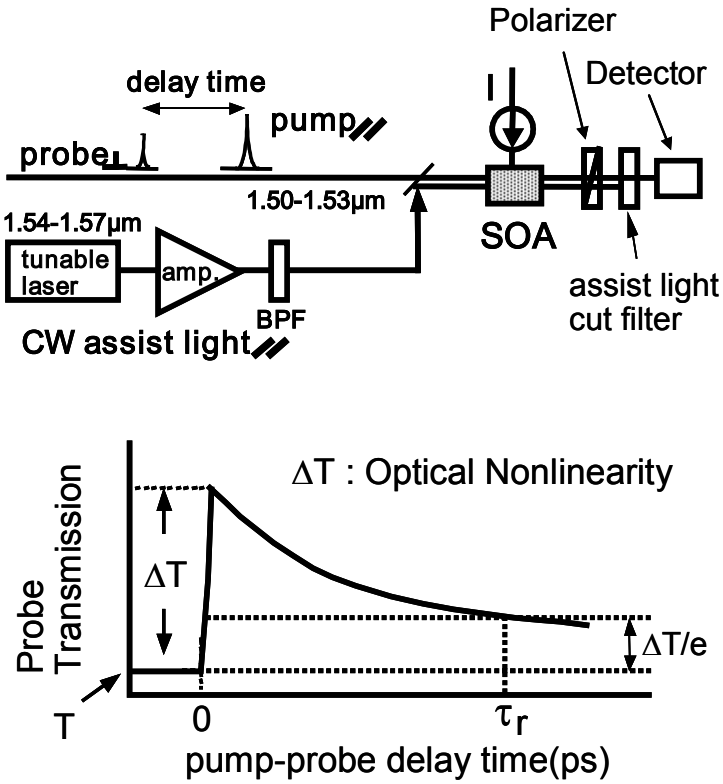

Figure 2-10: Experimental setup of the pump-probe measurement and the definition of the parameter in the measurement results.

.

The polarizations of pump, probe, and the assist light beams were TE, TM, and TE, respectively. The pump beam was cut by the polarizer, and the assist light was cut by the polarizer and the optical low-pass filter, after passing through the SOA. The lower schematic image depicts the definition of the parameter in the pump-probe measurement. When the measurement time equals to 0, immediately after a pump pulse is passing through the SOA, the carrier population increases due to the absorption. The excess carriers are decreasing due to the spontaneous emission. The absorption recovery time is defined by the point that equals to the 1/e of the initial change of the probe transmission expressed by ΔT. When the CW assist light make a contribution to the stimulated emission of the excess carriers, the 1/e recovery time can

be expected to quickly go back to the steady state.

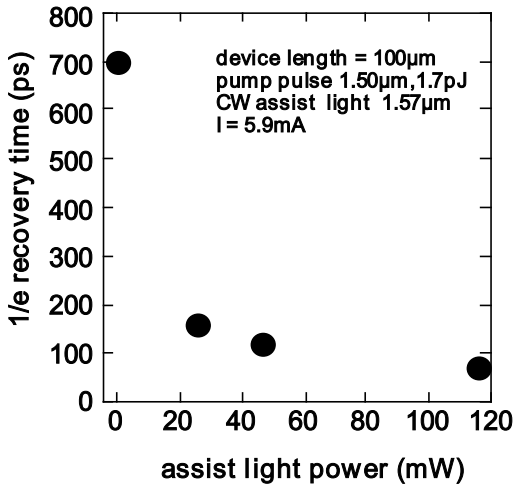

Figure 2-11: 1/e recovery time as a function of the assist light power

Figure 2-11 shows the 1/e absorption recovery time, in which the change of probe transmission decreases to 1/e of the initial value as a function of the assist light power. The signal wavelength was 1.50 μm and the transparent wavelength of the CW assist light was 1.57 μm when the SOA was operated at 5.9 mA injections. The 1/e recovery time is drastically reduced from 700 ps to 70 ps by increasing the assist light power, because the total quantity of stimulated recombinations is proportional to the number of incident photons

Figure 2-12 shows 1/e recovery time as a function of injection current. The wavelengths of the signal and the assist lights are 1.50 μm and 1.56 μm, respectively. The squares, the triangles, and the circles indicate data at the loss region, the transparent point, and the gain region for the assist light, respectively. The 1/e recovery time was decreased from 96 ps to 66 ps by increasing the injection current. By using the assist light in the gain region of SOAs, the intensity of the assist light is amplified in the active layer along the waveguide. Therefore, a larger number of photons combine

with the excess carriers in the active layer in comparison with the case of using the assist light set at the transparent point.

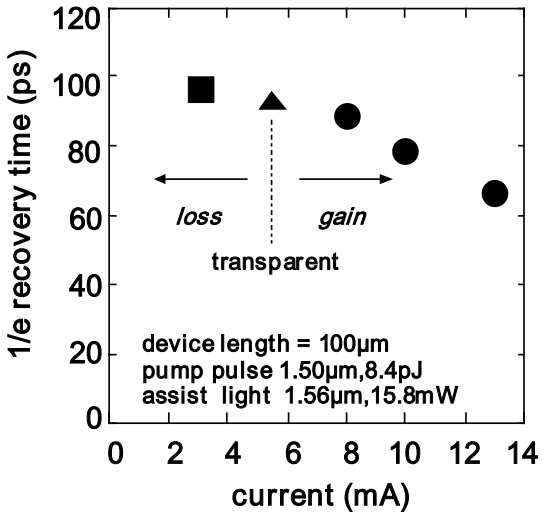

Figure 2-12: 1/e recovery time as a function of the injection current.

The optimum wavelength of the assist light was also investigated to obtain a shorter 1/e recovery time. Figure 2-13 shows the 1/e absorption recovery time as a function of the wavelength of the assist light. An injection current of 6.5 mA was set to make the waveguide transparent for the assist light wavelength of 1.54 μm, as indicated by filled circles. The coupled power of the assist light was about 30 mW. A shorter 1/e recovery time of 97 ps was obtained at 1.55 μm (gain) in comparison with 117 ps obtained at 1.54 μm (TP). Since the assist light at 1.55 μm (gain) has a positive gain, the intensity of the assist light at 1.55 μm (gain) is amplified in the active layer along the waveguide. Therefore, a large number of excess carriers are recombined by the stimulated recombination of the amplified assist light. While in the longer wavelength range of the assist light, the 1/e recovery time increases to exceed 120 ps.

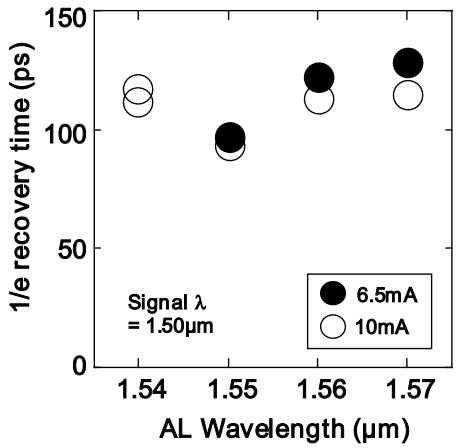

Figure 2-13: Measured result of the 1/e absorption recovery time as a function of the wavelength of the assist light.

This is because the gain of the assist light becomes smaller as the wavelength of the assist light approaches the band-gap energy. Increasing the injection current up to 10 mA, as indicated by open circles did not change this trend. Consequently, setting the wavelength of the assist light in the gain region of an SOA is not always the best way to obtain a shorter 1/e recovery time. To obtain the shortest 1/e recovery time, the assist light has to be set at the optimum wavelength in the gain region of the forward-biased SOA.

Figure 2-14 shows the wavelength dependence of the optical gain of the forward-biased SOA to clarify the optimum wavelength of the assist light. The experimental setup was almost the same as the one shown in Fig. 2-10, except that only the probe beam was irradiated to the SOA and the assist light cut filter (optical low-pass filter) was removed for the measurement of the amplified signal intensities, which were calculated by the output power and the width of the pulses in the probe beam. The wavelength of the probe beam was changed from 1.54 μm to 1.58 μm.

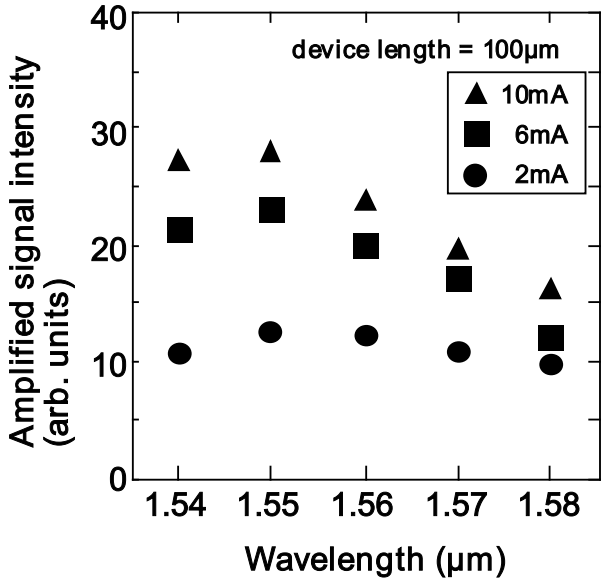

Figure 2-14: Amplified signal intensity as a function of the wavelength of the assist light. The parameters are the injection current to the SOA.

The estimated energy of the coupled optical pulse was 4 pJ. All data were readjusted by subtracting the optical background, which is the signal level of 0 mA injection. As the experimental result shows, the maximum point of the gain for the signal pulse was 1.55 μm in the active layer for each condition. In other words, since 1.55 μm is the maximum point of dg/dn in the active layer when excess carriers are generated due to the absorption of the signal pulse, the positive gain for 1.55 μm assist light becomes maximum valued compared with other wavelengths of the assist light. This is the reason why the optimum wavelength of the assist light to obtain the shortest 1/e recovery time was 1.55 μm, as shown in Fig. 2-13. Therefore, the assist light has to be set at the wavelength of the peak of gain profile. We have also confirmed that the 1/e recovery time was reduced from about 600 ps to 46 ps with 77 mW assist light power at 1.55 μm, which is the result of the optimum wavelength operating under 9.6 mA injections.

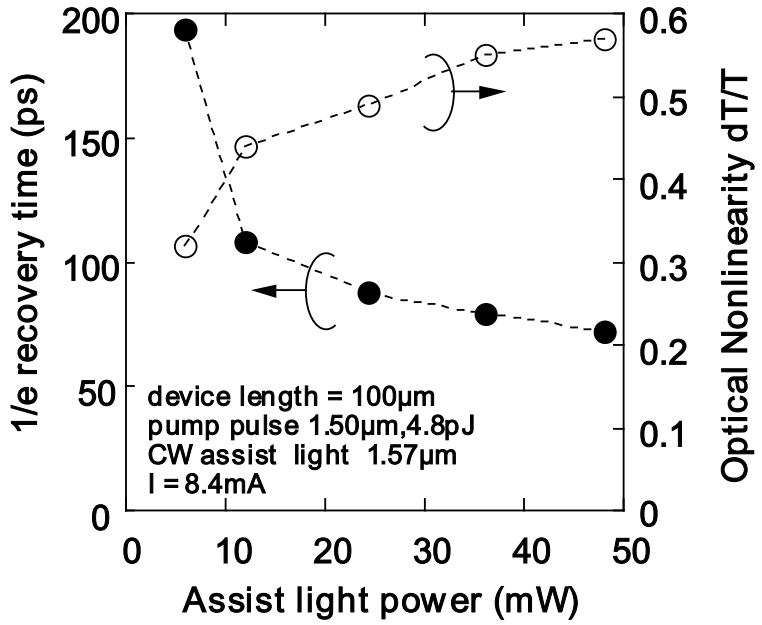

Figure 2-15: 1/e recovery time and optical nonlinearity as a function of the launched power of the assist light.

The 1/e recovery time and the nonlinearity as a function of the assist light power in the case of setting the wavelength of the assist light in the gain region are shown in Fig. 2-15. The filled and open circles represent the 1/e recovery time and the optical nonlinearity dT/T defined in Fig. 2-10, respectively. The optical nonlinearity dT/T is defined as follows: dT represents an initial change of probe transmission against the signal (pump) pulse and T represents the initial probe transmission through the waveguide. The wavelengths of signal and assist lights are 1.50 μm and 1.57 μm, respectively. The injection current of 8.4 mA was twice the transparent current of 4.2 mA for the assist light of 1.57 μm. By increasing the assist light power, the optical nonlinearity dT/T increased from 0.32 to 0.57, while the 1/e recovery time decreased from 194 ps to 70 ps. In the case of setting the wavelength of the assist light in the gain region, since the assist light causes the stimulated recombination, the initial carrier population is reduced and the absorption coefficient is larger than the case of setting the wavelength of the assist light at the transparent point on the gain curve at the same injection current. Setting the wavelength of the assist light in the gain

region has an advantage in terms of not only recovery speed but also optical nonlinearity. According to the evaluation results from section 3.2 to 3.4, the nonlinear absorption in an SOA with the proposed methodology for reducing the recovery time can be applied for an ultrafast saturable absorber. To introduce the technique to the actual transmission line, the feasibility of optical 2R regeneration is investigated in following sections by using a modulated optical data signal.

2.5 Optical noise reduction in 5 Gbit/s NRZ signal

To evaluate the effectiveness of the optical 2R regeneration by using the proposed methodologies, the transmission performance of the 5 Gbit/s NRZ signals due to the noise reduction effect is investigated by comparison of the receiver sensitivity in the BER measurement. The relationship between the Q-factor improvement of the optical signals and nonlinear absorption parameters in an SOA is investigated by the numerical calculation.

2.5.1 Experimental setup

The experimental setup is shown in Fig. 2-16. The input optical data signal was a 2^7-1 PRBS of 5 Gbps NRZ from a $LiNbO_3$ modulator driven by a pulse pattern generator. The amplified optical signal pulse was coupled into the noise reduction device through a tapered fiber.

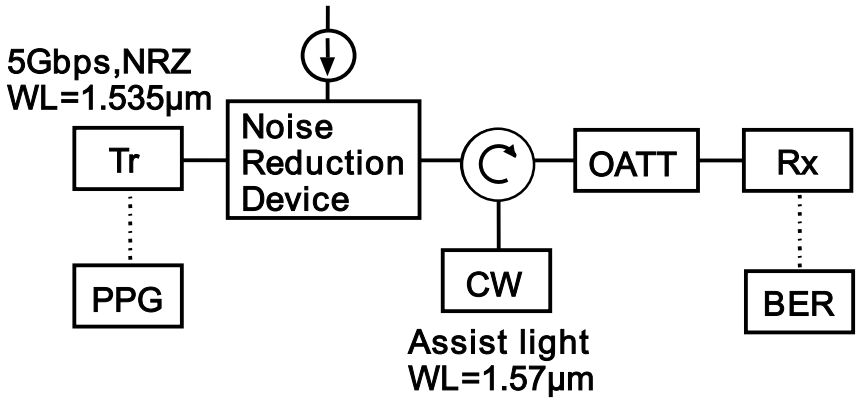

Figure 2-16: Experimental setup for the evaluation of the optical 2R regeneration.

The CW assist light was coupled into the backside of the device through an optical circulator because there was no need to insert a band pass filter that was one of the causes for

reducing optical power of the signal in the case of this experiment. Although, there should be some differences in the optical field distribution of the CW assist light and efficiency of stimulated emission according to the input direction of the CW assist light, the experimental results of as regards the absorption recovery time were almost the same in case of using the 100 μm long device. The signal output from the noise reduction device was attenuated in front of the receiver. The receiver sensitivity was measured by a bit error rate (BER) tester synchronized by a pulse pattern generator at 5 Gbit/s repetition rate.

2.5.2 Experimental results

Figure 2-17 shows the optical output intensity versus the optical input intensity coupled to the waveguide without the assist light. Parameters are injection currents.

The width of pulse is 100 ps with 5 Gbit/s repetition rate. Nonlinear absorption characteristics still exist for a signal wavelength of 1.535 μm up to 4 mA under which the waveguide was determined to be transparent for the CW assist light of 1.57 μm. The unsaturated absorption coefficient α_0 of 44.1 cm^{-1} and the saturation intensity I_s of 11.1 mW were obtained by the fitting of the Equation (2) indicated by the dashed line.

$$I_{out} = I_{in} \exp\left\{ -\alpha_0 \exp\left(-\frac{I_{in}}{I_S} \right) L \right\} \qquad (2)$$

It was experimentally confirmed that the saturation intensity I_s was scarcely changed with/without the assist light. Strictly speaking, the unsaturated absorption coefficient increases about several percent due to the faster absorption recovery time by means of the assist light. Since it did not seem to be a significant difference, α_0 and I_s deduced from the result without the assist light were used in the later discussion. Note that the insertion loss of the noise reduction device against the signal pulse is as low

as -0.9 dB with 4 mA injection. The low loss feature is a great advantage for inline devices such as the noise reduction device in the repeater.

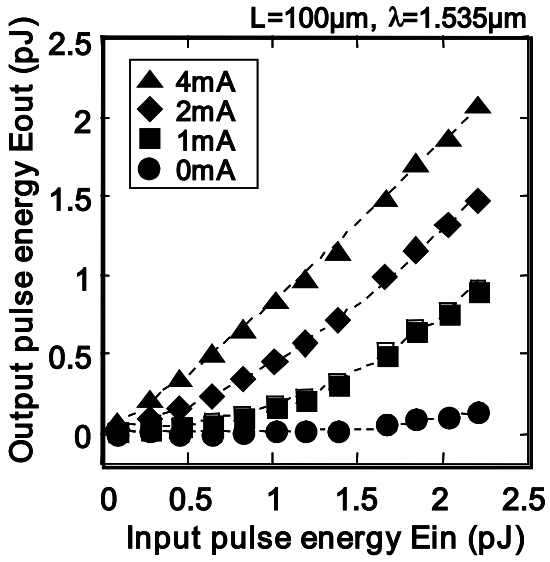

Figure 2-17: I/O characteristics of the noise reduction device.

The BER measurement was carried out for evaluation the performance as shown in Fig. 2-17. The wavelength and injected intensity of the optical data signal were 1.535 μm and +8 dBm, respectively. The 1.57 μm CW assist light of 20 mW, which was transparent, was injected from the backside of the SOA. The coupling coefficient between the waveguide and the tapered fiber at both sides was about 40 %. The absorption recovery times with and without the assist light were about 100 ps and 700 ps, respectively. Figure 2-18 shows the measured BER as a function of the received power. The BER characteristics with the assist light indicated by closed circles were improved in receiver sensitivity by 0.5 dB compared with the results of back-to-back (B-B) measurement without the noise reduction device indicated by closed squares. This result may be due to the fast noise suppression effect on the space level. However, the BER without the assist light indicated by open circles was

worse than the result of B-B. The remaining noise on the space level and/or word pattern effect on mark level due to the rather slow absorption recovery may impair performance. In comparison with SOA with and without the assist light, the receiver sensitivity was improved by 1.5 dB at a BER equal to 10^{-9}.

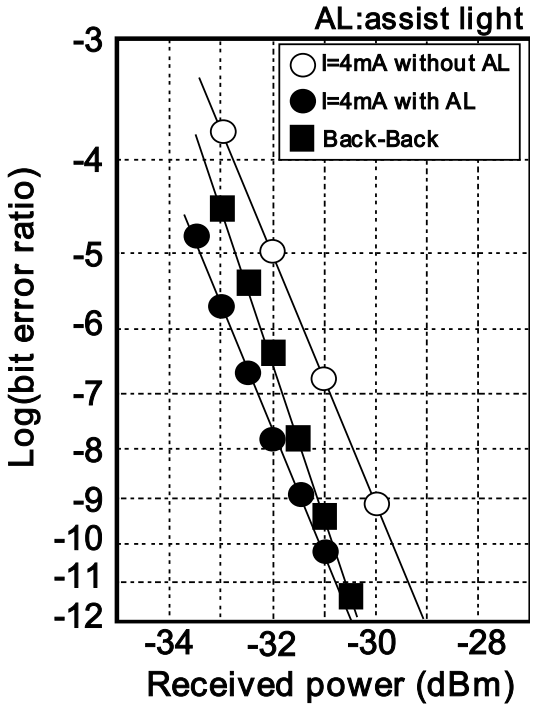

Figure 2-18: Measured BER as a function of the received power.

2.5.3 Numerical calculation

In this part, the performance of the noise reduction device, which depends on the noise distribution on the signal and the device parameters such as α_0, I_s, and L, is investigated by numerical calculation. The performance of the noise reduction device is calculated by Q-factor, which consists of the four parameters as shown in Fig. 2-6. They are the mean energy of the mark (one) level E_{p1}, the mean energy of the space (zero) level E_{p0}, the standard deviation of the noise on the mark level σ_1, and the standard deviation of the noise on the space level σ_0. The Q-factor of the input optical signal pulse is defined by the formula,

$$Q = \frac{\left(E_{p1} - E_{p0}\right)}{\left(\sigma_1 + \sigma_0\right)} \tag{3}$$

which is usually used for the Gaussian noise distribution. In the same way, the Q-factor of the output optical pulse defined by the formula,

$$Q' = \frac{\left(E'_{p1} - E'_{p0}\right)}{\left(\sigma'_1 + \sigma'_0\right)} \tag{4}$$

as shown in Fig. 2-6. Since, the transformed noise distribution is not Gaussian shape, the Q-factor of the output optical pulse does not directly relate to the exact signal to noise ratio (SNR) of the optical pulse. In other words, it does not mean an improvement of attainable BER. The quantity of Q' defined here represents the degree of the eye opening in the eye diagram, which is usually obtained by a sampling oscilloscope. The improvement of the degree of the eye opening makes the receiver sensitivity better in weak received power. Q-factor can be derived

Figure 2-19 shows the Q value improvement as a function of the input optical pulse energy using the device parameters that are the α_0 of 44.1 cm^{-1}, the Es = 1.11 pJ, and the L of 100 μm. The device parameters were empirically determined by the experimental results of I/O characteristics and the fitting curve expressed in eq. (2). The improvement of Q value, which equals to 20*Log

(Q-factor), was calculated by difference between input and output Q values that were able to be estimated by using eq. (3) and eq. (4). The Q value of the input signal was set to be 15.56 dB, which was equivalent to BER of 10^{-9}, where the σ_1 and the σ_0 were 8 % of the mark level E_{p1} deduced from the experimental result. The Q' value was estimated to 15.96 dB by utilizing eq. (2) and the determined device parameters when the optical pulse energy was as large as 1.26 pJ, which corresponds to the input intensity deduced from the condition of the input signal in the BER experiment. The average power, the repetition rate, and the duty ratio were +8 dBm, 5 Gbps, and 50 %, respectively.

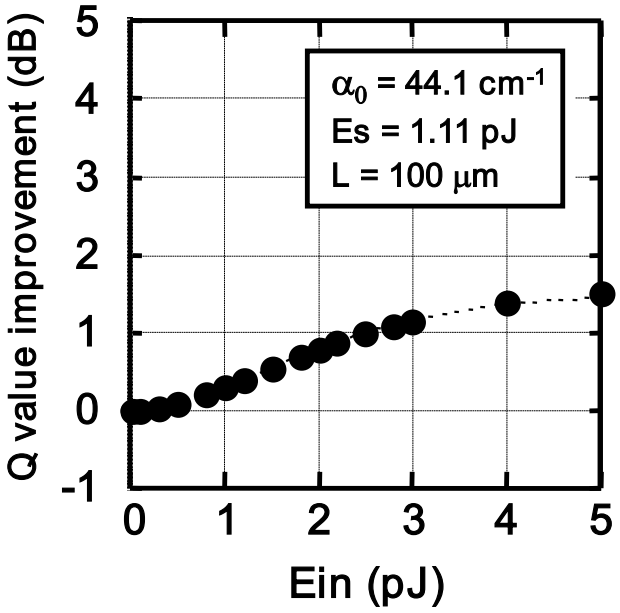

Figure 2-19: Q-factor improvement as a function of input pulse energy using the experimental device parameters.

Assuming that the only cause of the improvement from the Q value of 15.56 dB to 15.96 dB is the change of noise distribution on the space level, this improvement can be considered equivalent to the

9 % decrease from the σ_0 to the σ'_0. The small absorption coefficient of 44.1 cm^{-1} and the large saturation energy of 1.11 pJ comparable to the input pulse energy were the reasons why there was the small improvement. In order to obtain larger improvement, we can modify the device parameters α_0, I_s, and L by changing the material of the active layer or the length of the device. An ideal nonlinear absorption function for noise reduction is that mark level is not absorbed and space level is completely absorbed by the active layer of the device. The total amount of the optical signal absorption is determined by the $\alpha_0 L$. The low loss for the mark level is realized when saturation energy is sufficiently small in comparison with the optical signal pulse energy. The shorter device has the smaller saturation intensity.

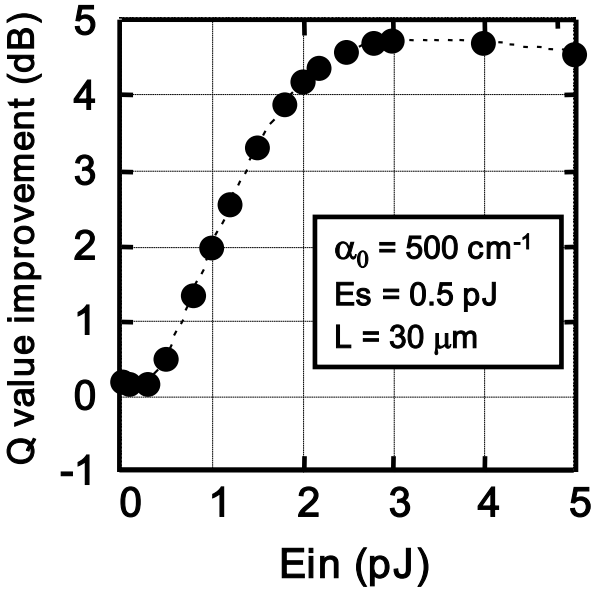

Figure 2-20: Q-factor improvement as a function of input pulse intensity using the assumed device parameters.

On the other hand, the absorption coefficient α_0 has to be larger than this case for sufficient nonlinear absorption effect. The assumed parameters were the α_0 of 500 cm^{-1}, the L of 30 μm, and the E_s of 0.5

pJ. The absorption coefficient of 500 cm^{-1} of the waveguide against the light of a 1.5 μm range was deduced by the property of the InGaAs bulk material with a carrier density of $1x10^{18}$ cm^{-3} and a confinement factor of 0.3. The saturation energy of 0.5 pJ in the 30 μm device was deduced from our experimental results on length dependency of E_s. Figure 2-20 shows the Q value improvement with the optimized device parameters as a function of input pulse energy. The calculated Q' value of 17.79 dB, which meant the improvement of 2.23 dB, was obtained with the 1.26 pJ optical pulse energy that was the same as the previous estimation. This improvement can be considered equivalent to the 41 % decrease from the σ_0 to the σ'_0 under the same assumption in respect to the relation of the Q' value and the σ'_0. The suppression effect of the noise distribution on the space level due to the saturable absorption was enhanced from 9 % to 41 % by optimizing the device parameters. Additionally, much more reduction of the absorption recovery time may be expected for a shorter device in our method.

2.6 Optical noise reduction in 10 Gbit/s RZ signal

For the long haul transmission as well as the metro area transport application, 10 Gbit/s return-to-zero (RZ) format of the optical data signal is the dominant methodology from viewpoint of the transmission performance. It is useful to realize a simple optical 2R regeneration device for both TDM and WDM transmission systems. In this section, evaluation results of the transmission performance of the 10 Gbit/s RZ signals with and without the optical 2R regeneration device are experimentally described by both the BER measurement and the optical signal to noise ratio (OSNR) measurement as well as the extinction ratio of the optical data signals. The optical 2R regeneration device is an ultrafast SA by using an SOA with the CW assist light for reducing the recovery time just same as the previous section.

2.6.1 Experimental Setup

An optical 2R regeneration device, so-called optical reshaping device (ORD) in this section, was a ridge waveguide MQW-SOA of 100 μm length with an anti reflection coat on both facets. Figure 2-21 shows the optical output intensity versus the optical input intensity coupled to the waveguide with the assist light. The closed circles are experimental results. Nonlinear absorption characteristics still exist, since the signal light of 1.55 μm was the wavelength region of absorption under applying voltage of 0.2 V. Wavelength and induced power of CW assist light were 1.58 μm and 20 dBm, respectively. It was the transparent wavelength on gain profile of ORD determined by the bias voltage and average power of CW assist light.

The dashed line is the fitting curve, which expressed as follows,

$$I_{out} = I_{in} \exp\left\{-\alpha_0 \exp\left(-\frac{I_{in}}{I_S}\right) L\right\} \qquad (5)$$

Where α_0 is the unsaturated absorption coefficient, I_s is the saturation intensity and L is the length of the absorption region. In this case, α_0 of 87cm^{-1} and I_s of 51 mW were calculated by eq. 5. Here, the relation between the optical pulse intensity and the optical pulse energy are explained by using the formulas.

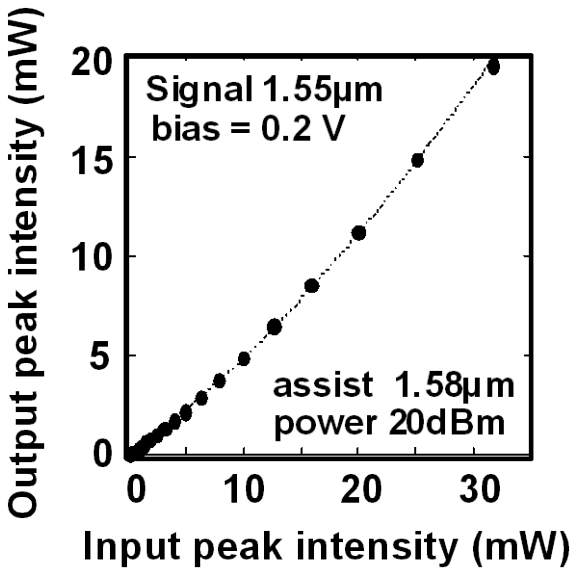

Figure 2-21: Nonlinear I/O characteristics of the device with the assist light.

The optical pulse energy means the summation of the energy of photons. The optical pulse intensity means the peak power of pulse, which is corresponding to the height of optical pulse. Therefore, the optical pulse energy is derived from the product of the optical pulse intensity and the time width of the optical pulse. Figure 2-22 shows the experimental setup for the evaluation of 10 Gbit/s optical 2R regeneration. The input optical signal pulse was a 2^{23}-1 PRBS of 10 Gbit/s RZ from an electro-absorption modulator (EAM) for generating the RZ pulse and a $LiNbO_3$ modulators for the PRBS encoding. An ASE light was added by the optical coupler to the signals for emulating the accumulation of ASE noise from concatenated EDFAs in transmission line.

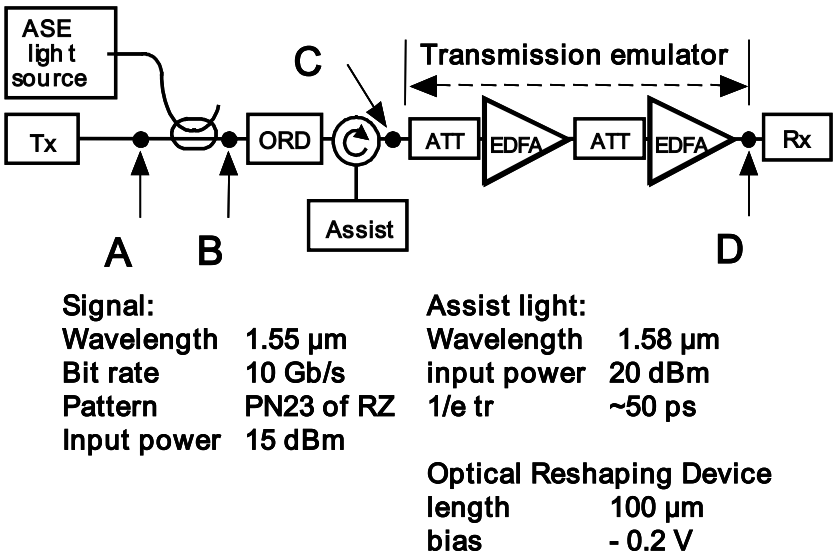

Figure 2-22: Experimental setup for the evaluation for 10 Gbit/s optical 2R regeneration

The CW assist light was coupled into the backside of the device through an optical circulator. At the back of the optical 2R regeneration device, optical attenuators and EDFAs were deployed for emulating the transmission line, which included optical fibers and repeaters. Four measurement points indicated by A, B, C and D were defined as shown in Fig. 2-22. The measurement points A and B are defined for evaluating the reference quality of the transmission signal and the impaired signal by ASE noise before regeneration, respectively. The other measurement points C and D are defined for evaluating the signal quality after the regeneration and the transmission performance after passing through the transmission emulator, respectively.

2.6.2 Experimental Result

The OSNR measurement with resolution of 0.2 nm was carried out at points A, B, and C as

shown in Fig. 2-23.

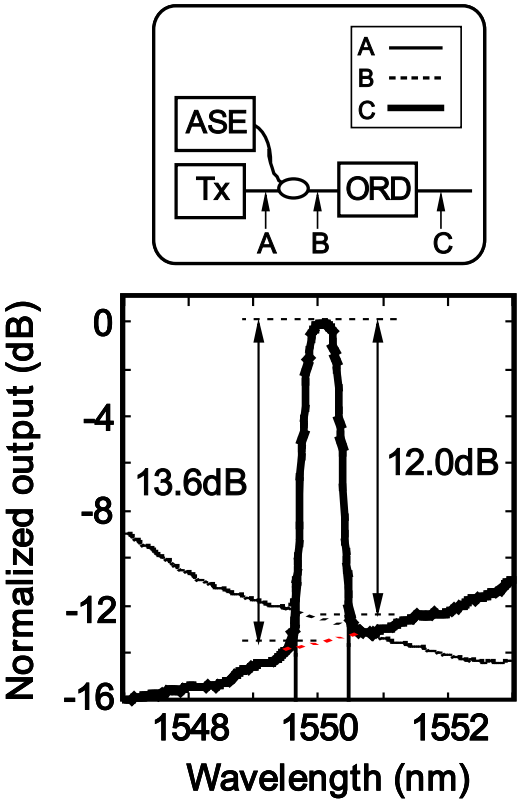

Figure 2-23: Normalized optical power of the data signal measured at the points A, B and C.

The measured results of each optical spectrum were normalized by the peak power at 1550 nm of each result. The OSNR of the transmitter measured in the point A as a reference was more than 30 dB. The measured OSNR of point at B drawn by the dashed line and point C drawn by the thick solid line were 12.0 dB and 13.6 dB, respectively. The improvement of 1.6 dB was observed in the OSNR evaluation due to the noise reduction at the space level of the optical data signal. Figure 2-24 shows the measurement result of the BER evaluation at the defined points A, B and C.

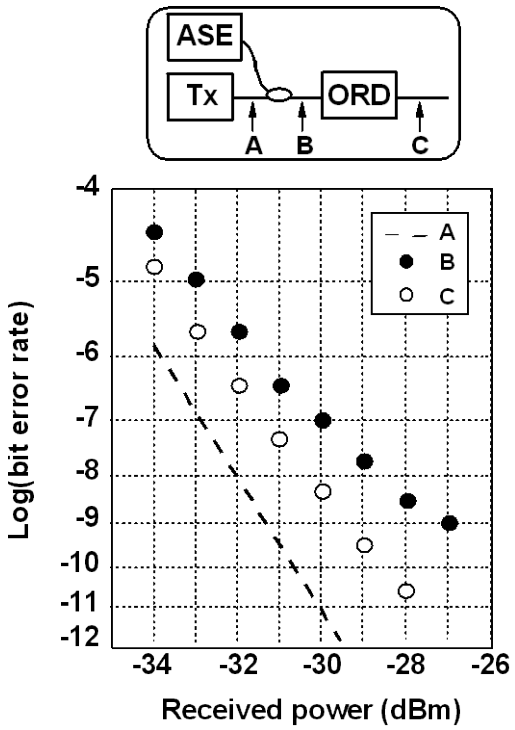

Figure 2-24: BER measurement results at point A, B and C as a function of the received power.

The result of point B indicated by closed circles showed a power penalty against the result of point A due to the ASE noise on mark and space levels which impair the eye opening of signal pulses. The result of point C, which is after passing through the ORD indicated by opened circles, the receiver sensitivity of 2.5 dB was improved compared with the result of point B at a BER equal to 10^{-9} due to the noise suppression effect on space level.

Figure 2-25 shows the measurement results of the extinction ratio and the optical SNR and the estimated results of the Q-factor at each measurement point in Fig. 2-22. The extinction ratio and the Q-factor were calculated by the histogram of eye pattern measured by the high-speed electric oscilloscope. The effect of ORD was become clear in each characteristic comparing with point B and C. By introducing the 2R regeneration, the improvement of the transmission performance was able to

achieved not only at the points before and after the ORD but also at the point D. It is supposed that the noise distribution at space level is modified to the non-Gaussian distribution due to the nonlinear transfer function of the ORD. The final suppression effects of aggravation in extinction ratio and in optical SNR were 0.5 dB and 0.8 dB, respectively.

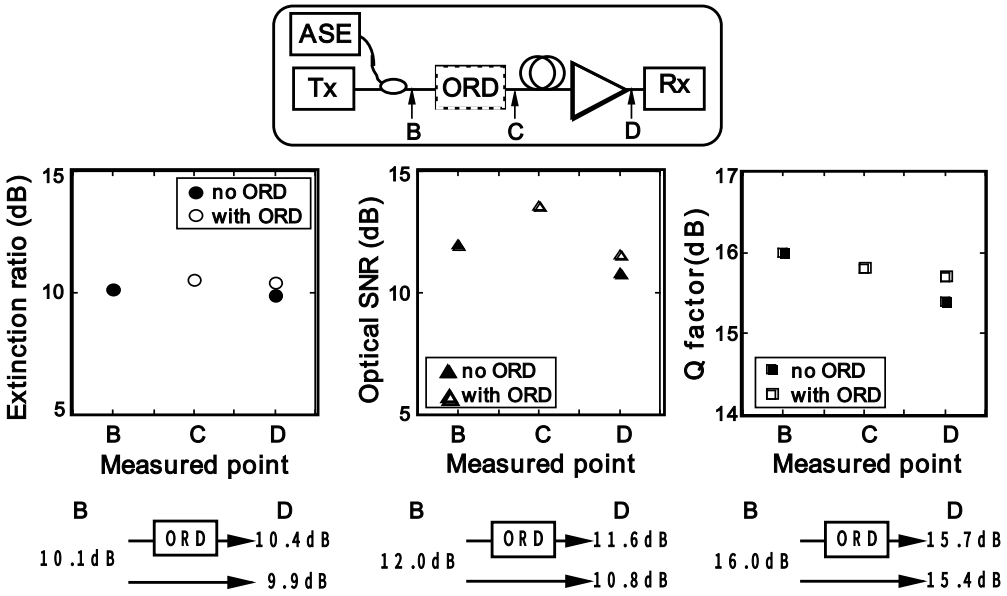

Figure 2-25: Measurement results of the extinction ratio, the optical SNR and the Q-factor of the optical data signal at points B, C and D.

The extinction ration can be theoretically estimated by the ASE noise accumulation and the noise suppression effect of the nonlinear absorption effect of the ORD. The ASE noise generated by the EDFA is expressed as follows,

$$P_{ase} = \frac{hc}{\lambda} \cdot NF \cdot B_o \cdot (G-1) \qquad (6)$$

where P_{ase} is the power of ASE noise, h is the Plank constant, c is the light speed, NF is the noise figure of EDFA, Bo is the bandwidth of the filter and G is the small signal gain of EDFA. The extinction

ratio of the each point can be estimated by calculating the mean value of the mark level and the space level of the optical signals.

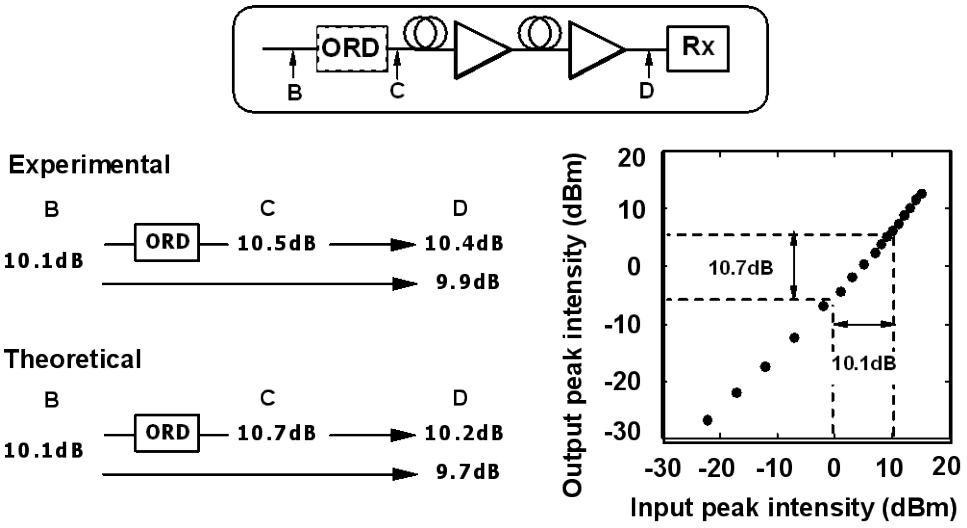

Figure 2-26: Experimental and theoretical evaluation of the extinction ratio at each point. The left side viewgraph shows the measured I/O characteristics.

Figure 2-26 shows the measurement and the theoretical estimation of the extinction ratio as well as the measurement result of the I/O characteristics. The experimental results are the same as the previous results as shown in Fig. 2-25. The extinction ratio of point B can be calculated by the mean value of the mark and the space level by adding the ASE noise to the reference signal generated by the transmitter. The nonlinear transfer function expressed by the eq (5) and the device parameters derive the extinction ratio at point C. The α_0 of 87 cm^{-1}, I_s of 51 mW and L of 100 μm were used as the device parameters that were estimated by the measured I/O results. The extinction ratio at point D was estimated by adding the ASE noise to the calculation result of point C. The theoretical estimation well corresponds to the experimental result. This result suggests that the improvement of the transmission performance by using the optical 2R regeneration can be simply estimated by using the

proposed estimation procedure.

2.7 Conclusion

In this section, novel methodology to realize an ultrafast SA for the all-optical 2R regeneration was proposed and investigated by using an SOA with external CW light. Nonlinear absorption effect in the active layer of SOA was investigated experimentally and numerically. By introducing the conception of Q-factor, the device parameter and the actual performance were tied up for designing the device and the system for the optical 2R regeneration. For reducing the absorption recovery time to realize the ultrafast SA, external CW assist light was deployed. The absorption recovery time, which is governed by the spontaneous emission, was drastically reduced from 700 ps to 66 ps evaluated by the conventional pump-prove technique. Experimental evaluation for verifying the optimum condition was carrier out with regard to the assist light. Using the assist light at transparent wavelength in the gain profile of the SOA was basic idea that did not change the condition of the gain profile. For further reducing the recovery time, using the assist light at gain region was proposed and proved by the experimental evaluation. To evaluate the feasibility of the all-optical 2R regeneration, performance tests were demonstrated by using the 5 Gbit/s NRZ signal and the 10 Gbit/s RZ signal. The improvement of the performance was observed in each evaluation. In the 5 Gbit/s experiment, the improvement of receiver sensitivity was successfully confirmed to be 0.5 dB compared with the back-to-back measurement. According to the simple calculations, the noise suppression effect on the space level of more than 40 % for the initial noise distribution at the input pulse intensity of 1.26 pJ would be possible by changing the material of the active layer to an InGaAs bulk semiconductor and the device length of 30 μm. Moreover, in the experiment using 10 Gbit/s RZ signals, the ASE noise suppression effect on space level of optical signal in the optical reshaping device was confirmed. In the BER measurement, receiver sensitivity improvement of 2.5 dB was confirmed by using ORD. Improvements of extinction ratio of 0.5 dB and optical SNR of 0.8 dB

were obtained in front of receiver by superimposing the ORD.

These results are promising to realize the quite simple all-optical 2R regeneration device using nonlinear absorption in an SOA in ultra-high repetition rate operation.

CHAPTER 3 ALL-OPTICAL 3R REGENERATION

3.1 Introduction

The all-optical 3R regeneration, as mentioned in the chapter 2, is defined that re-shaping, re-amplifying and re-timing can be simultaneously realized by the optical means. A lot of methodologies for the all-optical 3R regeneration as well as the all-optical signal processing are proposed by using the different material and the devices. Figure 3-1 shows the schematic image of the all-optical 3R regeneration. Basically there are two parts in the 3R regeneration system.

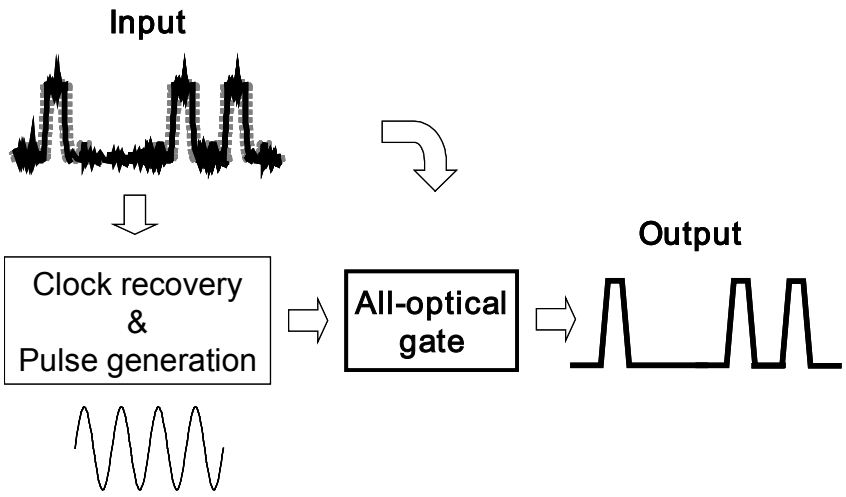

Figure 3-1: Schematic diagram of the all-optical 3R regeneration.

The clock recovery section extracts an accurate clock and generates a continuing optical clock from the input optical data signal with timing jitter and power fluctuation. The all-optical gate section works like an optical shutter, which is opened by the optical pulse input. It is straightforward that the semiconductor waveguide device can be expected to realize the all-optical regeneration device with high-efficiency, small volume and low-cost manner. Especially the semiconductor waveguide

device has a large nonlinear response of the optical properties such as a refractive index to the input optical pulse due to the absorption or emission through the interaction between carriers and photons in the semiconductor active layer of the device. However, there still exists a problem, for utilizing the device in the ultra-high speed optical communication system, that is the recovery time from the excitation state to the steady state of the carriers in the semiconductor device. The slow recovery time of the gain as well as absorption degrades the operation performance due to the inadequate performance and the word pattern effect in the optical fiber communication system. Therefore, it is essential for the high-speed operation of the device to introduce the novel mechanism.

In this chapter, a new technique to shorten the gain recovery time of SOA is introduced by using the external CW light. Moreover, the methodology is applied for the UNI switch for the high-speed operation. To apply the UNI switch for the actual deployment in the optical fiber communication system, the new material is used for the birefringent media compared to the original proposal. To investigate the feasibility of this methodology, the all-optical regenerative wavelength conversion is demonstrated at the repetition rate of 40 Gbit/s as well as 80 Gbit/s. Section 4.2 proposes the new technique for reducing a gain recovery time for SOA using external CW assist light. Section 4.3 describes the operation principle of the UNI switch. The experimental evaluations of the all-optical regenerative wavelength conversion at the repetition rate of 40 Gbit/s and 80 Gbit/s are expressed in section 4.4 and 4.5, respectively.

3.2 Reducing a gain recovery time of SOA by external CW light

The semiconductor waveguide based regeneration devices utilize the nonlinear I/O characteristics and the refractive index change to control the phase of the optical pulse [92-104]. The dominant factor of the inadequate performance of the device is the word pattern effect due to the gain

fluctuation for the data signals. Therefore, suppression of the gain fluctuation is effective method to improve the regeneration performance.

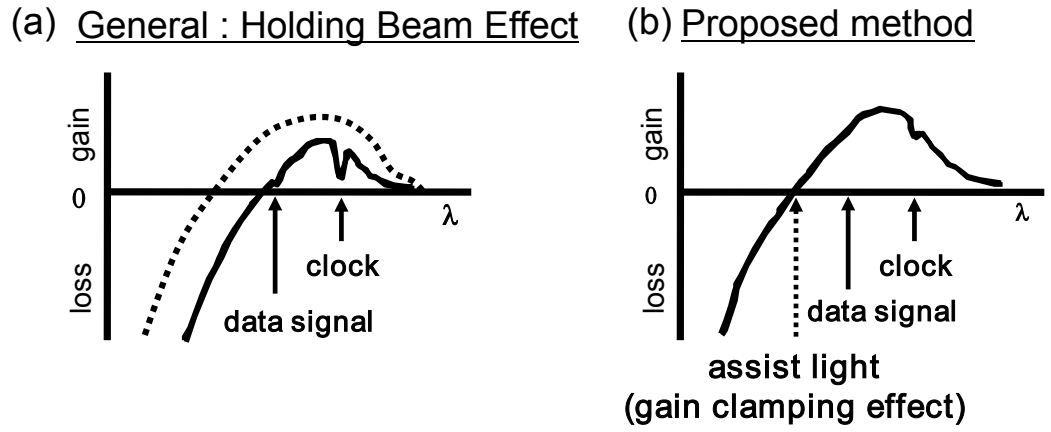

Figure 3-2: Simplified gain curves of an SOA using (a) the holding beam effect and (b) the gain clamping effect.

One of the techniques for high-speed operation of optical 3R regeneration as well as wavelength conversion is the holding beam effect [34, 105-106] as shown in Fig. 3-2(a). The holding beam effect by the clock pulse injection makes gain profile stable because the positive gain for the data signal become small. However, a large average power of the optical clock pulse is needed to make the gain saturated condition. Moreover, a large power of the data signal is also needed to change the refractive index of the semiconductor waveguide since the positive gain for the optical data signal is small. Consequently, a large power of both the optical clock pulse and the optical data signal are required for the high-speed operation.

On the other hand, the proposed technique, which is depicted in the Fig. 3-2(b), utilizes the CW assist light at the transparent wavelength of the gain profile. The CW assist light clamps the gain curve of the SOA due to the stimulated emission or the absorption at the wavelength of itself when the

control signal changes the gain curve of the SOA. In this condition, the positive gain for the optical data signal is maintained at the same level as an initial state. Therefore, the refractive index change can be carried out by the small optical power compared to the holding beam effect. Furthermore, the faster gain recovery time can be expected by the very fast excess carrier generation due to the stimulated absorption caused by the CW assist light.

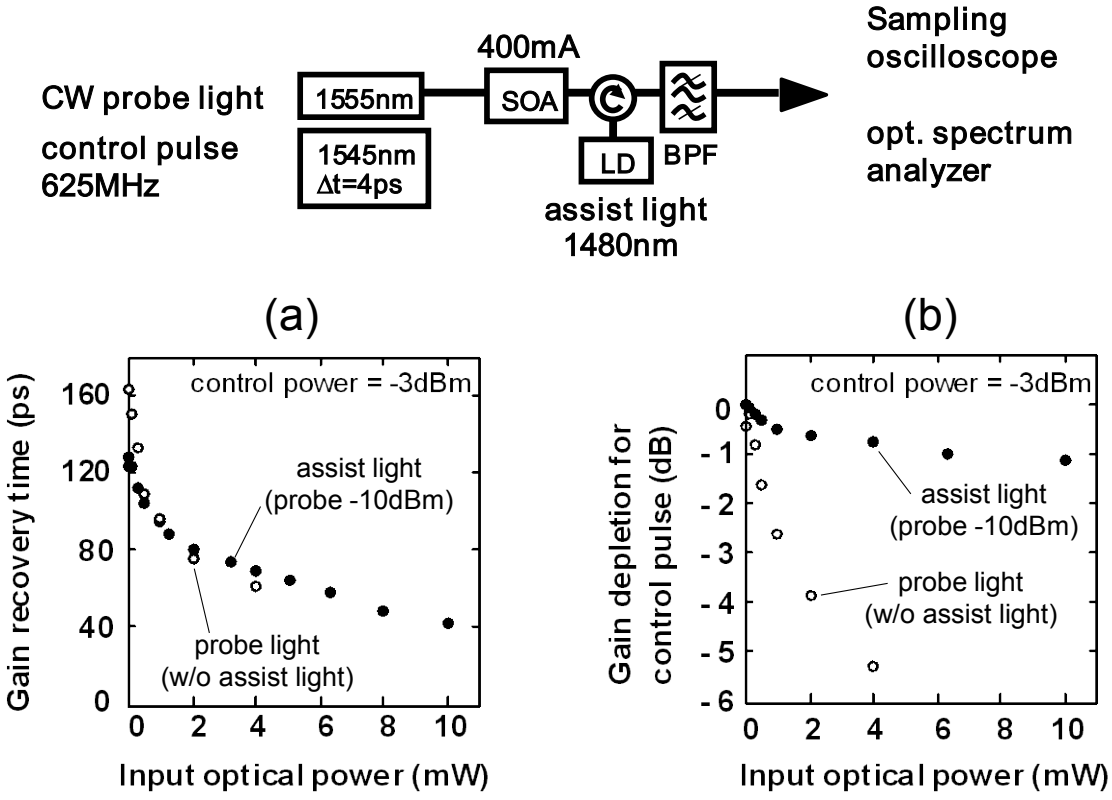

Figure 3-3: (a) Gain recovery time as a function of the input optical power. (b) Gain depletion for control pulse as a function of the input optical power.

Figure 3-3(a) shows the gain recovery time of an SOA as a function of the input optical power of either the probe or the assist light, which was measured using the experimental setup shown in the inset. The measurement was carrier out by using the cross gain modulation in the SOA and

captured by the high-speed sampling oscilloscope. The recovery time was defined as the 1/e recovery point of the initial change of the probe light. The SOA was InGaAsP/InP bulk type with gain peak wavelength of 1525 nm and the injection current was 400 mA. The wavelengths of the CW probe light and the control pulse with 625 MHz repetition rate were 1555 nm and 1545 nm, respectively. The assist light at 1480 nm was generated by the Fiber-Bragg-Grating-locked laser diode. Open and close circles indicate the data measured varying the probe light power without assist light and those measured varying the assist light power with a fixed probe light power of -10 dBm, respectively.

The gain recovery time monotonically decreased with increasing either the probe or the assist light power with similar power dependence. The gain recovery time of 40 ps was obtained when the assist light power was 10 mW. Figure 3-3(b) shows the gain depletion of the SOA to the control pulse measured with the same setup. The measured results were normalized by the peak power of the signal wavelength measured by the optical spectrum analyzer. The gain depletion was only -1 dB when the assist light power was increased as large as 10 mW since its wavelength was almost transparent to the active layer of the SOA. On the other hand, the gain depletion was as large as –5.5 dB in the case of the CW probe light power of 4 mW without assist light. It means that, a large control pulse power is required to induce a refractive index change corresponding to π-phase shift, which is important property for the interferometric switch utilizing the SOA. These results apparently prove the advantage of the method to utilize a transparent assist light as a gain clamping beam, because the fast gain recovery time and the low control pulse power can be realized simultaneously.

To prove the effectiveness of the proposed methodology, 40 Gbit/s data streams before and after passing through SOA with and without the CW assist light were observed by a sampling oscilloscope. Figure 3-4 shows the experimental setup and the trace curve of 40 Gbit/s data streams

that are the input signal, output signal without assist light and output signal with assist light. The data stream was generated by utilizing the optical time domain multiplexing (OTDM) technique and 10 Gbit/s RZ data signals, which was the pseudo random bit sequence (PRBS) of 2^7-1. There was obvious word pattern effect in the output signal without assist light as shown in Fig. 3-4(b). When the continuous "1" is fed into the SOA, the intensity of the output signal from the SOA becomes low gradually since the gain for the signal does not recover. The gain recovery time is supposed to be not enough fast for the 40 Gbit/s data stream. On the other hand, the reduction of the pattern effect of the SOA due to the assist light was observed at 40 Gbit/s as shown in Fig. 3-4(c). These results proved that the proposed methodology could be applied for the 40 Gbit/s.

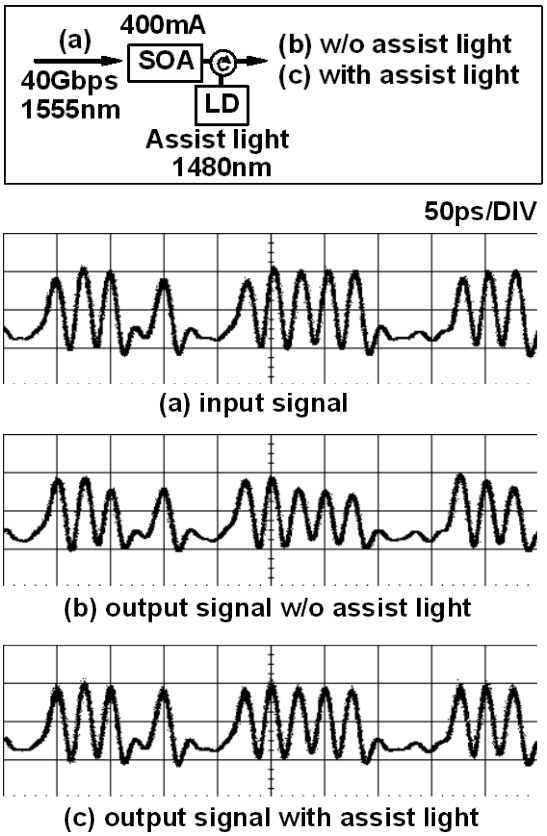

Figure 3-4: Experimental setup and the trace curves of the 40 Gbit/s data streams that are (a) input signal, (b) output signal without assist light and (c) output signal with assist light.

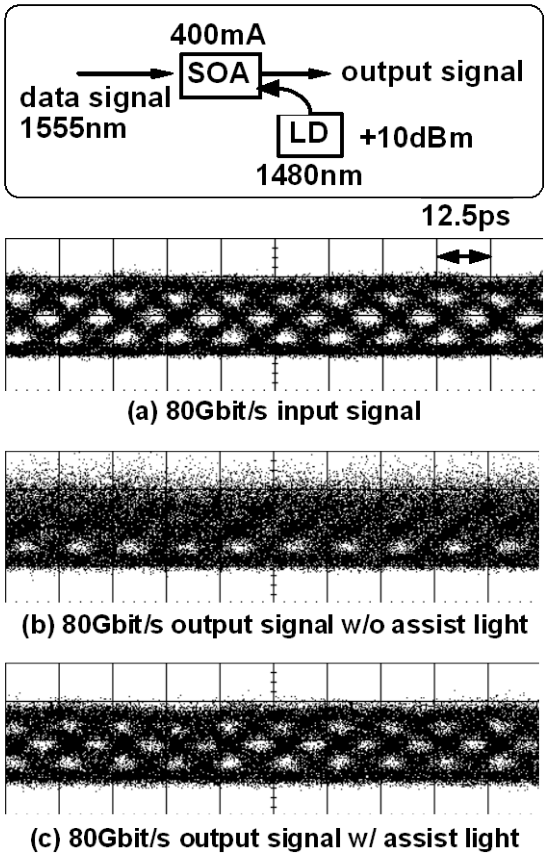

Figure 3-5: Experimental setup and the trace curves of the 80 Gbit/s data streams that are (a) input signal, (b) output signal without assist light and (c) output signal with assist light.

Furthermore, the same evaluation was carried out at the repetition rate of 80 Gbit/s. data stream generated by 10 Gbit/s based OTDM technique. Figure 3-5 shows the experimental setup, which is the same as the previous one, and the eye pattern of 80 Gbit/s data streams that are the input signal, output signal without assist light and output signal with assist light. The eye diagram of 80 Gbit/s data signal of 0 dBm was captured by sampling oscilloscope equipped with 30 GHz bandwidth

photo detector. Figure 3-5(b) apparently shows the pattern effect on the mark level of the signal, i.e., the impaired pulse height uniformity of the output signal of the SOA without assist light. The pattern effect was almost eliminated by using assist light, as shown in Fig. 3-5(c). Note that the gain recovery time accelerated by the CW assist light was applicable to the 80 Gbit/s application. These results indicate that the proposed method can be utilized in the ultra high-speed all-optical 3R regeneration as well as the all-optical signal processing.

3.3 All-optical regenerative wavelength conversion by UNI switch

The optical interferometric devices incorporating SOA, such as an SOA-MZI [42, 45, 57], an SOA-delayed interferometer [7-9, 56, 58] and an SOA-one-arm MZI which is so called "UNI (ultrafast nonlinear interferometer) [28, 107-111]" have been extensively investigated at the bit rate of 40 Gbit/s or higher and are promising candidates for the ultra-high-speed all-optical signal processing. Especially, the differential operation technique of SOA-based MZI devices allows their response speeds to easily overcome the limitation due to the slow gain recovery of the individual SOA. Since UNI employing one SOA has a structural simplicity that intrinsically assures good balance in both gain and phase in the one-arm MZI, it is easy to be tuned at the optimized condition and to stabilize the regeneration performance. In this section, operational principle of the UNI switch is described before the experimental evaluation.

Figure 3-6 shows the switching principle of the UNI configuration. The upper side schematic diagram and the lower one express the off state of the switch and the on state, respectively. The basic configuration of UNI switch consists of the two highly birefringent (HiBi) media, one SOA and a polarizer. Note that all components used here are compact in-line packaged components. In the off state of the UNI, a pair of orthogonally polarized clock pulses that are divided by the first HiBi

medium are recombined by the second one after passing through the SOA.

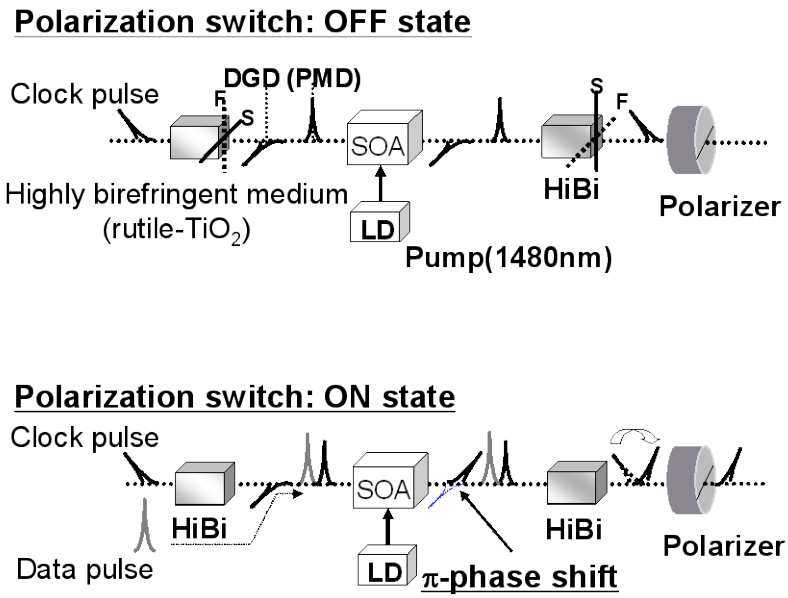

Figure 3-6: Schematic diagram of the fundamental configuration of the UNI switch.

To recombine the split pulse divided in the first HiBi medium, the second HiBi medium is set so that the slow and the fast axes may differ by 90 degrees. The polarizer placed at the end of the optical path is set not to pass the recombined clock pulse for making the UNI switch off state. In the on state of the UNI switch, the control pulse is fed into the middle of two separated pulses before launching the SOA. In the SOA, the trailing pulse of the split clock pulse experience π-phase shift induced by the control pulse. When the clock pulse pair is then launched into the second HiBi medium, the delay between the pulses is reversed and the two components are recombined before passing through the polarizer. The polarization of the recombined clock pulse is corresponding to the polarization direction of the polarizer. Hence the on state of the UNI switch can be realized. When the CW assist light is needed to deploy for reducing gain recovery time, the laser light can be irradiated

to the SOA by using an optical coupler from the front side or the backside.

3.4 All-optical regenerative wavelength conversion at 40 Gbit/s

For the actual deployment of the all-optical regenerator in the optical fiber communication system, it is important to verify the feasibility of the proposed methodology by using the actual data signals. The new technique has already proposed and evaluated in the previous section, which is that the CW assist light at the wavelength transparent to an SOA could clamp the gain profile of the SOA without changing gain or loss for control signals. In this section, a transparent assist light for gain clamping effect is applied for reducing a pattern effect of an SOA-based all-optical switch that is UNI. The proposed scheme in the UNI at 40 Gbps operation is evaluated by the BER test with various lengths of the (PRBS).

3.4.1 Experimental setup

The experimental setup of the UNI with the assist light is shown in Fig. 3-7. It consists of two TiO_2 rutile crystals, which has the respective refractive indexes for ordinary and extraordinary rays of n_o = 2.45 and n_e = 2.70, with the polarization mode dispersion (PMD) of 10 ps as the polarization discrimination devices. The same SOA as that used in the former experiment was deployed in between the two HiBi media. Both the 40 GHz probe pulse at 1555 nm and the 40 Gbit/s control signal pulse at 1545 nm were generated by the fiber ring mode-locked lasers with 10 GHz repetition rates and OTDM technique. The optical delay line was deployed for adjusting the time position of the optical data signal between the split clock pulses before launching to the SOA. The powers of the clock pulse and data signal launched to the SOA were –6 dBm and –3 dBm, respectively. The assist light of +10 dBm at 1480 nm was launched via optical circulator from the backside of the

SOA. A Babinet-Soleil compensator consisting of two TiO_2 rutile wedges precisely tuned the relative phase difference between two polarization components. The polarizer and the optical band pass filter were deployed for extracting the polarization switched signal at 1555 nm. The switched signal of 40 Gbit/s was demultiplexed into 10 Gbit/s signal by an EA modulator and the signal quality was estimated by the BER test system.

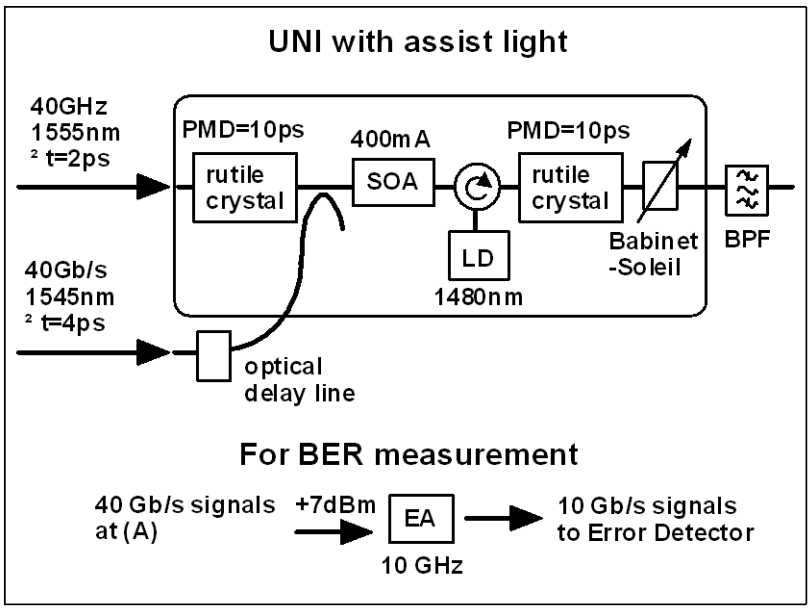

Figure 3-7: Experimental setup of the UNI switch with the CW assist light at 40 Gbit/s operation.

3.4.2 Experimental results

The eye diagrams of the back-to-back signal at 1545 nm, the switched signal at 1555 nm without (case A) and with (case B) assist light are shown in Fig. 3-8. The switched signal without the assist light was impaired by the pattern effect on the mark level as observed in the case B as shown in Fig. 3-8. The impairment of the mark level was suppressed due to the reduction of the pattern effect

by the CW assist light in the case C as shown in Fig. 3-8. The quality of each signal is quantitatively assessed by BER measurement. The results of BER measurements are also shown in Fig. 3-8.

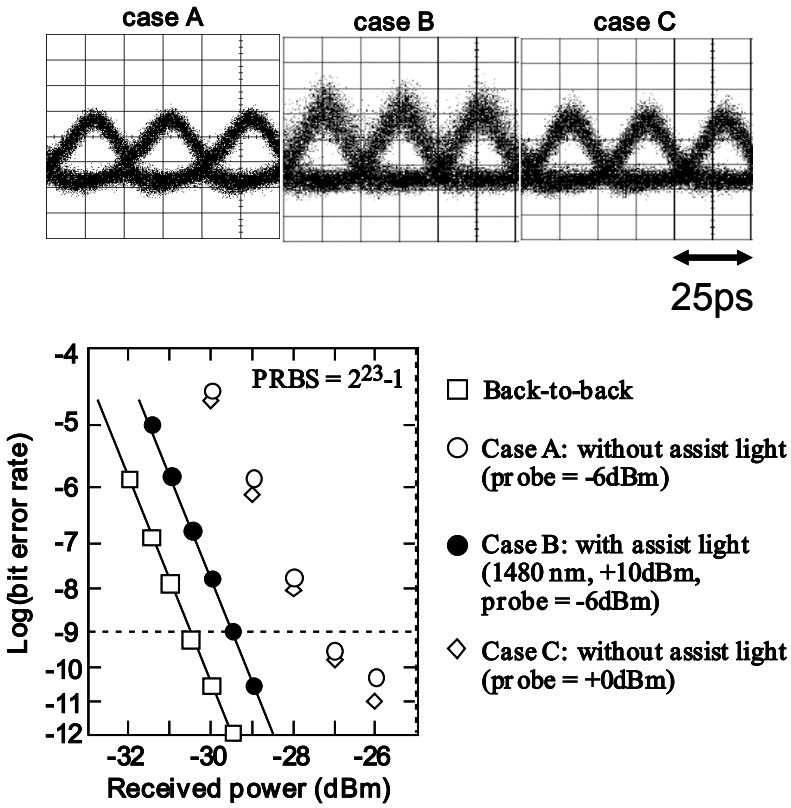

Figure 3-8: The eye diagrams of the 40 Gbit/s PRBS signals that are the input signal (case A), the output signal without assist light (case B) and the output signal with assist light (case C). The lower view graph is the measured BER results that are the back-to-back and the case A, B and C as a function of the received power.

The power penalty of 3.3 dB in case A (without assist light), which was defined at BER = 10^{-9} with reference to the back-to-back. In case B (with assist light), the power penalty was improved as small as 1.0 dB. In addition, no error floor was observed in case B, whereas a slight error floor (BER≈10^{-11}) was observed in case A. On the other hand, increasing the probe power instead of using the assist light, the improvement in power penalty from that of the case A was only 0.3 dB at the optimum probe light power of +0 dBm because the required control pulse power increased.

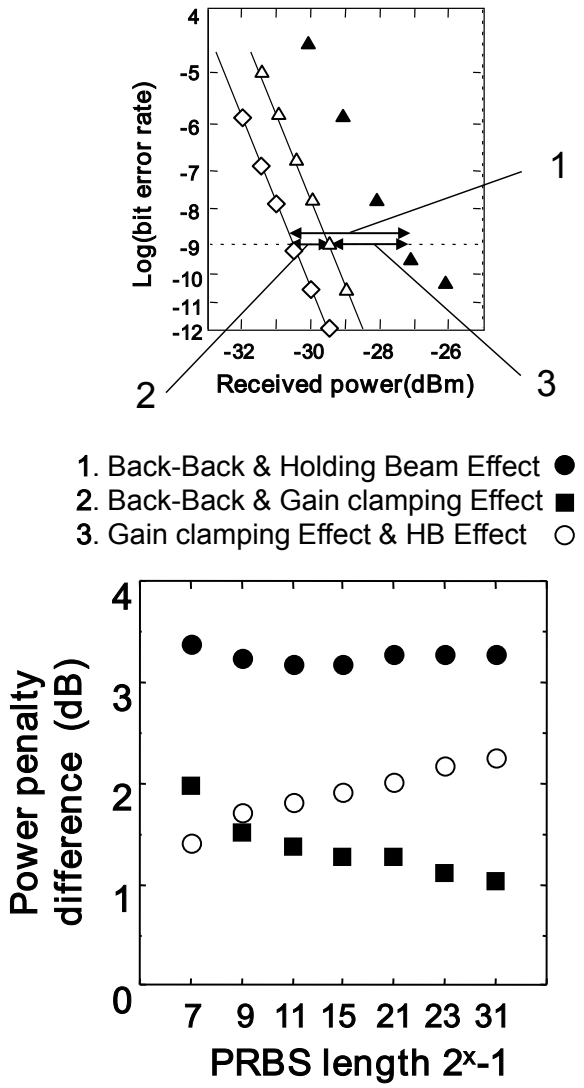

Figure 3-9: The power penalty difference as a function of the PRBS length.

Next, the BER's with various PRBS lengths were measured. Figure 3-9 shows the improvement in the power penalty achieved by the assist light as a function of the PRBS length. The upper figure is an example of BER measurement as a function of received power in the case that the PRBS of 2^{31}-1. The white diamonds, the white triangles and the black triangles indicate

measurement results of the back-to-back, the gain clamping effect and the holding beam effect, respectively. Each power penalty difference, which was indicated the number "1" or "2", was calculated by the two values of the received power when the BER equaled to $1x10^{-9}$. Furthermore, the difference between the two power penalty differences was calculated. The improvement was enhanced from 1.4 dB to 2.3 dB by increasing the PRBS length from 2^7-1 to 2^{31}-1 as shown in the lower figure of Fig. 3-9. This result also proves that the assist light effectively suppressed the pattern effect of the UNI. These results are promising that this proposed scheme can be utilized for the ultra-high-speed all-optical regenerative wavelength conversion, which is corresponding to the all-optical 3R regeneration at the repetition rate of 40 Gbit/s.

3.5 All-Optical wavelength conversion at 80 Gbit/s

In the previous section, 40 Gbit/s all-optical regenerative wavelength conversion was successfully demonstrated by the BER measurements. To evaluate the feasibility of the proposed scheme for the ultra high-speed optical communication system, the bit rate of the optical data signal fed into the UNI switch should be sped up. There are several discussions with regard to the next bit rate beyond 40 Gbit/s data stream, which is correctly expressed as 39.81312 Gbit/s as well as OC-768/STM-256 in the SONET/SDH networks. It is suitable for the SONET/SDH network to define the higher bit rate that is corresponding to the twice or four times of the OC-768/STM-256. On the other hand, 10 Gbit/s Ethernet network will need to have the ten times larger than the 10 Gbit/s interface, which means 100 Gbit/s. In this section, the all-optical wavelength conversion is evaluated at 80 Gbit/s for the initial evaluation of the next-generation ultra high-speed optical communication system.

3.5.1 Experimental setup

Figure 3-10 shows the experimental setup and the condition of the evaluation. The UNI switch consists of an SOA and two HiBi media as a polarization discriminated interferometer. The PMD of the HiBi media was corresponding to 6.25 ps. The injection current of the SOA was set at 400 mA, at which the small signal gain was about 17 dB with the polarization dependency less than 1 dB for 1555 nm wavelength. The transparent assist light of +10 dBm power at 1480 nm, which reduces a gain recovery time of the SOA, was induced via an optical circulator from the backside of the SOA. Pulse width of the 80 Gbit/s input data signal and 80 GHz clock pulses were 5 ps and 1.5 ps, respectively. Both the optical pulses were generated by 10 Gbit/s based OTDM technique. The other configuration was same as the previous experiment.

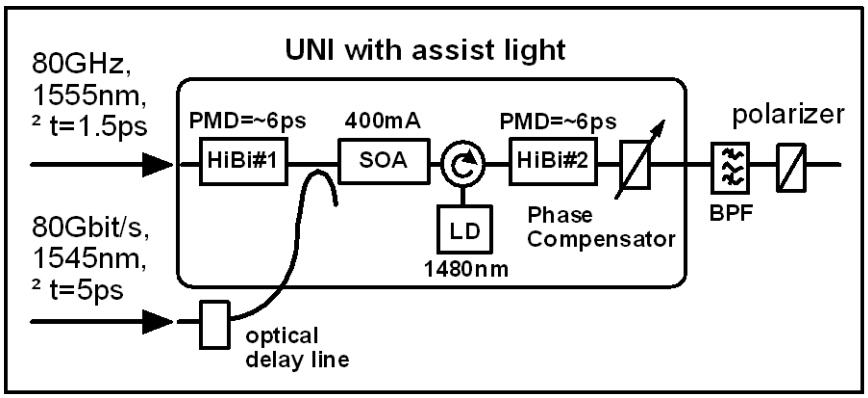

Figure 3-10: Experimental setup for evaluation of the 80 Gbit/s wavelength conversion by UNI switch.

The 80 Gbit/s data stream was modulated in PRBS 2^{31}-1 in the 10 Gbit/s repetition rate. It was difficult to generate the optical data signals and the optical clock pulse with accurate time interval of 12.5 ps for the 80 Gbit/s repetition rate, because the there was not measurement

equipment that could observe the 80 Gbit/s signal directly. When the OTDM technique is utilized to generate the higher bit rate, the RF spectrum analyzer and the photo-diode are used for evaluating the accuracy of the time interval. When the clock pulse at 20 GHz is generated by 10 GHz based OTDM technique, there is no frequency component of 10 GHz in the accurate 20 GHz clock pulse. Therefore, the OTDM equipment can be tuned to generate the accurate doubled bit rate by monitoring the suppression of the frequency component of the base frequency. By using this technique, the 80 GHz optical clock pulse and the 80 Gbit/s data stream were accurately generated for the experimental evaluation.

3.5.2 Experimental results

The eye diagrams of input and output signals at 80 Gbit/s are shown in Fig. 3-11.

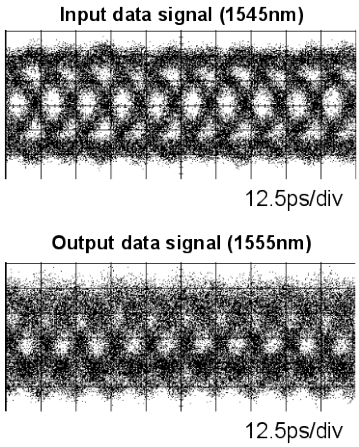

Figure 3-11: Eye diagrams of the input and the output signal of the 80 Gbit/s data stream.

The optical powers of the 80 Gbit/s data stream and the 80 GHz clock pulses fed into the SOA were 0 dBm and -5 dBm, respectively. Small switching power of 0 dBm for 80 Gbit/s wavelength conversion was realized by the transparent assist light. The operation logic of this

wavelength conversion was inversion from mark to space and vice versa, namely bit-inverted conversion.

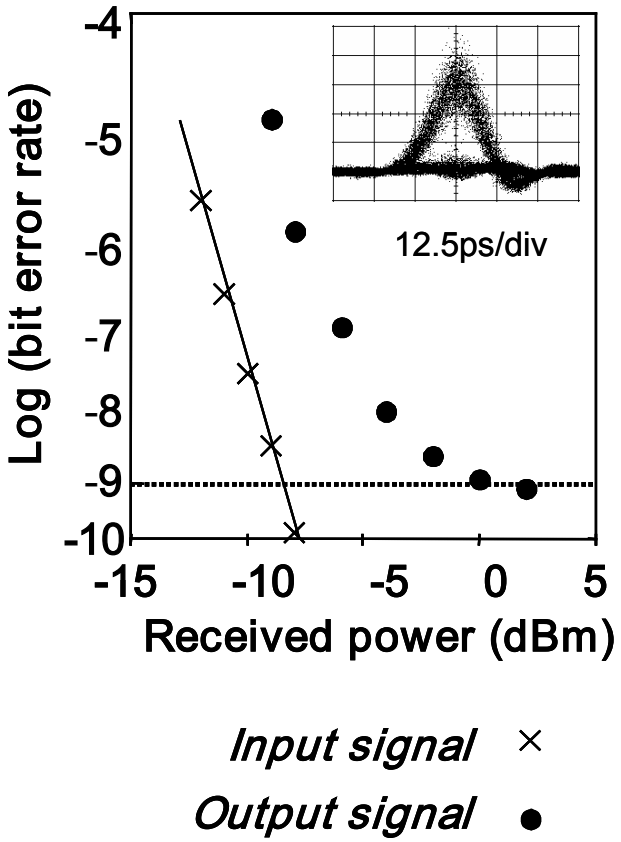

Figure 3-12: Measured BER result of the 80 Gbit/s wavelength conversion. The inset shows the 10 Gbit/s data signal demultiplexed by the EAM based conventional demultiplexing scheme.

The BER measurement was carried out at 10 Gbit/s after demultiplexing by two-cascaded EAMs that were driven at 20 GHz and 10 GHz. In Fig. 3-12, BER is plotted as a function of the received power. The inset shows the eye diagram of converted signal after demultiplexing 10 Gbit/s. Wavelength conversion with the error free operation was obtained. However, the power penalty of 8 dB compared to input signal was confirmed at the BER equals to 10^{-9} with error floor. The conversion penalty would be due to the remaining pattern effect in the SOA. The spread distribution on mark level was confirmed in the demultiplexed 10 Gbit/s signal as shown in the inset of Fig. 3-12.

3.6 Conclusion

In this chapter, a new technique to shorten the gain recovery time of an SOA by using the external CW light was proposed. Although the gain recovery time was almost same compared with the holding beam effect that was previous general technique, the advantage that the input power of the optical data signal became small was clarified by the experimental evaluation. The SOA gain recovery time of 40 ps was obtained utilizing the assist light with gain depletion as small as –1 dB. The operation principle of the UNI switch that was recognized as the polarization discrimination switch was described with regard to both the off state and the on state. To investigate the feasibility of this methodology, the all-optical regenerative wavelength conversion was demonstrated at the repetition rate of 40 Gbit/s as well as 80 Gbit/s. The reduction of the pattern effect of the UNI at 40 Gbps by the transparent assist light was successfully demonstrated while keeping the control pulse power as low as –3 dBm. The receiver sensitivity improvement of 2.3 dB was confirmed at BER = 10^{-9}. Moreover, the improvement in the power penalty was enhanced from 1.4 dB to 2.3 dB by increasing the PRBS length from 2^{7}-1 to 2^{31}-1.

The 80 Gbit/s wavelength conversion by the UNI switch was also demonstrated by using the CW assist light. The BER characteristic was measured at 10 Gbit/s after demultiplexing. Although the power penalty of 8 dB with error floor was confirmed in 80 Gbit/s wavelength conversion, error-free operation was obtained. The elimination of the conversion penalty would be possible by optimization of the SOA. It can be said that the SOA-UNI switch with injection of the transparent assist light is able to be an attractive method for an ultra high-speed all-optical signal processing.

CHAPTER 4 REGENERATION CAPABILITY OF ALL-OPTICAL 3R REGENERATOR AT 40 Gbit/s RETURN-TO-ZERO SIGNAL

4.1 Introduction

Most of the all-optical 3R regeneration schemes are experimentally investigated in the test bed of laboratories. It is necessary to evaluate the working principle and the potential of the new idea in laboratories for initial stage of the investigation. However, the evaluation condition or the numerical calculation may not be corresponding to the actual deployment. Therefore, it is important to verify their tolerances against various transmission impairments attempting to put them in the real fields. On the other hand, it is essential for the all-optical 3R regeneration device to make known the distinct regeneration capability of the proposed devices.

In this chapter, the operation margin of the all-optical 3R regenerator that is UNI switch with the CW assist light and the operation margin of the UNI switch against the intentionally impaired optical data signal are experimentally investigated at 40 Gbit/s. In section 5.2, the operation margin for the condition is experimentally evaluated in terms of the tolerance against the relative time position between the input data and the clock, the input power, and pulse widths of both input-data and clock. The tolerances are evaluated by the BER penalties of the regenerated signal with respect to the back-to-back (B-B) measurement. In the experimental evaluation of the all-optical 3R regeneration, it is essential to determine the optimal operation condition by monitoring the optical properties. In the same section, the regeneration schemes that are the bit inversion conversion and the bit non-inversion one are described as well as the methodology for determination of the optimal operation

condition by using an optical power meter. In section 5.3, the regeneration capability of an all-optical 3R regenerator placed just in front of the receiver is experimentally investigated by using simulated optical signal impairment due to both amplitude noise and timing jitter. The improvement in the minimum attainable BER that corresponds to the Q-factor and the broadening of the threshold-voltage window are described. The timing jitter reduction resulting in Q-factor improvement is also demonstrated.

4.2 Operation margin of the all-optical 3R regenerator

In this section, the operation margin of the UNI switch is investigated. Before the experimental evaluation, the Pros. and Cons. of the regeneration scheme with regard to the bit inversion and the bit non-inversion operation are expressed. Figure 4-1 shows the typical relative output optical power of the UNI switch as a function of the input average power. The interferometric switch shows the cyclic I/O characteristics both in the bit inverted regeneration and the bit noninverted one. For improvement of the regeneration performance, the bit inverted regeneration is better than the bit noninverted scheme that is simply expressed in the lower diagram of Fig. 4-1. By utilizing the bit-inverted regeneration, a mark level with fluctuated amplitude and a space level with an ASE noise can be converted to a clear space level and a stable mark level, respectively. Comparable extinction ratios were achieved for both modes. Since the relatively flat response was obtained in low input power region, fluctuation (*i.e.*, noise) in the regenerated mark level was expected to be reduced in the bit-inverted mode. In the following experiments, the regeneration was conducted in the bit-inverted mode.

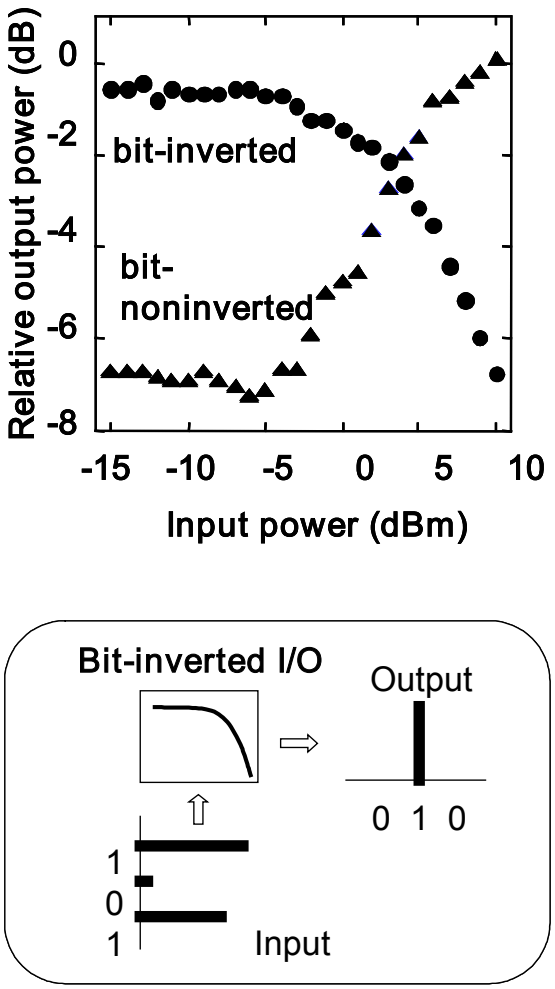

Figure 4-1: Measured I/O characteristics of the UNI switch and the schematic diagram of the transfer image of the bit-inverted conversion.

It is very important that the fluctuation of an input signal is not transcribed to the new signal in the all-optical 3R regeneration. Figure 4-2 shows the two I/O characteristics that were measured by the optical power meter (OPM) indicated by the open circles and the optical spectrum analyzer (OSA) indicated by the open triangles as well as the eye diagrams of the input and the converted optical signal around the optimal operation condition of the UNI switch.

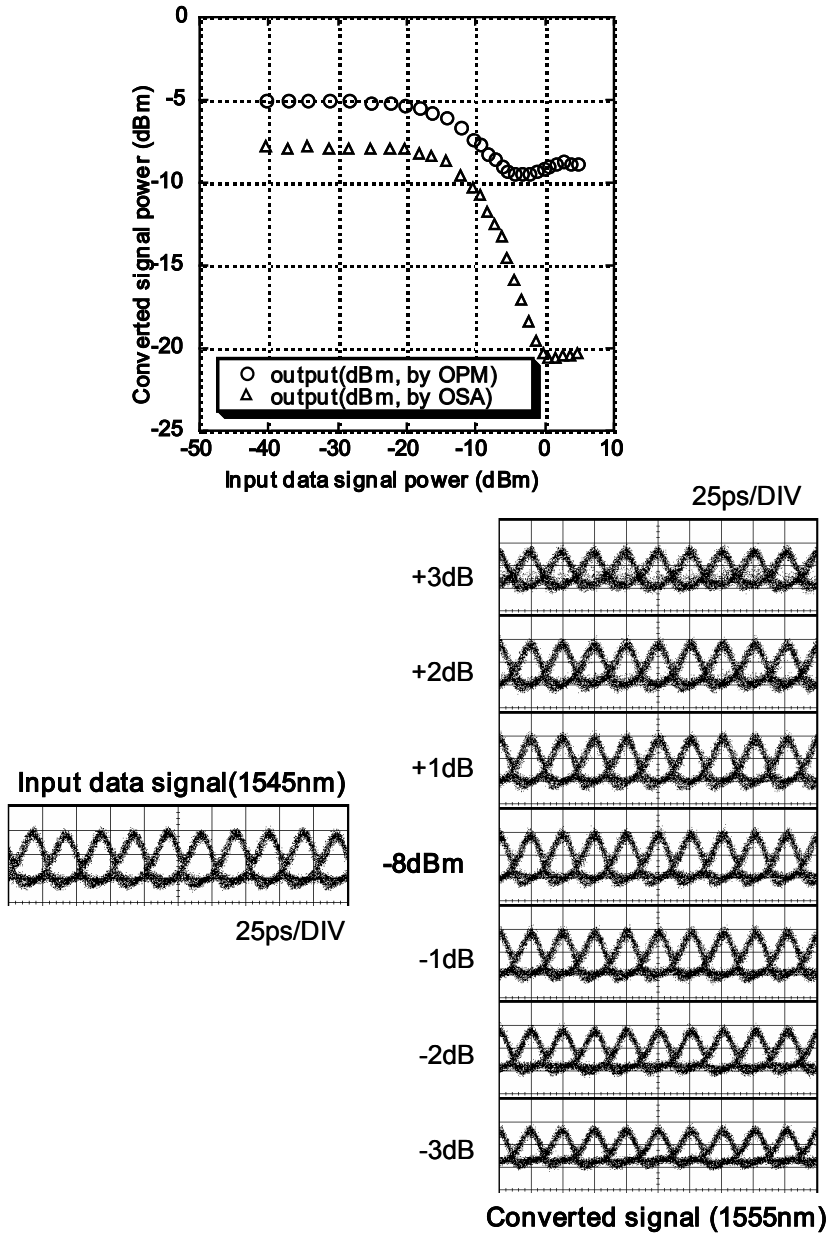

Figure 4-2: I/O characteristics of the bit-inverted conversion. The eye diagrams are the input and the output signal corresponding to the input optical power.

The optimal operation condition can be determined to be around -8 dBm or smaller power by assessment of the eye diagrams. Although the input optical power for the optimal operation

condition can be supposed by the I/O characteristic measured by the OPM, the optimal operation condition is not able be determined by the I/O characteristic measured by the OSA. The difference between the OPM measurement and the OSA one has a cause in lack of the information of modulation sideband.

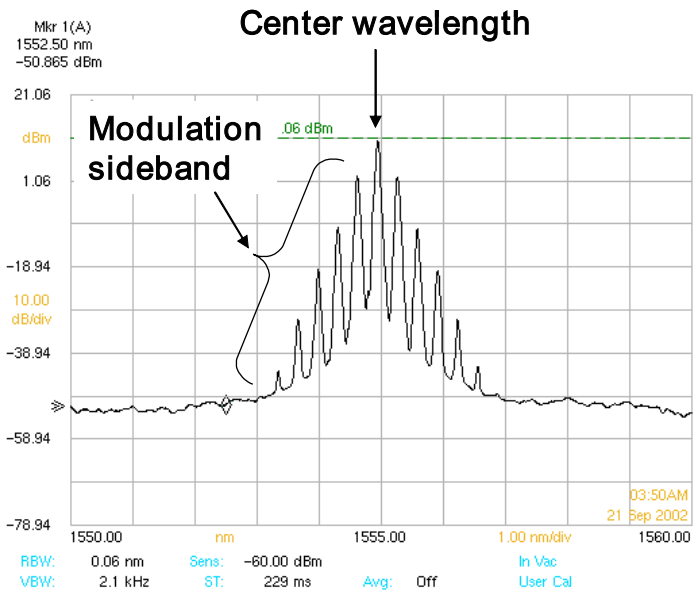

Figure 4-3: The optical spectra of the 40 Gbit/s signal at 1555 nm.

Figure 4-3 shows the optical spectra of 40 Gbit/s signal measured by the OSA of 0.06-nm resolution. When the OSA is used for the measurement, the measured optical power is determined by the peak power of the center wavelength of the signal. On the other hand, the measurement by utilizing the OPM is including the amount of the optical power of the modulation sideband. Consequently, the accurate evaluation for the optimal operation condition of the optical 3R regenerator with cyclic transfer function should be carried out by using the OPM. When the all-optical signal processing and the photonic cross connect are deployed in the network, the electric

performance monitoring, such as the B1/B2 byte in SONET/SDH header or the packet counter in the Ethernet interface, is not available due to the transparency for the optical signal. Therefore, it is essential for the all-optical networks to clarify the correlation between the actual performance and the monitored information as well as the establishment of the monitoring methodology. The following sections describe the operation margin of the all-optical 3R regenerator.

4.2.1 Experimental setup

The experimental setup is schematically shown in Fig. 4-4. The UNI switch was comprised of two HiBi media, a bulk-type InGaAsP-based SOA (800 μm long), a Babinet-Soleil phase compensator, an optical band pass filter and a polarizer. The transparent assist light at 1455 nm, which reduced the gain recovery time of the SOA, was injected from backside of the SOA. The clock pulse at 1555 nm having the pulse width in the range from 5 ps to 10 ps was directly generated by an EAM at 40 GHz.

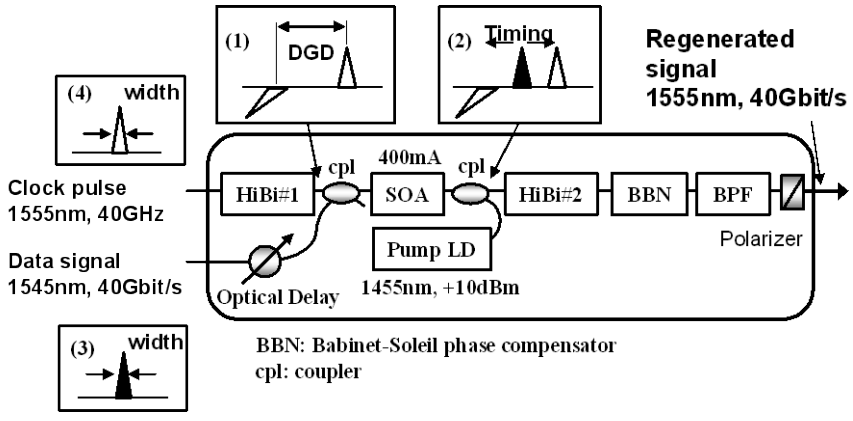

(1) Differential group delay (DGD) of HiBi media
(2) Relative position among the data signal and the clock pulses
(3) Pulse width of data signal
(4) Pulse width of clock pulse

Figure 4-4: Experimental setup for the operation margin and the evaluated articles.

The data signal at 1545 nm was generated by a fiber ring mode-locked laser for pulse width of 6 ps or by another EAM for pulse width of 15 ps. The optical time division multiplexing technique was used to make the 40 Gbit/s signal after coding at 10 Gbit/s with PRBS 2^{31}-1 in all the cases. As for 10Gbit/s-based BER measurement, post-amplified demultiplexer consisting of an EAM and an EDFA was used to demultiplex 40Gbit/s signal into 10Gbit/s. The tolerance parameters examined in this evaluation were illustrated and denoted in Fig. 4-4. The DGD of the HiBi medium, the relative timing position of the input data signal between two split clock pulses, the pulse width of the data signal and the clock pulse were configured with several different conditions in this evaluation.

4.2.2 Tolerance evaluation of the two DGDs of HiBi medium

The tolerances against the input power variance of data signal (6 ps) in respect to the different time window of the split clock pulses (5 ps), which was determined by the differential group delay (DGD) of the HiBi, were plotted in Fig. 4-5(a).

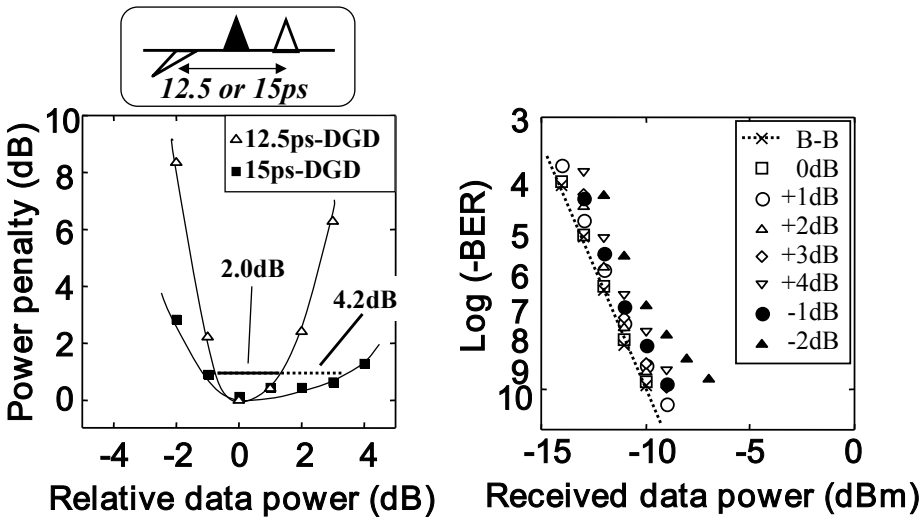

Figure 4-5: (a) Measured power penalty against the variance of input power. The pulse widths of the data and the clock were 6 ps and 5 ps, respectively. (b) Measured BER results with the input optical power variation as a function of the received power. The pulse widths of the data and the clock, and the DGD value were 6 ps, 5 ps and 15 ps, respectively.

No measurable power penalties on the regenerated signals were confirmed for both DGDs (12.5ps, 15ps) at the optimized input power. However, the tolerance against the input power deviation, which is defined that the increase of the power penalty was within 1 dB from the optimum condition, was 4.2 dB for the 15-ps DGD that was wider than that for 12.5-ps DGD. Because the cross phase modulation (XPM) in the SOA is exponentially recovered to the initial state, the amount of the XPM is less sensitive when time difference between the data pulse and the trailing clock pulse is apart. An increase margin of 2.2 dB might be attributed to the expansion of the split time window of the clock pulses. Hereafter, the condition set of 6 ps data signal, 5 ps clock pulse and 15-ps DGD is defined as "the reference condition". Figure 4-5(b) shows the BER measurement results of the reference condition corresponding to the result of Fig. 4-5(a). There is no error floor in the data at the optimum power, although the data under the power deviated by -2 dB from the optimum condition showed slight error floors.

4.2.3 Operation margin for the timing position of data signal

On the reference condition, the tolerance for the relative timing of data pulse was investigated by the power penalty with respect to the B-B as shown in Fig. 4-6(a). The 1dB margin of the relative timing of the data was confirmed to be 10 ps, which was as wide as two thirds of split time window of 15 ps. The best position of the data signal was just at the middle of the split clock pulses. Basically the relative timing position of the input data signal for the orthogonally split clock pulses is not changed drastically after the optical delay line is configured. The accurate clock that is extracted from the input data signal generates the optical clock pulse. In other words, the timing phase of the optical clock pulse is governed by the timing of the data signal. Therefore, the operation margin of 10 ps inside the 15-ps DGD is supposed to be large enough for the actual deployment.

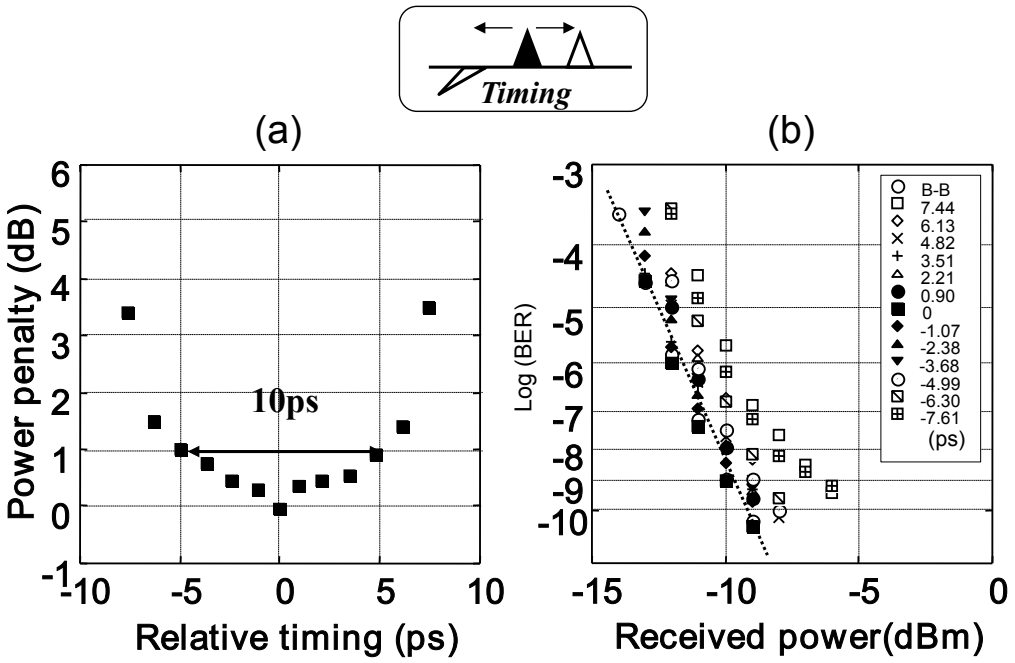

Figure 4-6: (a) Power penalty as a function of the relative timing of the input optical data signal. (b) BER results that are corresponding to the each point of the left side viewgraph as a function of the received power. The pulse widths of the data and the clock, and the DGD value were 6 ps, 5 ps and 15 ps, respectively.

Figure 4-6(b) shows the BER measurement results of the reference condition corresponding to the result of Fig. 4-6(a). There were error floors in the data that were more than +/- 7 ps apart from the optimum point. It seems that the correlation of the data signal and the split clock pulses strongly degrade the regeneration performance.

4.2.4 Operation margin for the DGD parameter of UNI switch

The impact of the pulse width against the regeneration performance was evaluated by expanding the pulse width of the data signal that was changed to 15 ps that was 2.5 times wider than the reference condition of 6 ps. The pulse width widening is a regular problem in the actual transmission line due to the chromatic dispersion of an optical fiber. The pulse width of 15 ps was not adequate for 40 Gbit/s repetition rate since the time interval of the 40 Gbit/s is 25 ps. Therefore, the pedestal of the optical signal of 15 ps might be overlapped each other in the case of continuous "1" signal. Moreover, the input optical data signal is overlapped with the split clock pulses since the

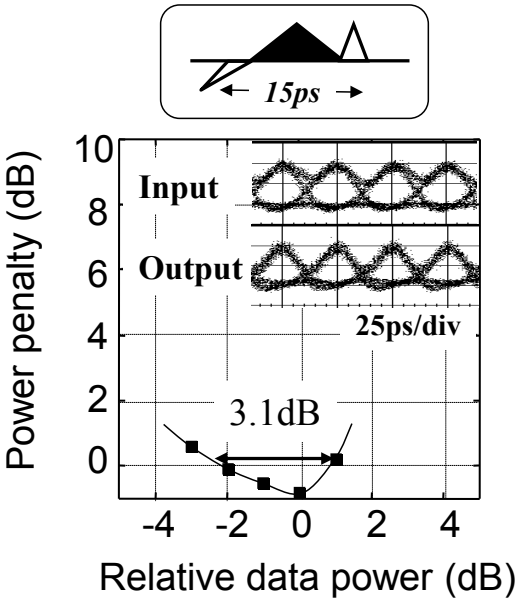

Figure 4-7: Power penalty of the output signal of the UNI switch for the power variance of the input data signal. The pulse widths of the data and clock were 15 ps and 5 ps, respectively.

pulse width of 15 ps is corresponding to the DGD of the HiBi media. The inset eye diagrams in Fig. 4-7 were the input and the output signal that operated at the optimal condition. The measured tolerance for the power variance of data signal is shown in Fig. 4-7. The tolerance was evaluated by the power penalty that was the difference of the Q values between the optimal operation and the changed input power. Negative power penalty of -0.9 dB, which meant the improvement of the

receiver sensitivity, was observed at the optimum condition, although the tail of the data signal should be overlapped with the split clock pulses. The input power tolerance of more than 3 dB has been confirmed. This result cannot be directly compared to the reference condition case, because the wider input data signal of 15 ps pulse width might be already degraded by a coherent cross talk when 40 Gbit/s signal was generated by OTDM technique as recognized from the waveform shown in the inset of Fig. 4-7. However, this result proved a high tolerance against the data pulse widening that might be induced by the chromatic dispersion and/or PMD of the optical fibers.

In the former reports, the UNI was operated using a relatively narrow clock pulses, which were a few pico seconds width for 40 Gbit/s, for instance, to avoid overlap among data pulse and split clock pulses. However, clock pulse width should be more flexible to adapt various kinds of transmission systems.

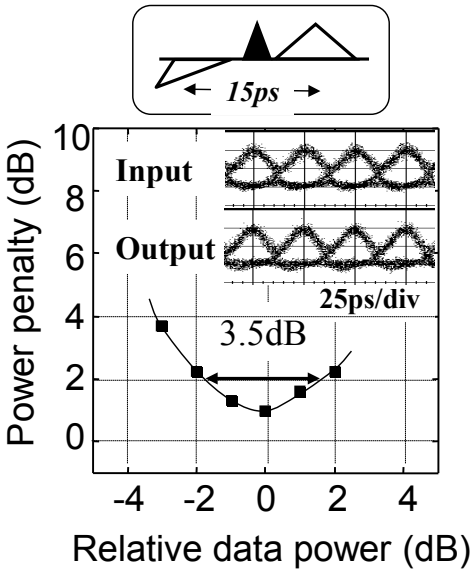

Figure 4-8: Power penalty of the output signal of the UNI switch for the power variance of the input data signal. The pulse widths of the data and clock were 6 ps and 10 ps, respectively.

Figure 4-8 shows the data power tolerance for the case that the clock pulse width was

changed to 10 ps from the reference condition of 5 ps. In this case, the pulse width of the input data signal was 6 ps. The power penalty from back-to-back was still remained as small as 1 dB. The eye diagram of the output signal with clear eye-opening was confirmed as shown in the inset of the Fig. 4-8. The tolerance of the input data signal of 3.5 dB was observed as well as the error-free operation in each condition.

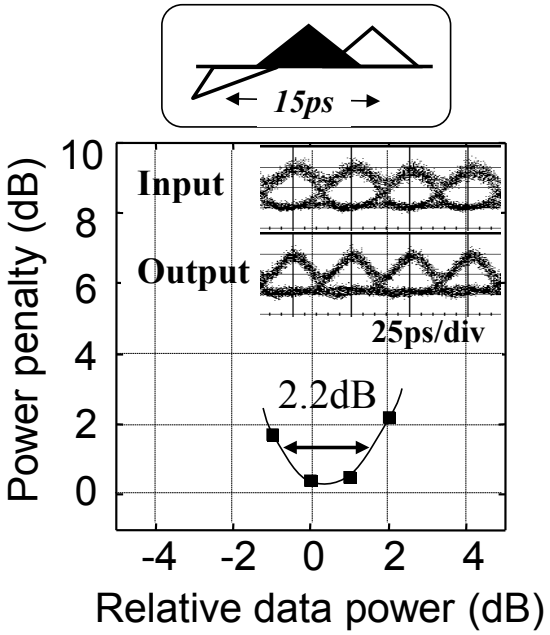

Figure 4-9: Power penalty of the output signal of the UNI switch for the power variance of the input data signal. The pulse widths of the data and clock were 15 ps and 10 ps, respectively.

Based on these two results, regeneration capability in the case of the 15 ps data pulse with 10 ps clock pulse was investigated as shown in Fig. 4-9. As described in the former section, the 15 ps input data signal was degraded to some extent as observed on the mark level in the waveform in the inset. Note that the power penalty at the optimum data power was as small as 0.4 dB in spite of the substantial overlap between the data signal and the split clock pulses. However, the input data power tolerance was somewhat decreased down to 2.2 dB.

4.3 Regeneration capability for impaired signal

In this section, the regeneration capability of the UNI switch as an all-optical 3R regenerator is evaluated by employing the intentionally impaired optical data signal. Figure 4-10 shows the impairment factor of the optical data signal in the EDFA based transmission line. The power fluctuation is occurred by an ASE noise generated from the concatenated EDFAs as well as the time-dependent optical loss in the transmission fibers. The ASE noise gives a fluctuation of timing, which is a timing jitter, along the long distance transmission line. A pulse width widening is mainly caused by the chromatic dispersion of fibers and the chirping of an optical data signals due to the refractive index change of the semiconductor optical device.

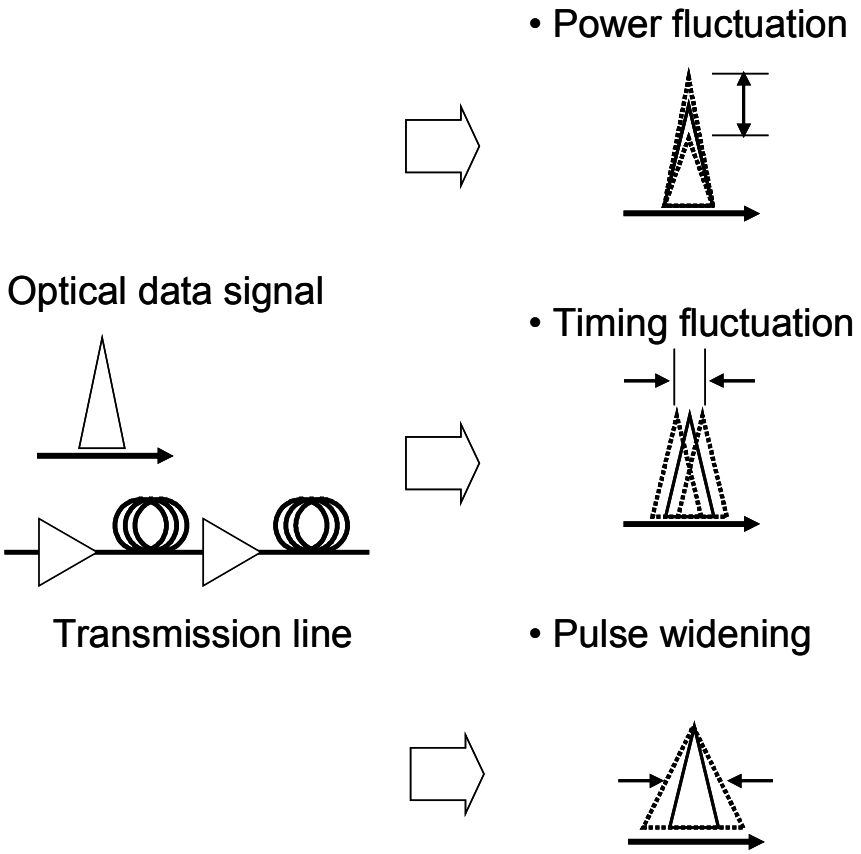

Figure 4-10: Schematic diagram of the impairment factors for the optical data signal in the EDFA based transmission line.

These three impairment factors are the major reason of the performance degradation of the optical signal. The all-optical 3R regenerator is expected to eliminate them by all-optical processing for the ultra high-speed repetition. The following sections describe the experimental evaluation.

4.3.1 Experimental setup

Figure 4-11 schematically shows the experimental setup. The basic configuration was same as the previous setup as shown in Fig. 4-4. The DGD of the two HiBi media was 12.5 ps. Both the 40Gbit/s data signal (1545 nm, 6 ps, -1~+1 dBm) and the 40GHz clock probe pulse (1555 nm, 2 ps, -2 dBm) were generated by 10Gbit/s-based OTDM technique.

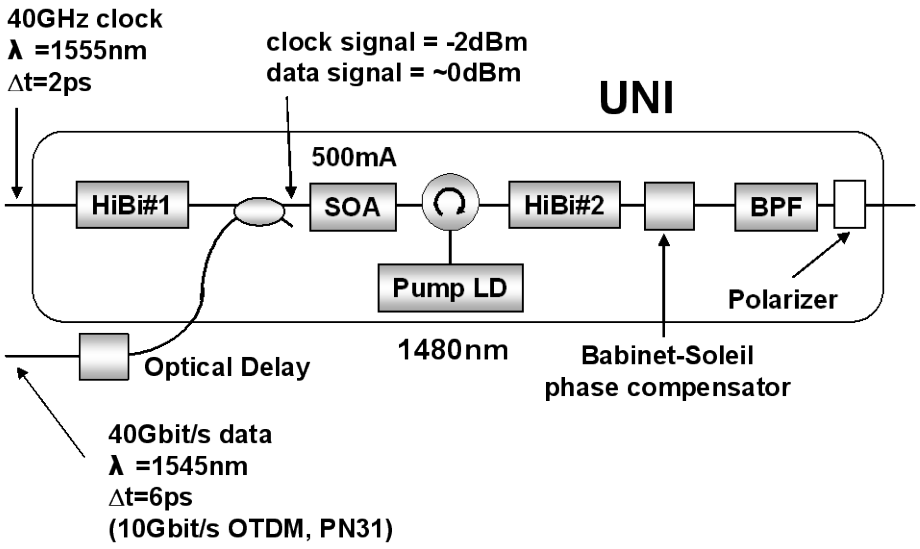

Figure 4-11: Experimental setup of the all-optical 3R regeneration for the intentionally impaired optical signal.

Figure 4-12 also shows the experimental configuration that enables to give the intentional impairment to the optical data signal. A high-power ASE light source was employed to superimpose amplitude noise onto the data signal for making a power fluctuation. The quasi-random timing jitter

was imposed on the data signal using a combination of a polarization scrambler and a polarization maintaining fiber with PMD of 8.5 ps that corresponded to the maximum timing jitter. It enables that the time position of the optical data signal is changed by the polarization of the output signal from the polarization scrambler. The intentionally degraded data signal was fed into the UNI switch via the optical band pass filter and the polarization controller, and the qualities of the original data and the regenerated signals were evaluated by means of eye-diagram observation and BER measurement. As for 10Gbit/s-based BER measurement, post-amplified demultiplexer consisting of an EAM and an EDFA was used to demultiplex 40Gbit/s signal into 10Gbit/s.

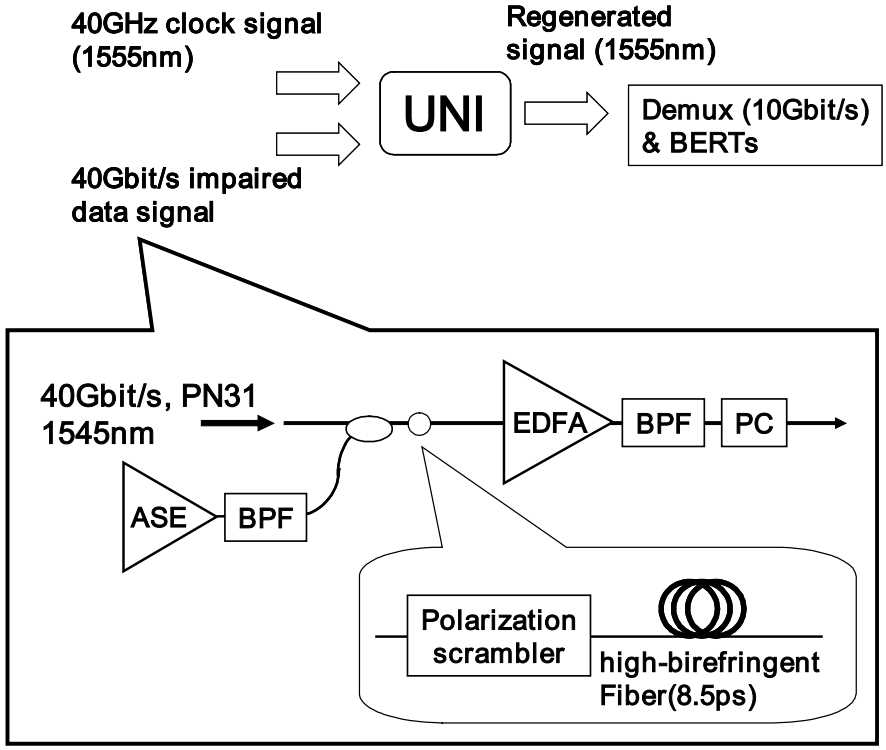

Figure 4-12: Schematic diagram of the configuration for giving the intentional impairment to the optical data signal.

4.3.2 Signal degradation by the amplitude noise

Figure 4-13 shows the amplitude distributions of the data signal degraded by ASE noise and the regenerated signal. The corresponding eye diagrams are shown in the insets. The distributions of both the mark and space levels became narrowed and non-Gaussian distributions after the regeneration owing to the nonlinear transfer function of the all-optical 3R regenerator, which was the bit-inverted conversion, while those of the control signal were Gaussian distributions.

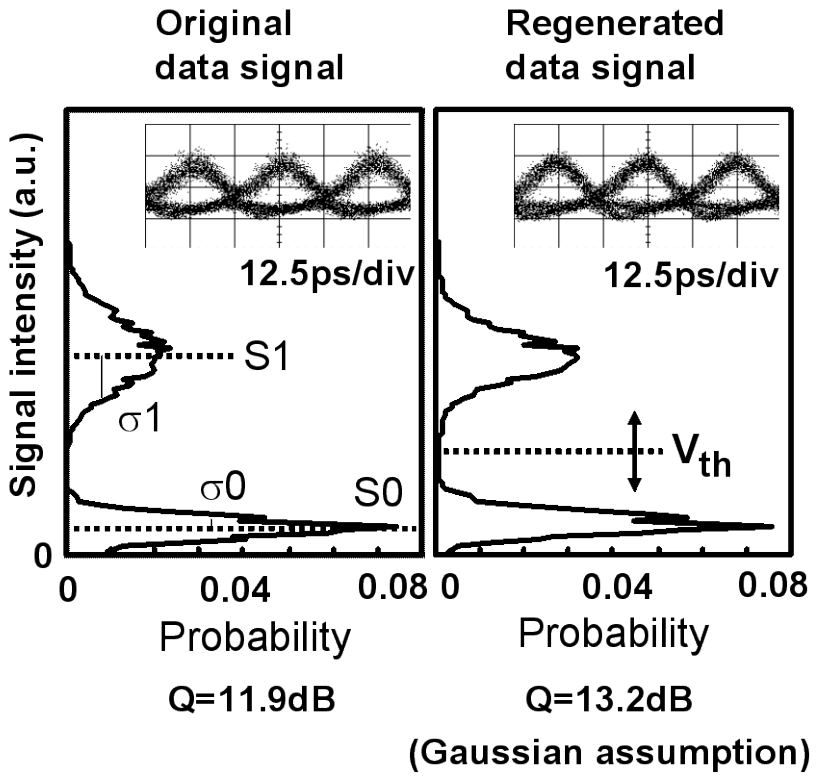

$$^{*}Q = 20\log\left\{\frac{(S1\text{-}S0)}{(\sigma 1+\sigma 0)}\right\}$$

Figure 4-13: Histograms of the signal intensity of the original data signal and the regenerated signal. The Q values of both signal were estimated by the measured factors and the expressed formula.

The Q value of the original and the regenerated signals were estimated by using the measured factors and the formula as shown in Fig. 4-13. The factors that were the mean value and the standard deviation of the histogram of the signals were measured by the electric sampling oscilloscope. The Q value of the original data signal and the assumed Q value of the regenerated signal were 11.9 dB and 13.2 dB, respectively. The improvement of 1.2 dB was obtained by the nonlinear transfer function of the 3R regenerator.

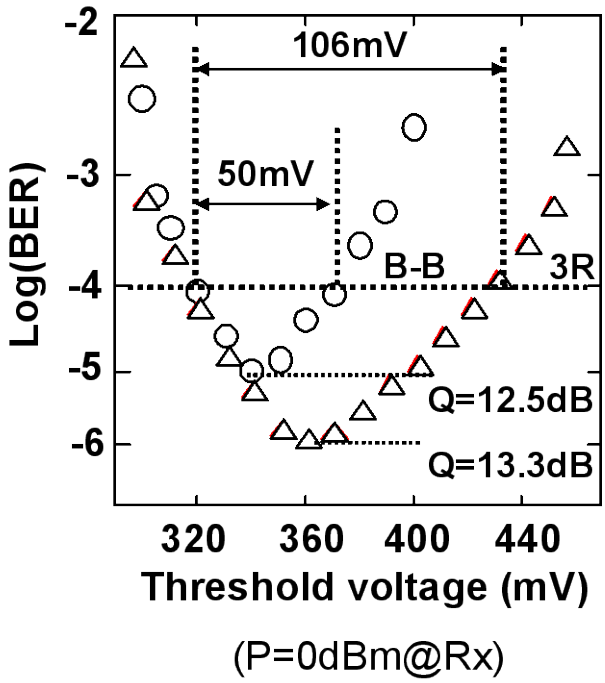

Figure 4-14: Measured BER of the original data signal and the regenerated signal as a function of the threshold voltage of the decision circuit in the reveiver.

Such reshaping function with eye opening effect of the 3R regenerator contributes to the widening of the threshold-voltage window at the receiver, as shown in Figure 4-14. The threshold-voltage window, within which the BER less than 10^{-4} that can be recovered to the BER of 10^{-9} by FEC was achievable, was 2.1 times broadened after the regeneration. The optical signal-to-noise

ratio was estimated to be 8.2 dB for the degraded control signal, and 27 dB for the regenerated signal. These highly tolerable characteristics of the receiver should be beneficial to the receiver to receive a seriously impaired FEC coded signal with little margin.

4.3.3 Timing jitter

The timing jitter reduction capability of the 3R regenerator was assessed separately from its reshaping function by intentionally adding timing jitter within 8.5 ps to the data signal. Figure 4-15 shows the waveforms of the original data signal, the data signal with timing jitter, and the corresponding regenerated signal, respectively. The timing position of the original data signal was changed by the polarization scrambler and the polarization maintaining fiber.

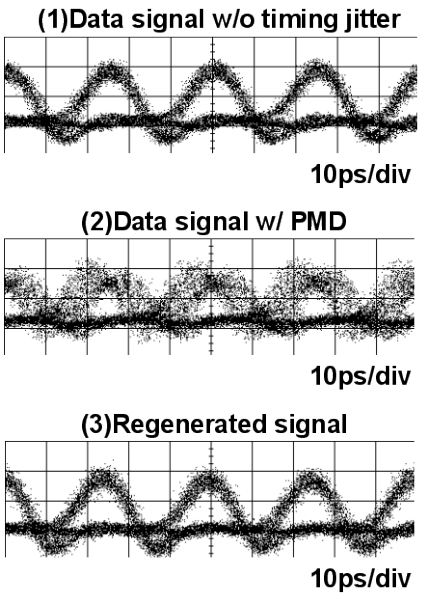

Figure 4-15: Measured waveforms of (1)the original data signal, (2)the data signal with quasi timing jitter of 8.5ps and (3)the regenerated signal by the all-optical 3R regenerator.

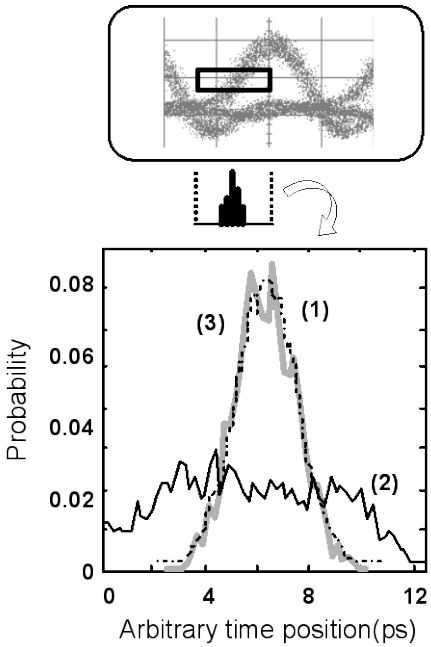

Figure 4-16: Histograms of the rise point of eye diagrams at the half of the mark level height. (1) Original data signal (dashed line) (2) Data signal with emulated timing jitter generated by the combination of a polarization maintain fiber and a polarization scrambler (solid line). (3) Regenerated signal (gray line).

The histogram shown in Fig. 4-16 was taken along the time axis for the rise curve of each waveform at the half of the mark level height. Each histogram from indicated by the dashed line (1), the solid line (2) and the gray line (3) are corresponding to the measured waveforms shown in Fig. 4-15. The standard deviation of 1.25 ps derived from the histogram of the regenerated pulse coincided with that of the original data signal, while that of the data signal with timing jitter was as large as 3.19 ps. Nevertheless, obtained power penalty improvement by the regeneration was as small as 1 dB at BER = 10^{-9}, that may be attributed to that the imposed timing jitter values were not random and/or too small for the 10 Gbit/s-based receiver to respond due to its limited bandwidth.

4.3.4 Amplitude noise and timing jitter

The employed data signal was simultaneously imposed both with moderate ASE noise and quasi-random timing jitter of 8.5 ps, which was generated by the polarization rotator and Hibi medium

whose DGD was 8.5 ps. The OSNR of the degraded control signal was estimated to be 12.4 dB.

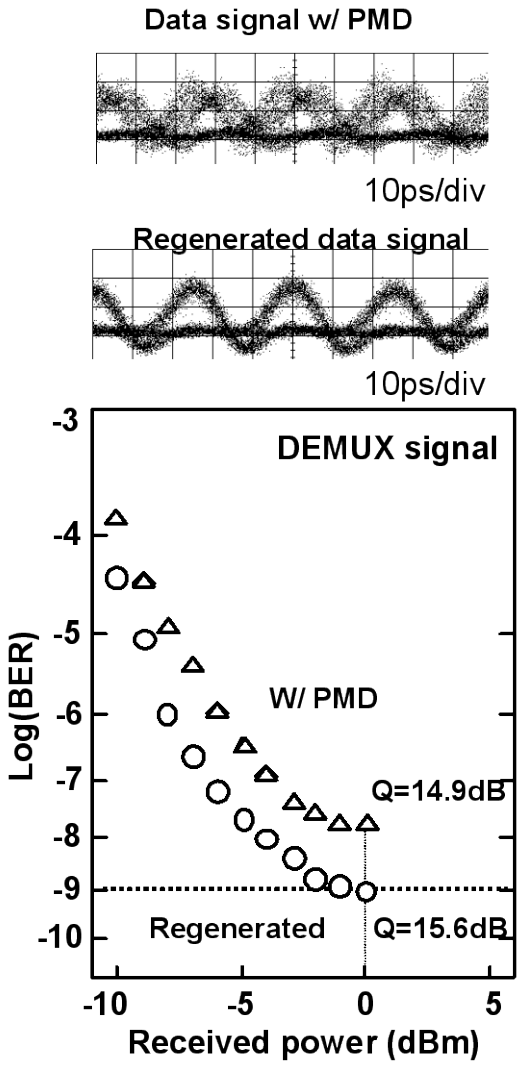

Figure 4-17: Measured BER results of the degraded data signal and the regenerated signal as a function of the received power. The corresponding eye diagrams are shown in the inset.

Figure 4-17 shows the measured BER results with the corresponding eye diagrams in the inset of the figure. The minimum attainable BER of 1.4×10^{-9} (Q-factor of 14.9 dB) for the degraded data signal was improved to BER = 8.5×10^{-10} (Q-factor of 15.6 dB) for the regenerated signal. The improvement of Q-factor by 0.7 dB proves that the all-optical 3R regenerator consisting of UNI switch

can work as a mitigater directly recover of signal impairments of both random amplitude noise and random timing jitter.

4.4 Conclusion

In this section, the advantage of the bit-inverted conversion and the experimental results due to the benefit of the conversion scheme were described. The operation margins of the UNI switch as an all-optical 3R regenerator were experimentally investigated at 40 Gbit/s by changing various parameters, which simulate a practical environment. The input power tolerance of 4.2 dB and the timing tolerance of 10 ps within the power penalty of 1 dB were observed. The optical regeneration with wider clock pulse of 10 ps was confirmed with the 1 dB penalty increase. When the data signal was widened up to 15 ps, the improvement of the receiver sensitivity of 0.9 dB was observed with respect to the degraded input data signal.

Next, the reshaping and retiming capability of the UNI switch were also experimentally evaluated by employing seriously impaired 40Gbit/s data signal. It was confirmed that the reshaping function of the 3R regenerator contributed to broadening of the threshold-voltage window at the receiver by a factor of 2.1. The timing jitter of 8.5 ps imposed on the control pulse was almost completely corrected after the regeneration. Finally, the Q-factor of 14.9 dB for the control pulse, on which both amplitude noise and timing jitter were imposed, was improved to 15.6 dB after the regeneration. These results indicate that the all-optical 3R regenerator is promising as a mitigator for recovering the signal impairments of the high-bit-rate signal placed directly in front of the receiver. In conclusion, UNI can be operated at 40 Gbit/s not only with zero-penalty at the optimum condition, but also with large tolerances against in timing jitter, power variation, and pulse widths changes.

CHAPTER 5 BIT RATE TUNABLE WAVELENGTH CONVERSION

5.1 Introduction

The UNI switch, which is a polarization Mach-Zehnder interferometer using one pair of DGD elements is an attractive candidate for over 100 Gbit/s operation as described in the previous section, because its simple one-SOA configuration results in easy control of the power balance between two optical arms and hence in superior stability. To simplify the configuration further, the UNI switch consisting of an SOA in a circulating configuration with only one DGD element has been reported [133]. However, all the reported UNIs so far have fixed switching gate windows equal to the DGD of the HiBi medium such as a polarization maintaining fiber in the most cases. For an actual deployment of the wavelength conversion device, a bit rate tunable feature is very useful functionality in the optical node or in front of the receiver. The photonic cross connect node for making a wavelength path is needed to change the bit rate of the optical data signal when the same optical path is required to use by several different input port. Moreover, the FEC functionality makes bit rate of the optical data signal to increase due to the redundant bit for the error correction. In addition to the simplifying the configuration of UNI switch, attaching a functionality of the bit rate tunability expands the applicable region of UNI switch in the all-optical networks.

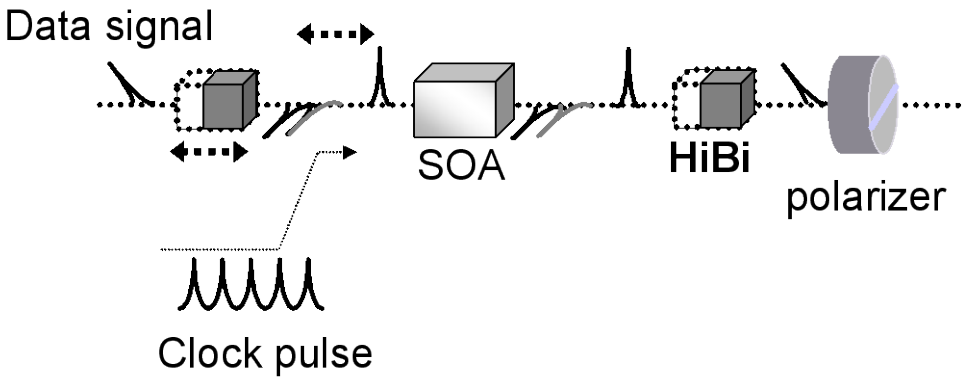

Figure 5-1: The configuration of the UNI switch using two fixed HiBi media.

Figure 5-1 depicts the basic configuration of UNI switch. To realize the bit rate tunable functionality by using UNI switch scheme, two issues have to be considered with regard to the optics in the configuration. The first one is that the quantity of the DGD of the HiBi media should be tunable in terms of the optical property for changing the optical delay of the split optical data pulse. This functionality has to be realized by the pico second order. Another is that the second HiBi has to be also tunable and the DGD should be corresponding to the first DGD of the tunable HiBi to recombine the split optical data pulse. Therefore, the mechanism for splitting and recombining the optical data pulse is ideally desired to be one module that realizes the tunable HiBi device and complete compensation the delay of the pulse.

In this chapter, a novel UNI configuration employing one variable DGD generator to control the switching gate window is proposed. A novel configuration for the bit-rate tunable all-optical regeneration is demonstrated by the combination of the one SOA and the reconfigurable optics with repetition rate from 10 Gbit/s to 80 Gbit/s.

5.2 Switching principle

Figure 5-2 shows the schematic diagram of a reflection type variable DGD generator that consists of a half wave plate (HWP), a polarization beam splitter (PBS) and a pair of movable mirrors.

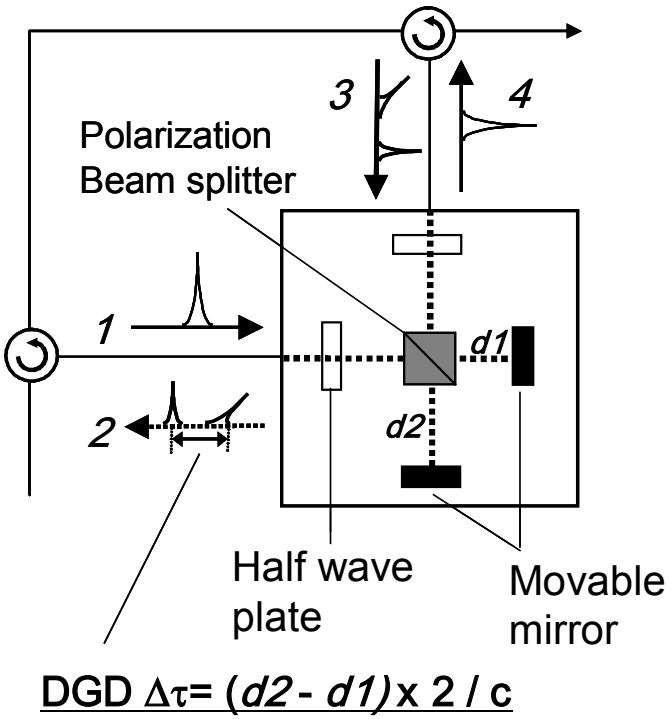

Figure 5-2: Schematic diagram of the tunable DGD generator for the bit rate tunable polarization discriminated switch.

A linearly polarized optical pulse, which is indicated by the number "1" in the fibure, is split into two orthogonally polarized pulses indicated by the number "2" by the difference in optical path lengths from PBS to each movable mirror, and consequently variable DGD of $\Delta\tau$ is generated. This variable DGD generator is equivalent to a birefringent medium with variable length. To recombine the split two pulses for the polarization switching, the split two pulses are fed into the variable DGD generator from another port as indicated by the number "3" in the Fig. 5-2. The leading pulse passes through the PBS and reaches to the movable mirror along the optical path indicated by d1. The trailing pulse is orthogonally reflected by the PBS and reaches to the movable mirror along the optical

path indicated by d2. Consequently, the time difference between the two pulses is eliminated by this operation. Thus, the two split pulses are recombined at the output of the variable DGD generator.

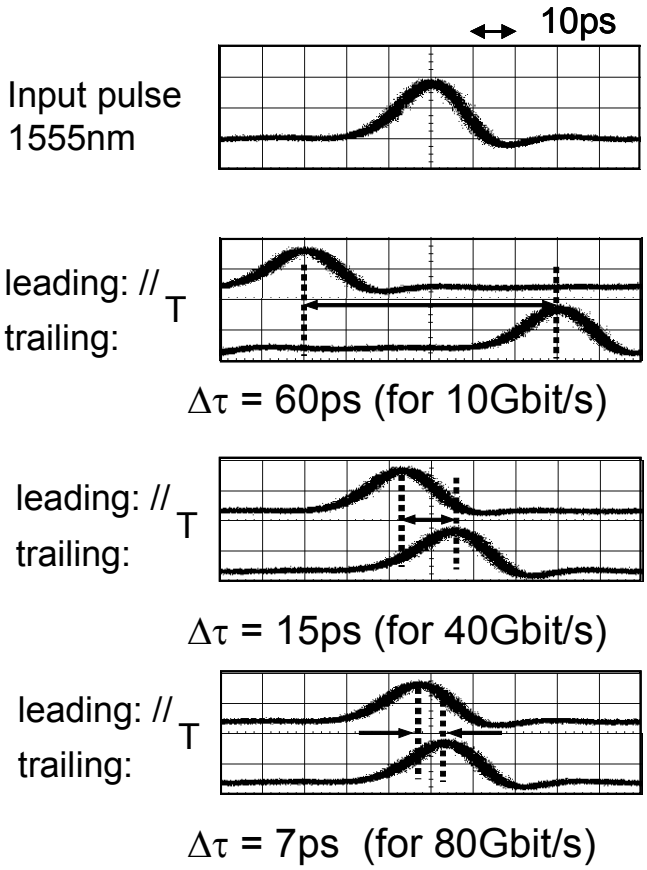

Figure 5-3: Waveforms of the orthogonally polarized pulses split by the variable DGD generator.

The waveforms of the orthogonally polarized pulses split by the variable DGD generator are shown in the Fig. 5-3. These waveforms were measured at the output port of the first optical circulator in the Fig. 5-2. The input pulse was 2 ps wide with 10 GHz repetition rate, which was generated by the fiber ring mode locked laser (FRML). The DGDs could be accurately controlled to be 60 ps, 15 ps and 7 ps by changing the position of the movable mirror, which corresponded to the

optimum switching gate windows (60 % of bit time slot) for 10 Gbit/s, 40 Gbit/s and 80 Gbit/s signals, respectively.

Figure 5-4 shows the picture of the variable DGD generator, which consists of the solid optics. The fiber receptor and the collimation lens were set at the left and the upper side of the picture. The λ/4 plate and the polarization beam splitter were anti-reflection coated by the multi-layered dielectric films. The movable mirrors were high reflection coated by a gold evaporation with the flatness less than λ/10 for 1550 nm range. Under the experimental evaluation, these optics were covered by a box for avoiding an air fluctuation.

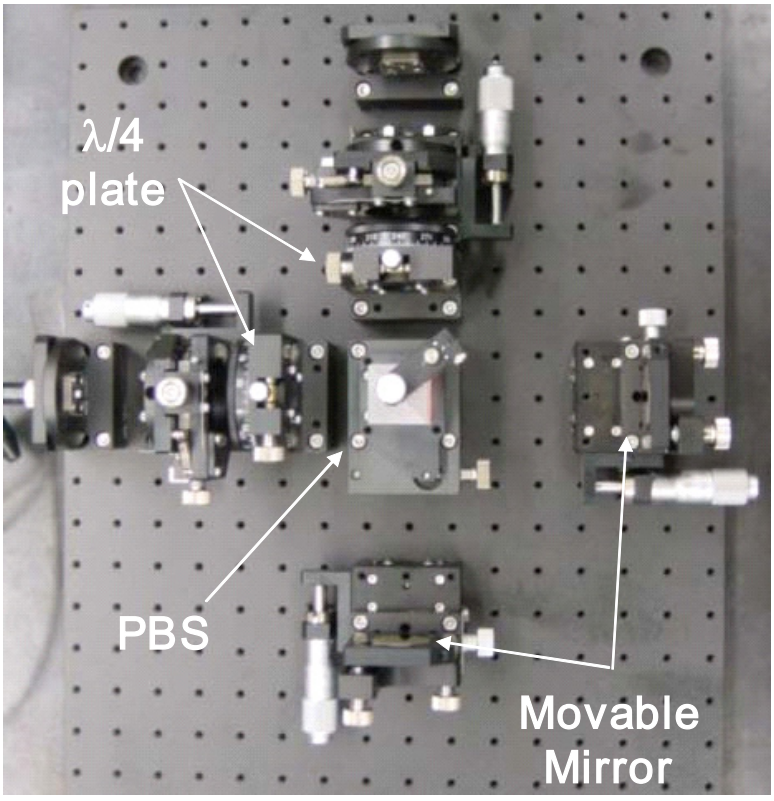

Figure 5-4: Top view of the optics for the variable DGD generator.

5.3 Bit rate tunable wavelength conversion from 10 Gbit/s to 80 Gbit/s

5.3.1 Experimental setup

The schematic experimental setup for the optical regeneration with various bit-rate data is shown in Fig. 5-5.

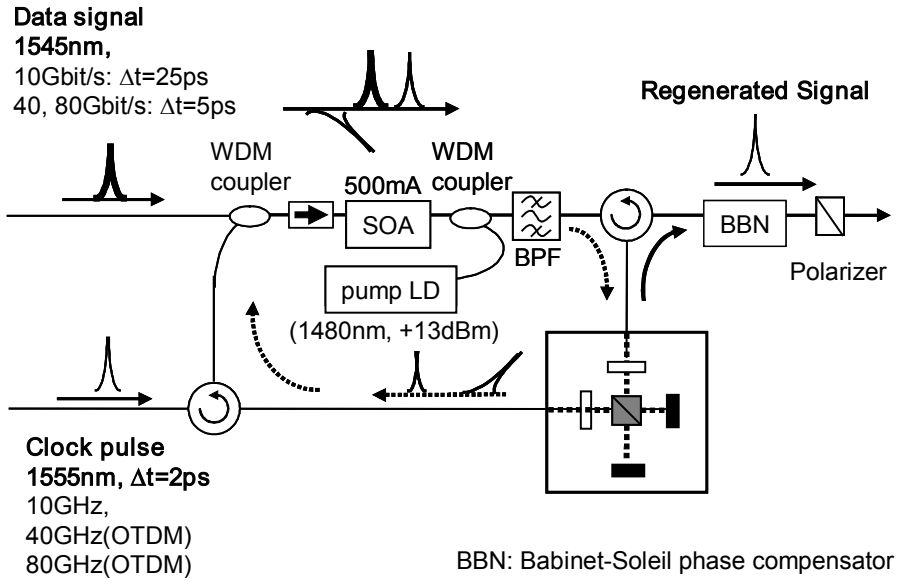

Figure 5-5: Experimental setup of the tunable wavelength conversion using the tunable DGD generator.

This is the UNI configuration consisting of only one variable DGD element instead of two separate fixed DGD elements in the conventional UNI. The clock pulse input into the port A was split into orthogonally polarized pulses by the variable DGD generator when it reflected in the mirrors and output from the port A again. The two-split clock pulses passed through the SOA, and were fed into the port B of the same variable DGD generator. Two-split clock pulses are recombined at the output of the port B, since the DGD between two polarizations given by the variable DGD generator from the port A is canceled. The data signal co-propagated between the leading and the trailing pulse in the

SOA. The relative time positions among the data pulse and the two-split clock pulses can also be individually adjusted by the DGD generator. Consequently, only the trailing pulse was cross-phase modulated by the data signal. When the phase shift reaches to π, the polarization of the recombined pulse is completely switched.

The SOA was the InGaAsP/InP bulk type with a gain peak of 1525 nm at injection current level of 500 mA. The wavelengths of the data signal and the clock pulse were 1545 nm and 1555 nm, respectively. The CW assist light of 1480 nm (+13 dBm) for reducing the gain recovery time of the SOA was injected from backside of the SOA via WDM coupler which allows to combine the wavelength of the 1550 nm range for the data signal and the clock signal and the 1480 nm for the CW light. The clock pulses of 10 GHz, 40 GHz and 80 GHz with 2 ps pulse width were generated by FRML with a 10 GHz repetition rate and multiplexed in optical domain. The clock powers into the SOA were –14 dBm (10 GHz), -12 dBm (40 GHz) and –4 dBm (80 GHz), respectively. The data pulses were generated using a combination of a CW laser and an EAM (25 ps wide) for 10 Gbit/s, and using a FRML (5 ps wide) for 40 and 80 Gbit/s. The data pulses with 10 GHz repetition rate were coded by an LN modulator with PRBS 2^{31}-1 and multiplexed in optical domain. The input powers of the data signals into the SOA were –3 dBm (10 Gbit/s), 0 dBm (40 Gbit/s) and +4 dBm (80 Gbit/s), respectively.

5.3.2 Experimental results

Figure 5-6 shows the eye-diagrams of the input (1545nm) and regenerated output (1555nm) data signals of 10 Gbit/s, 40 Gbit/s and 80 Gbit/s. Clear eye-openings were obtained in 10 – 80 Gbit/s regenerated data signals, although a slight mark level fluctuation was observed due to the word-pattern effect on the eye diagram of the 80 Gbit/s.

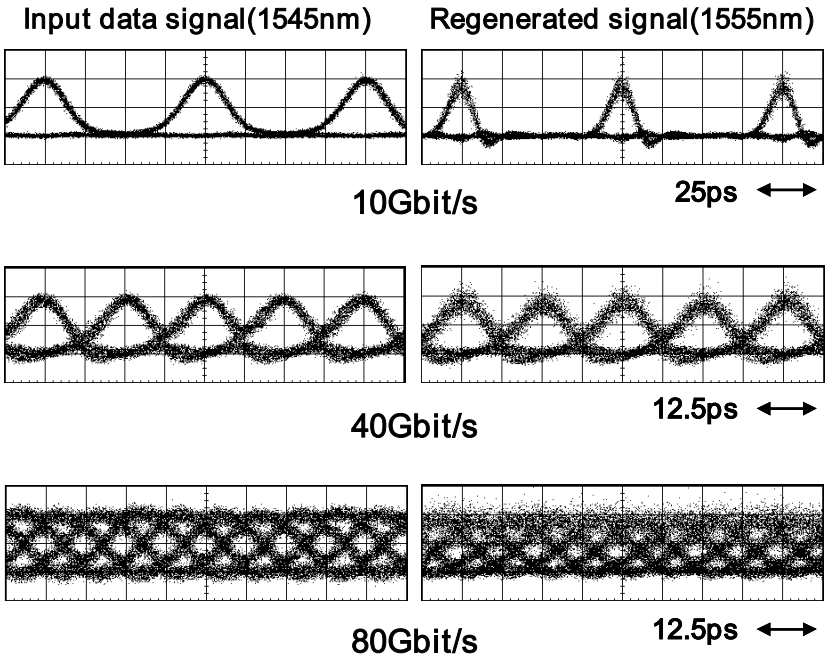

Figure 5-6: Eye diagrams of the input/output signal of the wavelength conversion.

Figure 5-7 shows the BER measurement results for 10, 40 and 80 Gbit/s regenerated signals after demultiplexing to 10 Gbit/s. EA modulator-based demultiplexing method was employed for 40 Gbit/s (40 Gbit/s to 10 Gbit/s) and 80 Gbit/s (80 Gbit/s to 20 Gbit/s, 20 Gbit/s to 10 Gbit/s) regenerated data signals as well as for the input data signal. The power penalties at BER equaled to 10^{-9} for 10 Gbit/s, 40 Gbit/s and 80 Gbit/s were 0.2 dB, 2.0 dB and 9.4 dB, respectively. A part of the power penalties at higher bit rates might be attributed to the wavelength dependency of the EA modulator-based demultiplexers, although the gain recovery time of SOA seems to be dominant factor.

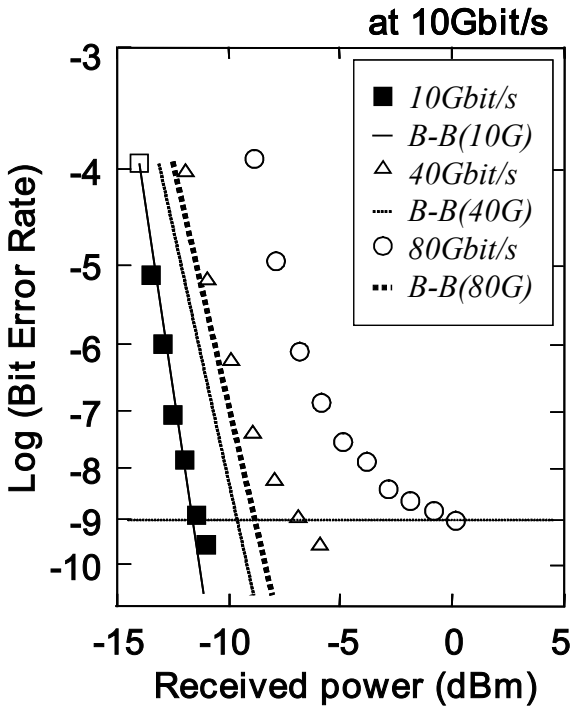

Figure 5-7: Measured BER results of the bit rate tunable wavelength conversion.

5.4 All-OPTICAL SIMULTANEOUS DEMULTIPLEXING

The all-optical demultiplexing is essential functionality in the high-speed photonic network. The future high-speed optical communication will be operated more than 40 Gbit/s, which will be up to around 100 Gbit/s. However, the electronics part of the receiving system will not be easily realized such a high-speed circuit as well as the semiconductor detectors. Therefore, before receiving the

optical data signal at the receiver, the bit rate should be decreased to low enough for the decision circuit in the receiver as well as the response of the photo diode. In this chapter, a novel methodology for simultaneous demultiplexing into two channels with half bit-rates and with equal signal qualities is proposed. A UNI switch changes the polarization direction of the input signal light pulse depending on the coexistence of the control signal pulse. Therefore, it is possible to achieve a simultaneous demultiplexing by extracting both the polarization-switched and non-switched outputs of the UNI deploying a PBS. In the following section, the proposed methodology is experimentally evaluated by utilizing 20 Gbit/s, 40 Gbit/s and 80 Gbit/s as an input optical data signal. The qualities of the demultiplexed signals are assessed by BER measurement with compared to the conventional demultiplexing method using EAM. The power advantage of our proposed demultiplexer is experimentally verified.

5.5 Principle of the all-optical simultaneous demultiplexing

As described in section four, the UNI switch realizes the switch states both on and off by using the polarizer as shown in Fig. 3-6. The UNI switch changes the polarization of the regenerated optical data signal due to the π-phase shift in the trailing pulse and the recombination of the split pulses. After recombination of the split pulse, the on and the off state is obtained due to the polarization direction of the polarizer placed at the end of the optical path of the UNI switch. Therefore, the both states of the polarization switch can be simultaneously extracted by introducing the polarization beam splitter as shown in Fig. 5-8.

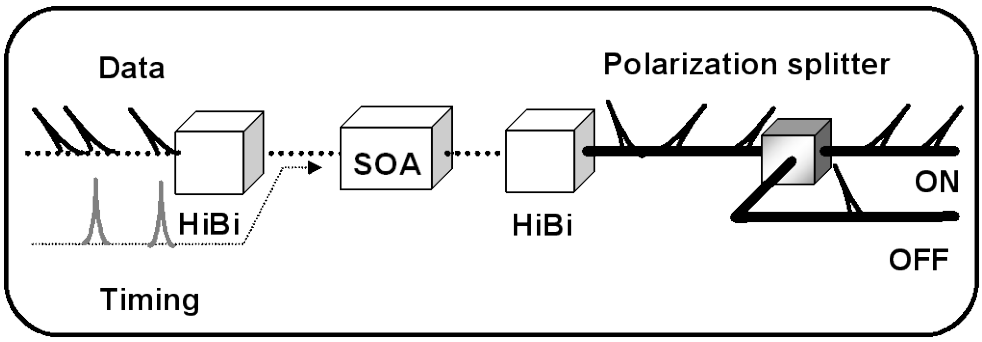

Figure 5-8: Schematic diagram of the simultaneous all-optical demultiplexer of the UNI switch with the polarization beam splitter.

In this scheme, it is essential for the simultaneous extraction of the both states to make the complete π-phase in the trailing pulse. In principle, however, all the SOA-based MZI switches including the UNI can not only gate the incoming data signal but also fully switch if the phase shift photo-induced in the SOA reaches π. Therefore both the switched and the un-switched signals can be simultaneously extracted using only one SOA-MZI all-optical switch. Nevertheless, no report has been presented to date that experimentally verifies such a full-switching capability of the SOA-MZI device, because it is relatively difficult to achieve an complete π phase shift with a reasonable input power and with an exact balance of signal intensities passing through two MZI arms. The use of the transparent assist light contributes to the reduction of the signal power required to achieve an complete π phase shift, and the one-arm MZI configuration of the UNI makes it easier to achieve the exact arm balance. The uses of both states of the output signal can double the efficiency of signal demultiplexing.

5.6 Experimental evaluation

5.6.1 All-optical demultiplexing from 20 Gbit/s into 2 x 10 Gbit/s

In this section, the proposed all-optical simultaneous demultiplexing is experimentally

evaluated by utilizing 20 Gbit/s optical data signal and 10 GHz optical clock pulses. Figure 5-9 shows the experimental setup and the eye diagrams. The basic configuration of the UNI switch was almost same as the previous evaluation. The DGD of each HiBi medium was 10 ps. The 20 Gbit/s data signal was generated by 10 Gbit/s based OTDM technique with PRBS of 2^{31}-1 encoding. The input optical power of the 20 Gbit/s data signal and the 10 GHz clock pulse were 0 dBm and –3 dBm, respectively. The half-wave plate was deployed in front of the polarization beam splitter for adjusting the polarization direction. The optical band pass filter cut the timing clock pulse of 1545 nm. CW assist light of 1480 nm was irradiated from backside of the SOA via optical circulator. The eye diagrams of the 20 Gbit/s input optical data signal, 10 GHz clock pulse and clear two outputs of 10 Gbit/s data signal were shown in Fig.5-9. In the case of absence of 10 GHz clock pulses, 20 Gbit/s optical data signal and no signal were observed from the channel 1 and 2, respectively. Figure 5-10 shows the measured BER results of the input data signal demultiplexed by the conventional 10 GHz driven EAM as a reference and the two 10 Gb/e signals demultiplexed by the proposed scheme. Almost the same results were observed in each 10 Gbit/s output in the BER results as well as in the eye diagram as shown in Fig. 5-9. The power penalty of 1.2 dB at the BER of 10^{-9} was confirmed in both channels. The optical power of the input data signal to the EAM demultiplexer must be amplified by EDFA up to +10 dBm for compensating the optical loss in the EAM. On the other hand, the optical power of the input data signal to the UNI switch was around +0 dBm. These results show the advantageous feature of the proposed scheme for the all-optical demultiplexer that is the low power switching for the simultaneous demultiplexing by the simple configuration with compared to the conventional optical demultiplexer using EAM with EDFAs.

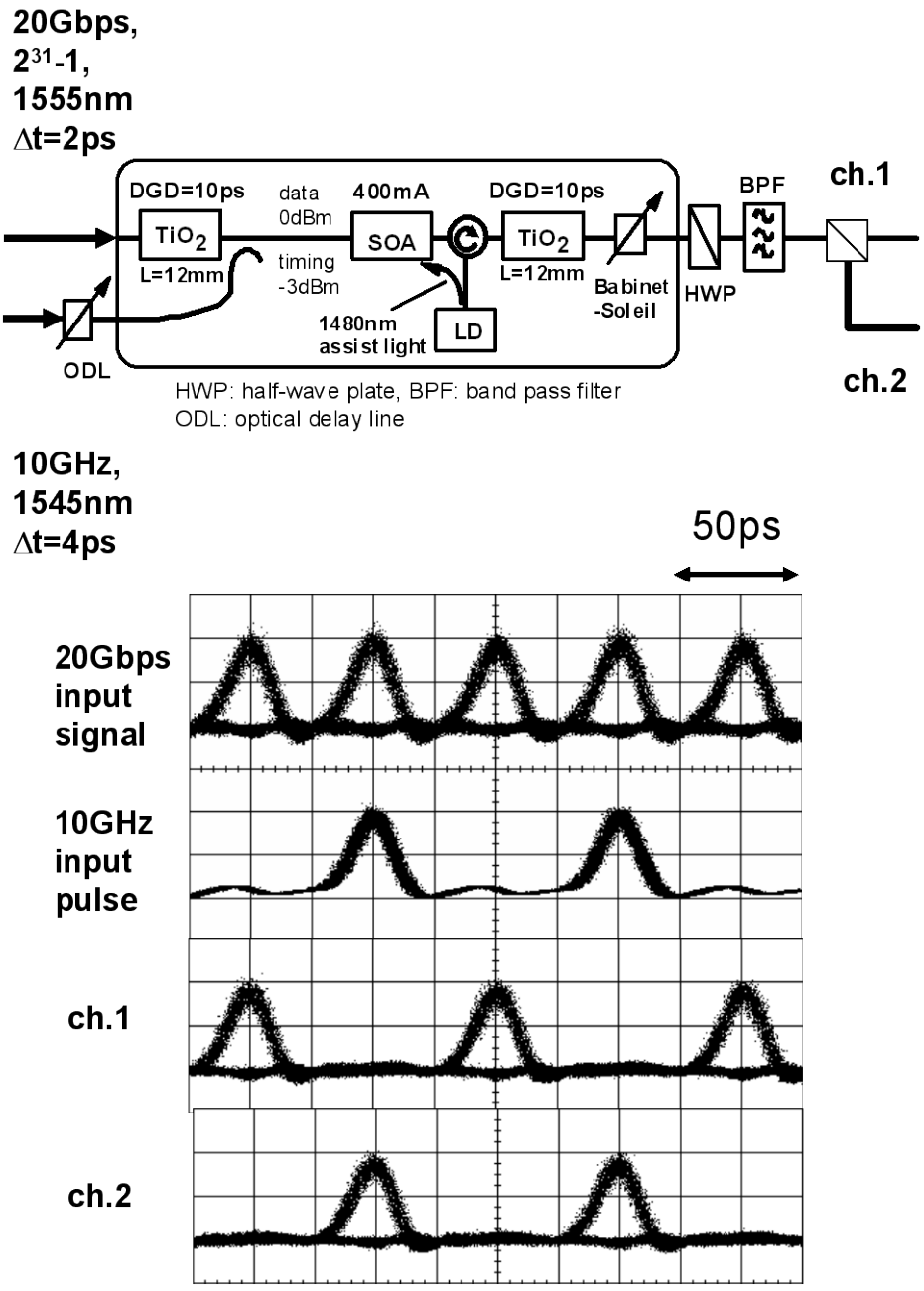

Figure 5-9: Experimental setup of the all-optical simultaneous demultiplexing by ugin UNI switch and the polarization beam splitter. The eye-diagrams are 20 Gbit/s input data signal, 10 GHz optical clock pulse and the output 10 Gbit/s data signals.

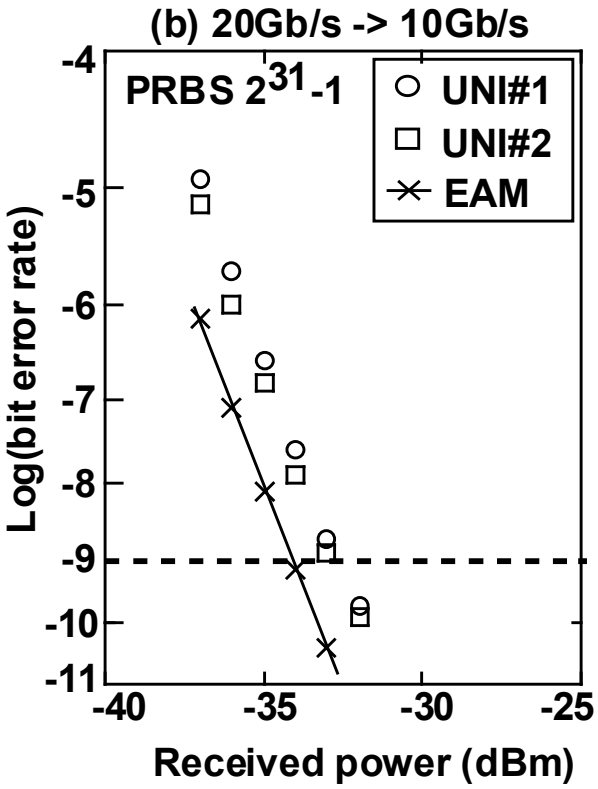

Figure 5-10: Measured BER results of all-optical simultaneous demultiplexing from 20 Gbit/s to two channels of 10 Gbit/s.

5.6.2 All-optical demultiplexing from 40 Gbit/s into 2 x 20 Gbit/s

In this section, a 40 Gbit/s data stream is simultaneously demultiplexed into two channels of 20 Gbit/s by the UNI switch demultiplexer. Comparing to the conventional demultiplexing method using EAM, it is verified that the demultiplexing scheme using the UNI switch has advantages in the viewpoints of power budget and simplicity. Figure 5-11 shows the experimental setup for simultaneous optical demultiplexing using the UNI, which consists of two rutile crystals and an InGaAsP/InP bulk type SOA.

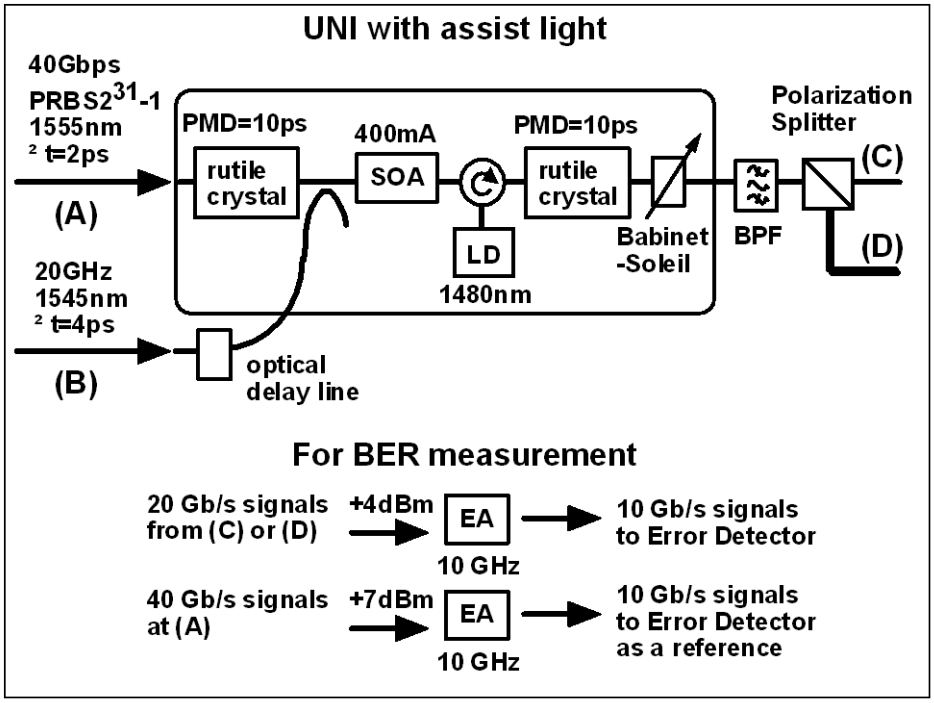

Figure 5-10: Experimental setup of the all-optical demultiplexer using UNI switch. The lower diagram schematically depicts the demultiplexing scheme for the BER measurement.

Both the 40 Gbit/s data signal and 20 GHz clock pulses were generated by 10 GHz based OTDM technique. The optical powers of the 40 Gbit/s data signal and the 20 GHz clock pulses injected into the SOA were -6 dBm and +1 dBm, respectively. The assist light of +10 dBm at 1480 nm was launched via optical circulator from the backside of the SOA. The PBS was employed to extract both polarization switched and non-switched signals simultaneously. The optical power of each demultiplexed signal was +4 dBm, which is 10 dB larger than that of input signal due to the SOA gain. Figure 5-11 shows the eye diagrams of the signals observed at the points (A)~(D) designated in Fig. 5-10. The eyes of both the 20 Gbit/s demultiplexed signals clearly opened as shown in Fig. 5-11 (C) and (D). The signal quality was assessed by measuring the BER after

demultiplexing the 20 Gbit/s output channel of the UNI into 10 Gbit/s using an EAM. The BER measurement of the input data signal that was directly demultiplexed from the 40 Gbit/s signal into 10 Gbit/s was carried out using the same EAM as a reference.

The BER characteristics of all the four 10 Gbit/s channels are shown in Fig. 5-12. The cross bars indicate the reference data with an input power of +7 dBm to the EAM. Error-free operations were observed for all the channels with no error floors. The distribution of the receiver sensitivity among four channels was within 0.5 dB. The small penalty of 1.2 dB against the EAM-based demultiplexing method was observed because the repetition rate of 20 GHz was low enough for the EAM to demultiplex the signal without impairment.

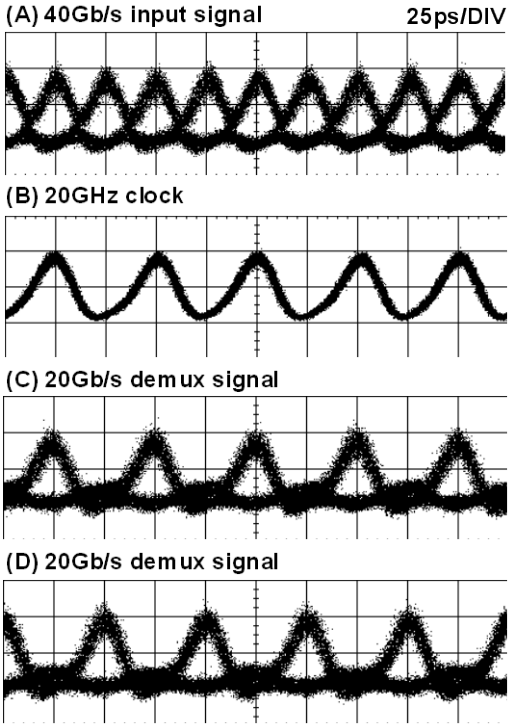

Figure 5-11: Eye diagrams of (A) the input 40 Gbit/s data signal, (B) 20 GHz clock pulse, (C) 20 Gbit/s demultiplexed signal of channel 1 and (D) 20 Gbit/s demultiplexed signal of channel 2.

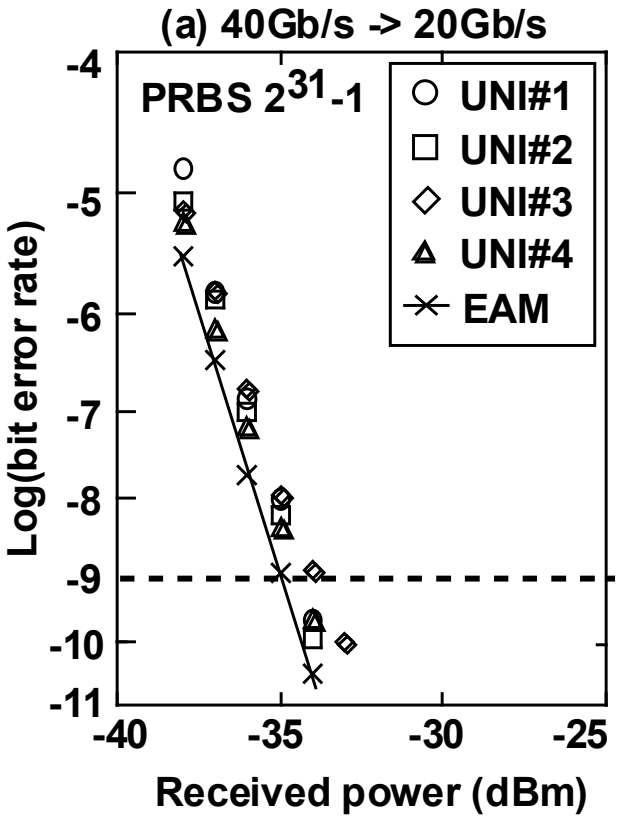

Figure 5-12: Measured BER results of the reference and the demultiplexed signals

5.6.3 All-optical demultiplexing from 80 Gbit/s into 2 x 40 Gbit/s

The UNI orthogonally switches the polarization angle of the input signal pulse owing to cross phase modulation generated by the control pulse. Therefore, it is possible to achieve a simultaneous demultiplexing by extracting both the polarization-switched and non-switched outputs of the UNI through a PBS with no power sacrifice. In this section, the all-optical simultaneous demultiplexing is applied for 80 Gbit/s data signal. A large advantage in power budget is expected in this method in comparison to an EAM-based demultiplexing because the EAM-based demultiplexing method requires intrinsically power-splitting loss. Consequently, an EDFA is required to insert in front of a receiver for the loss compensation, resulting in the increases of complexities as well as

system cost, and accumulation of additional ASE noise. For example, in the case of demultiplexing from 80 Gbit/s data into eight channels of 10 Gbit/s, it is required a one-to-eight power splitter which has inherent 9 dB loss and eight sets of an EAM, an EDFA and an optical band pass filter as shown in Fig. 5-13. In this configuration, the optical power of unselected channels is absorbed and wasted in each path after the splitting. On the other hand, the demultiplexing from 80 Gbps to eight channels of 10 Gbps by the UNI can be completed by concatenated three-stage UNI's with PBS's as shown in Fig. 5-14. No EDFA is required because of the SOA gain in the UNI. In an ultra high-speed optical communication, the low power operation is important feature for the actual system since the intensity of the optical data signal become the half of the 40 Gbit/s system due to the limitation of the average power fed into the fibers.

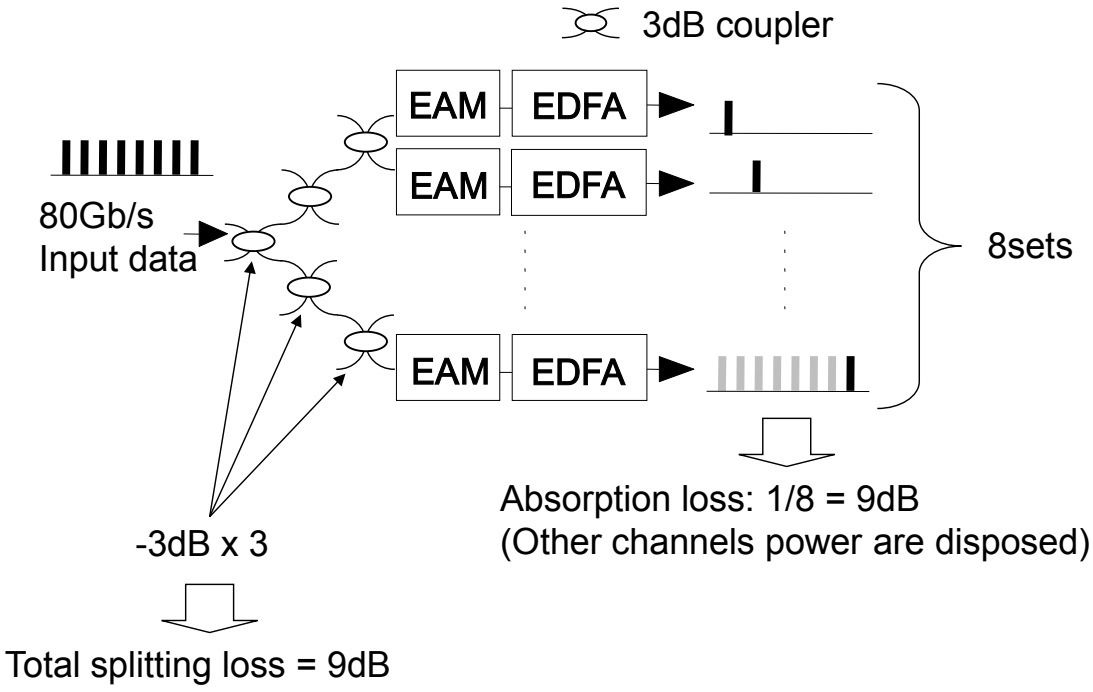

Figure 5-13: Schematic diagram of the demultiplexing scheme of EAM.

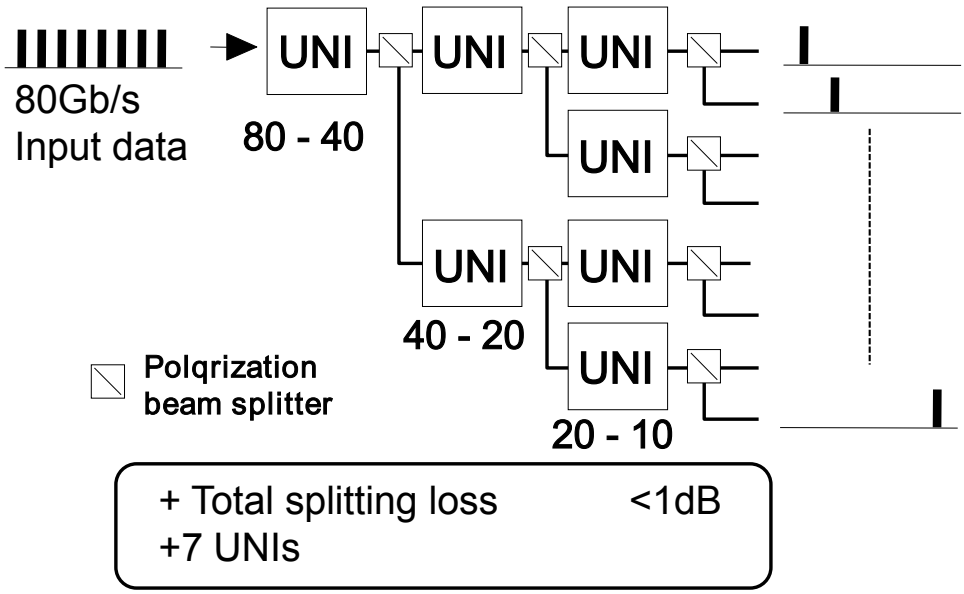

Figure 5-14: Schematic diagram of the demultiplexing scheme of UNI switch and the PBS.

The experimental setup for single-stage simultaneous optical demultiplexing using the UNI switch, which consists of two polarization-maintaining fibers (PMF) as a birefringent devices and an InGaAsP/InP bulk type SOA, is shown in Fig. 5-14. The polarization mode dispersion of the PMF was 6 ps, which corresponded to the half of the time slot of the 80 GHz. Both the 80 Gbit/s input data signal and 40 GHz clock pulses were generated by 10 GHz based OTDM technique. The optical powers of the 80 Gbit/s data signal and the 40 GHz clock pulses fed into the SOA were -5 dBm and +3 dBm, respectively. The transparent assist light with an input power of +10 dBm at 1480 nm, which was launched via optical circulator from the backside of the SOA, contributed to the reduction of the gain recovery time of the SOA from 160 ps to 40 ps as described in the chapter 4. Note that the smallness of the input 80 Gbit/s data signal was realized by the gain clamping effect owing to the transparent CW assist light. The PBS was employed to extract two orthogonally polarized signals simultaneously, which are both polarization switched and non-switched signals in the UNI. The

optical power of each extracted signal was about +1 dBm owing to the SOA gain. The output signal from the PBS was demultiplexed from 40 Gbit/s to 10 Gbit/s by an EAM-based demultiplexer for BER measurement as shown in the lower schematic diagram of Fig. 5-16. The reference BER of the 80 Gbit/s input data signal was also measured after demultiplexed by two cascaded EAM-based demultiplexers (80 Gbit/s to 20 Gbit/s, 20 Gbit/s to 10 Gbit/s). An EDFA and an optical band pass filter were set after each EAM in the EAM-based demultiplexer.

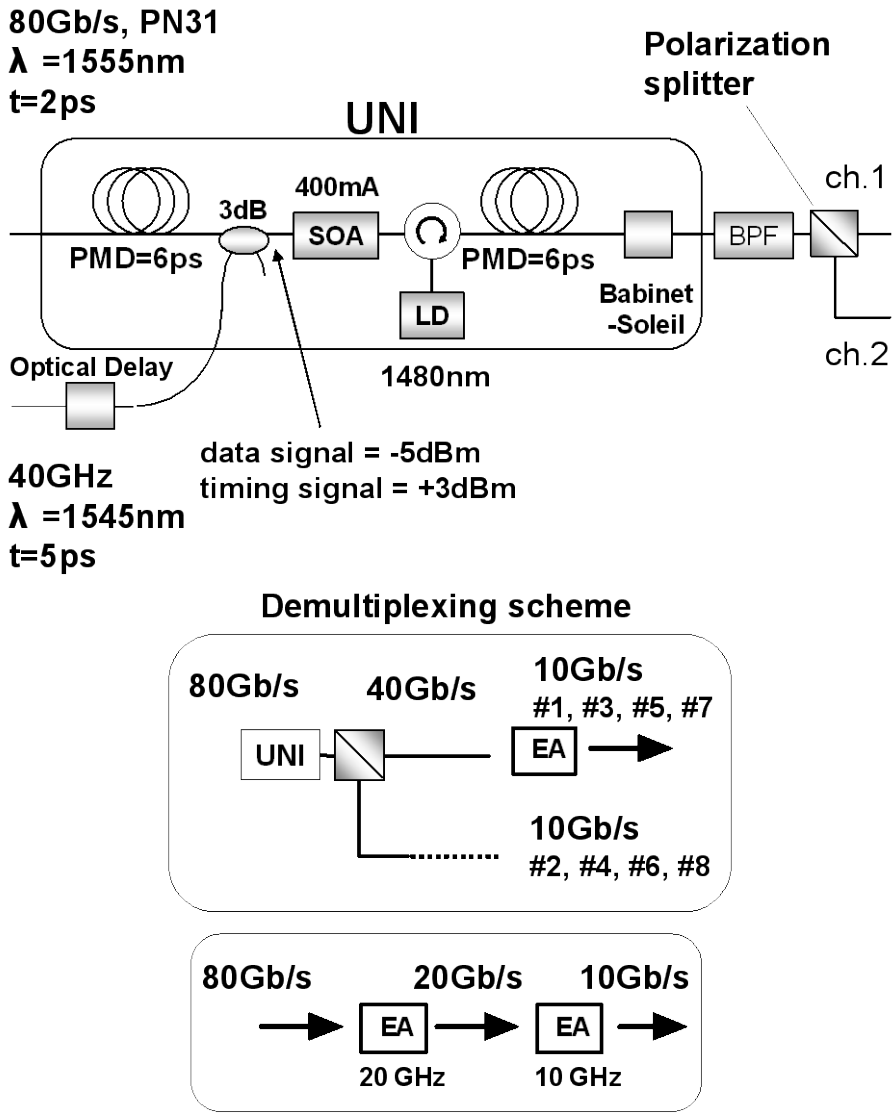

Figure 5-15: Experimental setup of all-optical demultiplexer using the UNI switch and PBS. The lower schematic diagrams show the demultiplexing scheme of the UNI switch and the conventional EAM demultiplexing as a reference.

Figure 5-16 shows the eye-diagrams of (a) the 80 Gbit/s input signal, (b) the 40 GHz clock pulses, (c) demultiplexed switched 40 Gbit/s signals and (d) non-switched 40 Gbit/s signals. The clear eye-openings were observed for all the channels.

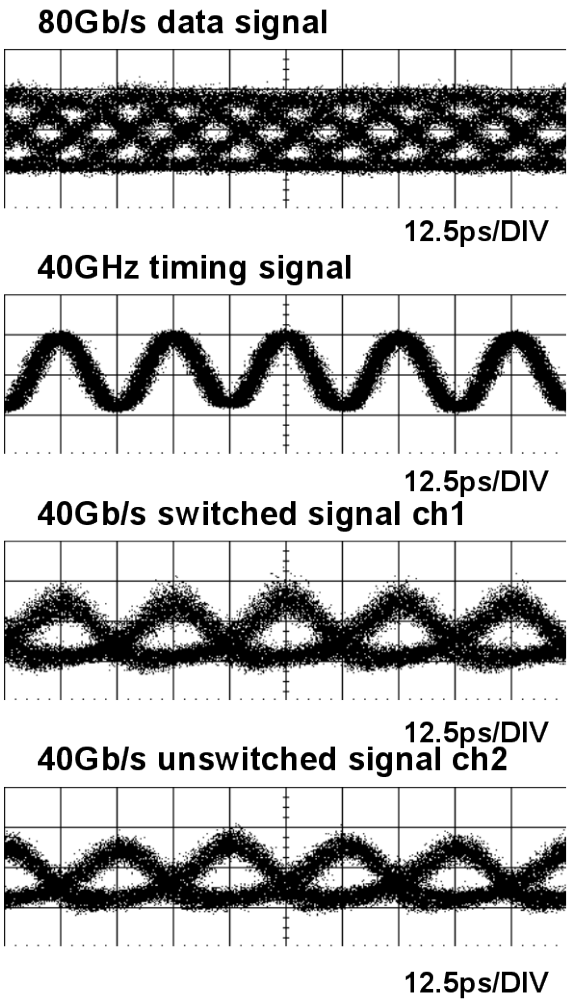

Figure 5-16: Eye diagrams of the 80 Gbit/s all-optical simultaneous demultiplexing.

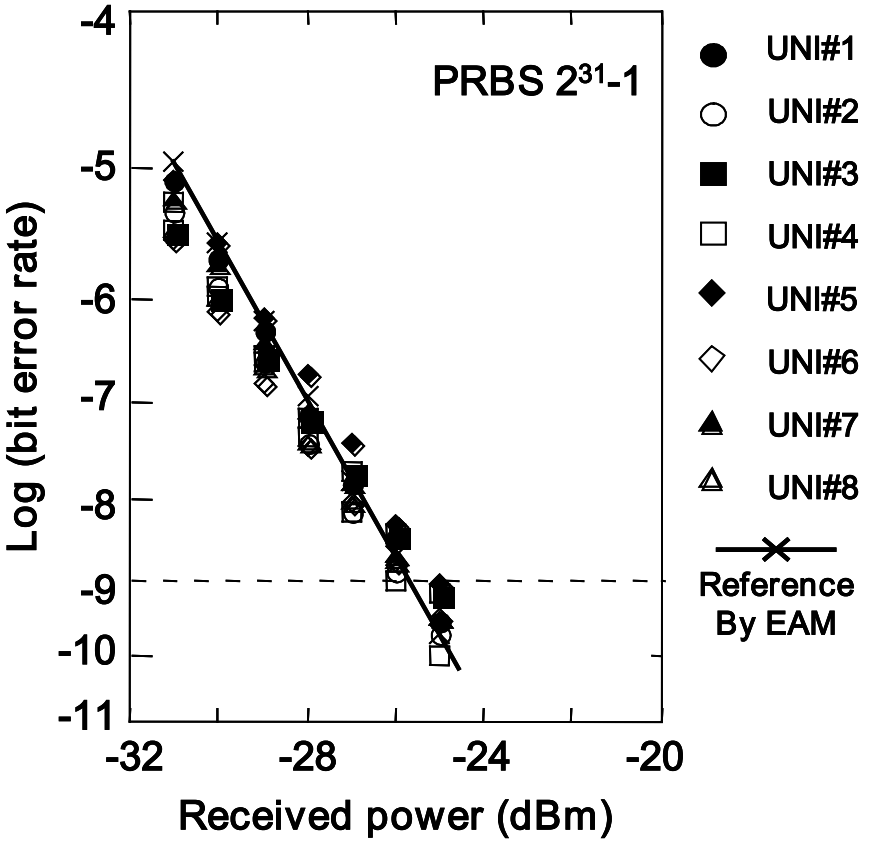

Figure 5-17: Measured BER results of the all 10 Gbit/s demultiplexed channels from 80 Gbit/s data signal by UNI switch based demultiplexer and the EAM based conventional demultiplexed 10 Gbit/s signal as a reference.

Figure 5-17 shows the BER measurement results as a function of the received power for all the channels demultiplexed by the UNI switch. Each open and closed mark indicates the 10 Gbit/s demultiplexed signals extracted from the channel 1 and 2 of the output from the UNI switch, respectively. The solid line indicates the reference BER result of the 10 Gbit/s demultiplexed signal by using the cascaded EAM. Little differences less than 1 dB in BER results among all the demultiplexed channels indicate that orthogonal polarization was switched perfectly in terms of the switching balance. This result shows, in other words, the π-phase shift can be completely achieved in

the UNI switch. Note that they were also somewhat improved from the reference case of EAM-based demultiplexing, resulting that the power penalty of the UNI-based demultiplexing from 80 Gbit/s data signal into two channels of 40 G/s data signal is observed to be negligible. From those results, the induced power penalty should be estimated only 2.0 dB if the three stages of the cascaded UNI-based demultiplexing architecture are utilized to demultiplex the 80 Gbit/s data signal into eight channels of 10 Gbit/s data tributaries. On the other hand, EAM-based demultiplexing intrinsically requires power-splitting loss of 9 dB to complete all the eight channels to be demultiplexed. The difference in power budget can be estimated as large as 7 dB. The advantage of the UNI switch based all-optical demultiplexer in power budget was obviously proved by these results. Moreover the simplicity of the configuration and the cost-effectiveness with regard to the EDFA-less feature of UNI-based demultiplexing methodology should also be recognized.

5.7 Conclusion

In this chapter, the significance of bit rate tunable functionality of the wavelength conversion device and the novel scheme were described. The bit rate tunable scheme for the all-optical regeneration utilizing the combination of an SOA and one variable DGD generator, which was constructed by using free space optics, was proposed and experimentally evaluated. The all-optical regenerative wavelength conversions were successfully demonstrated at bit rates of 10 Gbit/s, 40 Gbit/s and 80 Gbit/s. The proposed bit-rate tunable configuration can be promising method for a high-speed all-optical regenerator in the flexible transparent photonic network. Moreover, the novel methodology for the all-optical simultaneous demultiplexing by using the UNI switch with the transparent CW assist light and the PBS were proposed and experimentally evaluated. The bit-rates of the tested signals were 20 Gbit/s, 40 Gbit/s and 80 Gbit/s. In the all cases, the

capabilities of the all-optical simultaneous demultiplexing that were from 20 Gbit/s into two channels of 10 Gbit/s, from 40 Gbit/s into two channels of 20 Gbit/s and from 80 Gbit/s into two channels of 40 Gbit/s were successfully demonstrated by the eye diagram evaluation and the BER measurement. In the all BER measurements, error-free operations with no error floors were confirmed.

The receiver sensitivity in the 40 Gbit/s application, of which the distribution among the four channels was within 0.5 dB, was comparable to the reference data of direct demultiplexing by an EAM's, which verifies the signal quality was not changed after simultaneous demultiplexing. The high efficiency of demultiplexing is attributed to the full-switching capability of the SOA-MZI device, which was experimentally proved. The simultaneous demultiplexing from 80 Gbit/s data signal into two channels of 40 Gbit/s data signal was successfully demonstrated. The BER of all the eight channels of 10 Gbit/s demultiplexed by this proposed method were measured, and error-free operation with no error floors for all the channels were confirmed with received power variation less than 1 dB. No power penalty was also observed comparing to the conventional demultiplexing method by two stages of EAM. The three-stage cascaded UNI-based demultiplexers were estimated to have a significant power-budget advantage of 7 dB in comparison to the conventional EAM-based ones. These results indicated that the proposed scheme is an attractive method for a high-speed all-optical demultiplexing.

CHAPTER 6 CONCLUSION

This dissertation described that the ultra-high-speed all-optical signal processing based on an SOA with the CW assist light through chapter one to five. Chapter one expressed the overview of the optical fiber communication technology and the recent demand for the ultra-high-speed optical communication due to the rapid increase of the packet-centric services not only for the enterprise customer but also for the residential one. Section 1.1.1 and 1.1.2 expressed the abstract of the all-optical regeneration schemes that were the 2R and the 3R regenerations, and the other applications of the all-optical signal processing, respectively. Section 1.2 described the importance of the all-optical regeneration in future optical networks. The objectives of investigation of the all-optical 2R regeneration, which realizes the re-shaping and the re-amplification, and the all-optical 3R regeneration, which realizes the re-timing functionality in addition to the 2R regeneration were described in part 1.2.1 and 1.2.2, respectively. Section 1.3 expressed the applications of the ultra high-speed signal processing. In the section, the bit rate tunable wavelength conversion and the all-optical simultaneous demultiplexing were expressed in section 1.3.1 and 1.3.2, respectively.

Chapter 2 proposed and evaluated the new methodology of the ultra-high-speed saturable absorber by using the nonlinear absorption phenomena in the SOA with the CW assist light. The device parameters of the saturable absorber were considered by the experimental evaluation and numerical calculation using the measured results in the section 2.2 and 2.3. The proposed novel scheme for reducing the absorption recovery time by using the CW assist light was experimentally investigated in section 2.4. The effectiveness of the all-optical 2R regeneration by the SA with the CW assist light was experimentally investigated using 5 Gbit/s NRZ signal and 10 Gbit/s RZ signal in section 2.5 and 2.6, respectively. These results indicated that the simple 2R regeneration could be realized by this proposed method for the ultrafast optical communications.

Chapter 3 proposed the gain clamping effect for an SOA by the CW assist light and ultrafast polarization discrimination switch based on the one-arm Mach-Zehnder interferometer with the gain clamping effect. Section 3.2 described the effectiveness of the gain clamping effect by experimental evaluation. Especially, direct amplification of the 40 Gbit/s or the 80 Gbit/s optical data signal was successfully demonstrated by the SOA with the CW assist light. The UNI switch consists of the TiO_2 rutile crystalline as HiBi media was proposed in section 3.3. By introducing the CW assist light to the SOA in the UNI switch, the high-speed response of the switching and the low power operation were realized simultaneously. To evaluate the feasibility of this proposed methodology, the regenerative wavelength conversion was demonstrated at 40 Gbit/s and 80 Gbit/s. Especially, at the 40 Gbit/s regenerated data signal showed the advantage of the CW assist light compared to the conventional holding beam effect in the power budget. The error-free operation without error-floor was observed in the results of the wavelength conversion at the 40 Gbit/s repetition rate. Even though the 80 Gbit/s repetition rate, the error-free operation was successfully achieved. The proposed method for the ultra high-speed all-optical 3R regeneration could be the candidate for the future high-speed photonic networks.

Chapter 4 described the operational tolerance of the UNI switch based 3R regenerator and its regeneration capability by using the intentionally impaired signal at the repetition rate of 40 Gbit/s. The advantage of the bit-inverted regeneration was described in section 4.2. The operational margin of the UNI switch was experimentally evaluated by changing the device parameters and the system parameters that were the pulse width of both the data signal and the clock pulses, the DGD of the HiBi media and the relative position of the data signal between the split clock pulses. The operation margin more than 2 dB against the condition change was confirmed in each case. Moreover, the distinct regeneration capability was also demonstrated by changing the condition of the optical signal

degradation. An amplified spontaneous emission noise generated by an EDFA and a timing jitter of the optical data signal were intentionally lapped over the optical data signal. The expansion of the threshold voltage window was observed as large as two times of the original result. The improvement of the Q value and the attainable BER were confirmed in the impaired input data signal by ASE noise, the timing jitter and the doubled degradation of those factors. These results proved that the UNI switch based all-optical 3R regenerator could be applied for the future 40 Gbit/s all-optical networks.

Chapter 5 proposed the novel scheme for the bit rate tunable all-optical regeneration by using the combination of the SOA and reconfigurable optics. Section 5.2 expressed the operation principle of the variable DGD generator based polarization discrimination switch. The orthogonally split pulses with expected time difference could be generated by the variable DGD generator with simple operation. The bit rate tunable wavelength conversion was demonstrated at 10 Gbit/s, 40 Gbit/s and 80 Gbit/s using the almost same configuration of the devices excepting the bit rate of the local optical clock pulses in section 5.3. Error-free operation was confirmed in each bit rate. This proposed method could be promising technique for the flexible photonic networks. The all-optical simultaneous demultiplexing functionality by using the combination of the UNI switch and the polarization beam splitter was also proposed and successfully demonstrated in this chapter. Section 5.5 expressed the operation principle of the simultaneous demultiplexer. By introducing the CW assist light to the UNI switch, the complete π-phase shift was realized in the SOA as well as the low power operation. The all-optical simultaneous demultiplexing into the half bit rate was successfully demonstrated from 20 Gbit/s, 40 Gbit/s and 80 Gbit/s as described in section 5.6.

I would like to conclude that the proposed schemes for the all-optical 2R regeneration, the all-optical 3R regeneration, the bit rate tunable all-optical wavelength conversion and the all-optical

simultaneous demultiplexing were promising techniques in the future all-optical communication systems.

ACKNOWLEDGEMENTS

I would like to describe gratitude from my heart to Professor K. Utaka for giving me the opportunity to write this thesis. I also express my appreciation to Prof. I. Kato, Prof. H. Nakajima and Prof. M. Matsumoto for their fruitful discussion.

I would like to thank to Dr. S. Akiba, president of KDDI R&D Laboratories Inc. and Dr. M. Suzuki, executive director of KDDI R&D Laboratories Inc. for their continuous encouragement. I would like to express my acknowledgements to Prof. Y. Matsushima for giving suggestions to write this dissertation, as well as for his continuous encouragement. I must express my appreciation to Dr. H. Okinaka, Dr. T. Mizuike, Mr. H. Fujita and Mr. H. Tanaka for their continuous encouragement and the receptive attitude for this work. I also would like to express my acknowledgements to Dr. H. Mimura, CEO of Fiberlabs Inc., Dr. S. Tanaka, Director of NICT, Dr. H. Tanaka, Director of KDDI R&D Laboratories Inc. and Dr. N. Edagawa, Director of KDDI, for their warm encouragement while they worked for KDDI R&D Laboratories Inc.

I also wish to acknowledge fruitful discussions to Dr. M. Usami, Dr. K. Nishimura and Mr. R. Inohara on various issues, especially for their direction of my investigation and the evaluation of the experimental results, without which this dissertation would not have been possible. I am grateful to all the other members at photonic network division of KDDI R&D Laboratories Inc. for creating a wonderful circumstance. With support of the above colleagues, the present dissertation has been successfully accomplished.

Finally, I would like to thank to my wife Mami Tsurusawa for her continuous encouragement and kind support in my life.

REFERENCES

[1] S. Bischoff, B. Lading and J. Mørk, “BER Estimation for All-Optical Regenerators Influenced by Pattern Effects” IEEE Photon. Technol. Lett., vol. 14, pp. 33-35, Jan. 2002.

[2] J. D. Merlier, M. L. Nielsen, G. Morthier and R. Baets, “All-optical 2R regeneration of a 10 Gbit/s RZ signal in an MMI-SOA based device” Workshop on Optical Signal Processing, pp. 13-15, Nov. 2001.

[3] O. Leclerc, P. Brindel, S. Bigo, E. Brun-Maunand and E. Desurvire, “2 x 20 Gbit/s, 3500km regenerated WDM soliton transmission with all-optical Kerr fibre modulation”, Electronics Letters, vol.34, pp.l99-201, Jan 1998.

[4] U. Feiste, D. J. As and A. Ehrhardt, “18 GHz All-Optical Frequency Locking and Clock Recovery Using a Self-Pulsating Two-Section DFB-Laser” IEEE Photon. Technol. Lett., vol. 6, pp. 106-108, Jan. 1994.

[5] H. Kasuya, M. Mori, R. Goto, T. Goto and K. Yamane, “All optical mode locking of Fabry-Perot laser diode via mutual injection locking between two longitudinal modes” App. Phys. Lett., vol. 75, pp. 13-15, July 1999.

[6] H. J. Lee, J. Y. Choi and H. G. Kim, “Polarisation-independent, stable, all-optical clock recovery using an SOA/grating filter wavelength converter”, Electron. Lett. vol. 35, pp. 1368-1370, Aug. 1999.

[7] J. Leuthold, B. Mikkelsen, R. E. Behrmger, G. Raybon, C. H. Joyner and P. A. Besse, “Novel 3R Regenerator Based on Semiconductor Optical Amplifier Delayed-Interference Configuration” IEEE Photon. Technol. Lett., vol. 13, pp. 860-862, Aug. 2001.

[8] J. Leuthold, G. Raybon, Y. Su, and R. Essiambre, “All-Optical Transmission and Wavelength Conversion of 40 Gbit/s Signals over Ultra-Long Haul Distances” Conference Proceedings of Optical Fiber Communication Conference (OFC), WB1, Mar. 2002.

[9] J. Leuthold, C. H. Joyner, B. Mikkelsen, G. Raybon, J. L. Pleumeekers, B. I. Miller, K. Dreyer, C. and A. Burrus, “100Gbit/s all-optical wavelength conversion with integrated SOA delayed-interference configuration” Electron. Lett., vol. 36, pp. 1129-1130, Jun. 2000.

[10] H. J. Ki, Y. M. Jhon, Y. S. Lee and J. C. Jeong, “40 Gbit/s Clock Recovery with Optical Phase Lock Loop Based on a Terahertz Optical Asymmetric Demultiplexer” Conference Proceedings of Conference on Optical Internet (COIN), WeE16, pp. 344-346, Jul. 2002.

[11] H.-P. Nolting and M. Gravert, “Devices for 3R Signal Regeneration at 160 Gbit/s and faster” Workshop on Optical Signal Processing, pp. 19-22, Nov. 2001.

[12] L. D. Phillips, A. D. Ellis, H. J. Theiele, R. J. Manning and A. E. Kelly, “40 Gbit/s all-optical

data regeneration and demultiplexing with long pattern lengths using a semiconductor nonlinear interferometer" Electron. Lett., vol. 34, pp. 2340-2342, Nov. 1998.

[13] H. J. Thiele, A. D. Ellis and I. D. Phillips, "Recirculation loop demonstration of 40Gbit/s all-optical 3R data regeneration using a semiconductor nonlinear interferometer" Electron. Lett., vol. 35, pp. 230-231, Feb. 1999.

[14] D. T. K. Tomg, K.-L. Deng, B. Mikkelsen, G. Raybon, K. F. Dreyer and J. E. Johnson, "160Gbit/s clock recovery using electroabsorption modulator-based phase-locked loop" Electron. Lett., vol. 36, pp. 1951-1952, Nov. 2000.

[15] D. T. K. Tong, B. Mikkelsen, G. Raybon, T. N. Nielsen, K. F. Dreyer and J. E. Johnson, "Optoelectronic Phase-Locked Loop with Balanced Photodetection for Clock Recovery in High-Speed Optical Time-Division-Multiplexed Systems" IEEE Photon. Technol. Lett., vol. 12, pp. 1064-1066, Aug. 2000.

[16] K. Vlachos, G. Theophilopoulos, a. Hatziefremidis and H. Avramopoulos, "30 Gbit/s All-Optical Clock Recovery Circuit" IEEE Photon. Technol. Lett., vol. 12, pp.705-707, Jun. 2000.

[17] L. Wang, Y. Su, A. Agarwal and P. Kumar, "Polarization Insensitive Widely Tunable All-Optical Clock Recovery Based on AM Mode-Locking of a Fiber Ring Laser" IEEE Photon. Technol. Lett., vol. 12, pp. 211-213, Feb. 2000.

[18] T. Yamamoto, L. K. Oxenløwe, C. Schmidt, C. Schubert, B. Hilliger, U. Feiste, J. Berger, R. Ludwig and H. G. Weber, "Clock recovery from 160Gbit/s data signals using phase-locked loop with interferometric optical switch based on semiconductor optical amplifier" Electron. Lett., vol. 37, pp. 509-510, Apr. 2001.

[19] S. L. Danielsen, P. B. Hansen, K. E. Stubkjaer, M. Schilling, K. Wünstel, W. Idler, P. Doussiere, and F. Pommerau, "All Optical Wavelength Conversion Schemes for Increased Input Power Dynamic Range" IEEE Photon. Technol. Lett., vol. 10, pp. 60-62, Jan. 1998.

[20] C. Joergensen, S. L. Danielsen, K. E. Stubkjaer, M. Schilling, K. Daub, P. Doussiere, F. Pommerau, P. B. Hansen, H. N. Poulsen, A. Kloch, M. Vaa, B. Mikkelsen, E. Lach, G. Laube, W. Idler and K. Wunstel, "All-Optical Wavelength Conversion at Bit Rates Above 10 Gbit/s Using Semiconductor Optical Amplifiers" IEEE J. Selected Topics in Quantum Electron., vol. 3, pp.1168-1179, Oct. 1997.

[21] L. H. Spiekmen, U. Koren, M. D. Chien, B. I. Miller, J. M. Wiesenfeld and J. S. Perino, "All-Optical Mach-Zehnder Wavelength Converter with Monolithically Integrated DFB Probe Source" IEEE Photon. Technol. Lett., vol. 9, pp. 1349-1351, Oct. 1997.

[22] F. Ratovelomanana, N. Vodjdani, A. Enard, G. Glastre, D. Rondi, R. Blondeau, A. Dupas, L. Billès and J. C. Simon, "Regeneration improvement in all-optical wavelength converter, based on a Mach-Zehnder interferometer, by means of phase-shifter section" Electron. Lett., vol. 33, pp.

1629-1630, Sep. 1997.

[23] R. J. S. Pedersen, B. F. Jørgensen, B. Mikkelsen, M. Nissov, K. E. Stubkjaer, K. Wünstel, K. Daub, E. Lach, G. Laube, W.Idler, M. Schilling, P. Doussiere and F. Pmmerau, "Cascading of a non-blocking WDM cross-connect based on all-optical wavelength cnverters for routing and wavelength slot interchanging" Electron. Lett., vol. 33, pp.1647-1648, Sep. 1997.

[24]M. F. C. Stephens, M. Axghari, R. V. Penty and I. H. White, "Demonstration of Ultrafast All-Optical Wavelength Conversion Utilizing Birefringence in Semiconductor Optical Amplifiers" IEEE Photon. Technol. Lett., vol. 9, pp. 449-451, Apr. 1997.

[25] S. P. Yam and C. Shu, "All-optical wavelength switching in a semiconductor laser using self-seeding and external injection-seeding" Appl. Phys. Lett., vol.72, pp.1024-1026, Mar. 1998.

[26] M. F. C. Stephens, R. V. Penty, M. Ashari, I. H. White, K. Guild, M. J. O'Mahony, M. J. Roberston and P. J. Fiddyment, "Demonstration of an All-Optical Simultaneous Wavelength Converting/Space-Switching Cross-Point Device" IEEE Photon. Technol. Lett., vol. 10, pp. 224-226, Feb. 1998.

[27] W. Idler, K. Daub, G. Laube, M. Schilling, P. Wiedemann, K. Dütting, M. Klenk, E. Lach and K. Wünstel, "10 Gbit/s Wavelength Conversion with Integrated Multiquantum-Well-Based 3-Port Mach-Zehnder Interferometer," IEEE Photon. Technol. Lett., vol. 8, pp. 1163-1165, Sep. 1996.

[28] A. E. Kelly, I. D. Phillips, R. J. Manning, A. D. Ellis, D. Nessel, D. G. Moodie and R. Kashyap, "80 Gbit/s all-optical regenerative wavelength conversion using semiconductor optical amplifier based interferometer" Electron. Lett., vol. 35, pp. 1477-1478, Aug. 1999.

[28] L. H. Spiekman, J. M. Wiesenfeld, U. Koren, B. I. Miller and M. D. Chien, "All-Optical Mach-Zehnder Wavelength Converter with Monolithically Integrated Preamplifiers" IEEE Photon. Technol. Lett., vol. 10, pp. 1115-1117, Aug. 1998.

[29] J. A. Hudgings and K. Y. Lau, "Step-tunable All-Optical Wavelength Conversion Using Cavity-Enhanced Four-Wave Mixing," IEEE J. Quantum Electron., vol. 34, pp. 1349-1355, Aug. 1998.

[30] A. M. Kan'an and P Likamwa, "Ultrafast all-optical switching not limited by the carrier lifetime in an integrated multiple-quantum-well Mach-Zehnder interferometer" J. Opt. Soc. Am. B, vol. 14, pp. 3217-3223, Nov. 1997.

[31] S Bigo, O Leclerc and E Desurvire, "All-Optical Fiber Signal Processing and Regeneration for Soliton Communications" IEEE J. Selected Topics in Quantum Electron., vol. 3, pp. 1208-1221, Oct. 1997.

[32] M. Horita, S. Tanaka and Y. Matsushima, "Wavelength tunable optical add and drop multiplexer utilising coupled semiconductor waveguides and a striped thin-film heater" Electron. Lett., vol. 34, pp. 1-2, Nov. 1998.

[33] I. Ogura, Y. Hashimoto, H. Kurita, T. Shimizu and H. Yokoyama, "Picosecond All-Optical Gate

Using a Saturable Absorber in Mode-Locked Laser Diodes" IEEE Photon. Technol. Lett., vol. 10, pp.603-605, Apr. 1998.

[34] R. J. Manning and D. A. O. Davies, "Three-wavelength device for all-optical signal processing" Opt. Lett., vol. 19, pp.889-891, Jun. 1994.

[35] D. Taverner, N. G. Broderick, D. J. Richrdson, M. Ibsen and R. I. Laming, "All-optical AND gate based on coupled gap-soliton formation in a fiber Bragg grating" Opt. Lett., vol.23, pp. 259-261, Feb. 1998.

[36] I. Yokoyama, M. Asobe, A. Yokoo, H. Itoh and T. Kaino, "All-optical switching by use of cascading of phase-matched sum-frequency generation and difference-frequency generation processes" J. Opt. Soc. Am. B, vol. 14, pp. 3368-3377, Dec. 1997.

[37] A. Hirano, H. Tsuda, R. Takahashi, K. Sato, A. Sano, T. Kataoka and K. Hagimoto, "An All-optical Signal Discriminator: Applications to 2.4 Gbit/s All-optical Regeneration and Gbit/s Demultiplexing" Conference Proceedings of Opto-Electronics and Communications Conference (OECC), 18B4-3, pp. 342-343, Jul. 1996.

[38] F. Dorgeuille, B. Mersali, M. Feuillade, S. Sainson, S. Slempkès and M. Forcher, "Novel Approach for Simple Fabrication of High-Performance InP-Switch Matrix Based on Laser-Amplifier Gates" IEEE Photon. Technol. Lett., vol. 8, pp. 1178-1180, Sep. 1996.

[39] T. Akiyama, M. Tsuchiya and T. Kamiya, "Sub-pJ operation of broadband asymmetric Fabry-Perot all-optical gate with coupled cavity structure" Appl. Phys. Lett., vol. 72, pp. 1545-1547, Mar. 1998.

[40] A. Hirano, H. Kobayashi, H. Tsuda, R. Takahashi, M. Asobe, K. Sato and K. Hagimoto, "10 Gbit/s RZ all-optical; discrimination using refined saturable absorber optical gate" Electron. Lett., vol. 34, pp. 198-199, Jan. 1998.

[41] N. Finlayson, B. K. Nayar and N. J. Doran, "Switch inversion and polarization sensitivity of the nonlinear-optical loop mirror" Opt. Lett., vol. 17, pp. 112-114, Jan. 1992.

[42] R. Hess, M. Duelk, W. Vogi, E. Gamper, E. Gini, P. A. Basse, H. Melchior, K. S. Jepsen, B. Mikkelsen, M. Vaa, H. N. Poulsen, A. T. Clausen, K. E. Stubkjaer, S. Bouchoule and F. Devaux, "Simultaneous ass-optical add and drop multiplexing of 40Gbit/s OTDM signals using monolithically integrated Mach-Zehnder interferometer" Electron. Lett., vol. 34, pp. 579-580, Mar. 1998.

[43] S. Nakamura, Y. Ueno and K. Tajima, "Ultrafast (200-fs Switching, 1.5-Tb/s Demulitiplexing) and High-Repetition (10 GHz) Operations of a Polarization-Discriminating Symmetric Mach-Zehnder All-Optical Switch" IEEE Photon. Technol. Lett., vol. 10, pp. 1575-1577, Nov. 1998.

[44] S. Nakamura, K. Tajima, N. Hamao and Y. Sugimoto, "High-speed all-optical switching experiment in Mach-Zehnder configuration using GaAs waveguide" Appl. Phys. Lett., vol. 62, pp.

925-927, Mar. 1993.
[45] S. Nakamura, K. Tajima, and Y. Sugimoto, “Experimental investigation on high-speed switching characteristics of a novel symmetric Mach-Zehnder all-optical switch” Appl. Phys. Lett., vol. 65, pp. 283-285, Jul. 1994.
[46] K. Nakatsuhara, T. Mizumoto, E. Takahashi, S. Hossain, Y. Saka, B.-J. Ma and Y. Nakano, “All-optical switching in a distributed-feedback GaInAsP waveguide” Appl. Opt., vol. 38, pp. 3911-3916, Jun. 1999.
[47] V. Krajinovic, G. Remsak and S. Aleksic, “ADDRESS RECOGNITION USING SOA-BASED MACH-ZEHNDER INTERFEROMETER” Conference Proceedings of Opto-Electronics and Communications Conference (OECC), 11A3-6, pp. 416-417, Jul. 2002.
[48] K. Suzuki, T. Shimazu, S. Nakamura, Y. Ueno, M. Takahashi, T. Tamanuki, A. Furukawa, T. Sasaki and K. Tajima, “Hybrid integrated Symmetric Mach-Zehnder all-optical switch with phase controllers” The International Meetings on Optical Internet and Photonics in Switching (COIN+PS), MoB4, pp. 43-45, Jul. 2002.
[49] H. Avramopoulos, “Optical Signal Processing: Moving Towards Higher Functionality” Workshop on Optical Signal Processing, pp. 1-3, Nov. 2001.
[50] R. J. Manning, “Linear and Non-linear SOAs for ALL-optical Processing Circuits”
Workshop on Optical Signal Processing, pp. 4-6, Nov. 2001.
[51] B. Dagens, A. Labrousse, R. Brenot, B. Lavigne, P. Guerber, P.Brindel, O. Leclerc and M. Rcnaud, “SOA-based interferometer for all-optical signal processing” Workshop on Optical Signal Processing, pp. 7-9, Nov. 2001.
[52] U. Busolt, T. Tekin, C. Schubert, J. Berger, M. Schlak, B. Maul, W. Brinker, R. Molt , C. Schmidt and H. Ehlers, “Ultrafast all-optical signal processing by a monolithically integrated Mach-Zehnder-Interfermeter” Workshop on Optical Signal Processing, pp. 10-12, Nov. 2001.
[53] J. H. Kim, Y. T. Byum, Y. M. Jhon, S. Lee, D. H. Woo and S. H. Kim, “The Novel Design of All-Optical XOR Gate by using Cross Gain Modulation (EGM) in Semiconductor Optical Amplifiers” Workshop on Optical Signal Processing, pp. 102-104, Nov. 2001.
[54] M. L. Nielsen , A. T. Clausen, T. Fjelde, L. Oxenløwe, A. Klook, H. Poulsen and D. Wolfson, “All-optical signal processing employing interferometric structures,” Workshop on Optical Signal Processing, pp. 111-117, Nov. 2001.
[55] I. D. Phillips, A. Gloag, D. G. Moodie, N. J. Doran, I. Bennion and A. D. Ellis, “Drop and Insert Multiplexing with Simultaneous Clock Recovery Using an Electroabsorption Modulator” IEEE Photon. Technol. Lett., vol. 10, pp. 291-293, Feb. 1998.
[56] Y. Ueno, S. Nakamura, and K. Tajima, “Penalty-free error-free all-optical data pulse regeneration at 84 Gbit/s by using a symmetric-Mach-Zehnder-type semiconductor regenerator”,

IEEE Photonics Technol. Lett., vol. 13, pp. 469-471, May. 2001.

[57] S. Nakamura, Y. Ueno and K. Tajima, "168-Gbit/s all-optical wavelength conversion with a symmetric-Mach-Zehnder-type switch", IEEE Photonics Technol. Lett., vol.13, no.10, pp.1091-1093, Oct. 2001.

[58] Y. Ueno, S. Nakamura, K. Tajima and S. Kitamura, "3.8 THz wavelength conversion of picosecond pulses using a semiconductor delayed-interference signal-wavelength converter (DISC)", IEEE Photonics Technol. Lett., vol.10, no.3, pp.346-348, Mar. 1998.

[58] I. Gontijo, D. T. Neilson, A.C. Walker, G. T. Kennedy and W. Sibbett, "Nonlinear InGaAs-InGaAsP Single-Quantum-Well All-Optical Switch – Theory and Experiments" IEEE J. Quantum Electron., vol. 32, pp. 2112-2121, Dec. 1996.

[59] R. J. Manning, A. D. Ellis, A. J. Poustie and K. J. Blow, " Semiconductor laser amplifiers for ultrafast all-optical signal processing" J. Opt. Soc. Am., vol. 14, pp. 3204-3215, Nov. 1997.

[60] A. Melloni, M. Chinello and M. Martinelli, "All-Optical Switching in Phase-Shifted Fiber Bragg Grating" IEEE Photn. Technol. Lett., vol. 12, pp. 42-44, Jan. 2001.

[61] H. Ohta, S. Nogiwa, Y. Kawaguchi and Y. Endo, "Measurement of 200 Gbit/s optical eye diagram by optical sampling with gain-switched optical pulse" Electron. Lett. vol. 36, pp. 1-2, Apr. 2000.

[62] D. K. Jung, C. H. Kim and Y. C. Cung, "OSNR Monitoring Technique Using Polarization-Nulling Method" Conference Proceedings of Optical Fiber Communication Conference (OFC), WK4, pp. 176-178, Mar. 2000.

[63] R. Wiesmann, O. Bleck and H. Heppner, "Cost effective performance monitoring in WDM systems" Conference Proceedings of Optical Fiber Communication Conference (OFC), WK2, pp. 171-173, Mar. 2000.

[64] S.-L. Lee, C.-T. Pien and Y.-Y. Hsu, "Wavelength Monitoring in DWDM Networks Using Low Cost Semiconductor Laser Diode/Amplifiers" Conference Proceedings of Optical Fiber Communication Conference (OFC), WK1, pp. 168-170, Mar. 2000.

[65] R. Habel, K. Roberts, A. Solheim and J. Harley, "Optical Domain Performance Monitoring" Conference Proceedings of Optical Fiber Communication Conference (OFC), WK3, pp. 174-176, Mar. 2000.

[66] N. Hanik, A. Gladisch, C. Caspar and B. Streble, "Application of amplitude histograms to monitor performance of optical channels" Electron. Lett., vol. 35, pp. 403-404, Mar. 1999.

[67] Z. Tao, Z. Chen, L. Fu, D. Wu and A. Xu, "A Novel Method to Monitor OSNR Using a Mach-Zehnder Interferometer" Conference Proceedings of The Conference on Lasers and Electro-Optics (CLEO) / Pacific Rim, ThB2-4, Jul. 2001.

[68] I. Shake and H. Takara, "Flexible Performance Monitoring Using Amplitude Histogram Method

in Optical Fiber Communication" Conference Proceedings of Opto-Electronics and Communications Conference (OECC), 12B4-1, pp. 570, Jul. 2002.
[69] N. Hanik, A. Gladisch, C. Caspar and B. Streble, "Application of amplitude histograms to monitor performance of optical Channels" Electron. Lett., vol. 35, pp. 403-405, Mar. 1999.
[70] C. M. Weinert, L. Molle, C. Caspar and B. Streble, "Measurement and Modeling of Timing Jitter in Optoelectronic Repeaters and Frequency Converters" IEEE Photon. Technol. Lett., vol. 11, pp. 278-280, Feb. 1999.
[71] R. J. Manning, D. A. O. Davies, D. Cotter and J. K. Lucek, "Enhanced recovery rates in semiconductor laser amplifiers using optical pumping" Electron. Lett., pp. 787-788, May 1994.
[72] M. A. Dupertuis, J. L. Pleumeekers, T. P. Hessler, P. E. Selbmann, B. Deveaud, B. Dagens and J. Y. Emery, "Extremely Fast High-Gain and Low-Current SOA by Optical Speed-Up at Transparency" IEEE Photon. Technol. Lett., vol. 12, pp. 1453-1455, Nov. 2000.
[73] J. L. Pleumeekers, M. Kauer, K. Dreyer, C. Burrus, A. G. Dentai, S. Shunk, J. Leuthold and C. H. Joyner, "Acceleration of Gain Recovery in Semiconductor Optical Amplifiers by Optical Injection Near Transparency Wavelength" IEEE Photon. Technol. Lett., vol. 14, pp. 12-14, Jan. 2002.
[74] B. R. Bennett, R. A. Scref and J. A. D. Alamo, "Carrier-Induced Change in Refractive Index of InP, GaAs, and InGaAsP" IEEE J. Quantum Electron., vol. 26, pp. 113-122, Jan. 1990.
[75] J. S. Weiner, D. A. B. Miller and D. S. Chemla, "Quadratic electro-optic due to the quantum-confined Stark effect in quantum wells" Appl. Phys. Lett., vol. 50, pp.842-844, Mar. 1987.
[76] K. L. Hall, G. Lenz, A. M. Darwish and E. P. Ippen, "Subpicosecond gain and index nonlinearities in InGaAsP diode lasers" Optics Communications, vol. 111, pp. 589-612, Oct. 1994.
[77] J. E. Ehrlich, D. T. Neilson and A. C. Walker, "Carrier-Dependent Nonlinearities and Modulation in an InGaAs SQW Waveguide" IEEE J. Quantum Electron., vol. 29, pp. 2319-2324, Aug. 1993.
[78] I. Gontijo, G. Tessier, M. Livingstone, I. Galbraith and A. C. Walker, "Direct measurement of the polarization-dependent absorption and saturation in an InGaAs/InGaAsP single quantum well" J. Appl. Phys. Vol.80, pp. 4027-4032, Oct. 1996.
[79] R. Takahashi, Y. Kawamura and H. Iwamura, "Ultrafast 1.55 μm all-optical switching using low-temperature-grown multiple quantum wells" Appl. Phys. Lett., vol.68, pp. 153-155, Jan. 1996.
[80] A. Hirano, H. Tsuda, K. Hagimoto, R. Takahashi, Y. Kawamura and H. Iwamura, "10ps pulse all-optical discrimination using a high-speed saturable absorber optical gate" Electron. Lett., vol. 31, pp. 736-737, Apr. 1995.
[81] M. Hofman, K. Fröjdh, S. D. Brorson and J. Mørk, "Temporal and Spectral Dynamics in Multiquantum-Well Semiconductor Saturable Absorbers" IEEE Photon. Technol. Lett., vol. 9, pp.622-624, May 1997.

[82] I. Lahiri, D. D. Nolte, E. S. Harmon, M. R. Melloch and J. M. Woodall, “Ultrafast-lifetime quantum wells with sharp exciton spectra” Appl. Phys. Lett., vol. 66, pp. 2519-2521, May 1995.

[83] G. Lenz, E. P. Ippen, J. M. Wiesenfeld, M. A. Newkirk and U. Koren, “Femtosecond dynamics of the nonlinear anisotropy in polarization insensitive semiconductor optical amplifiers” Appl. Phys. Lett., vol. 68, pp. 2933-2935, May 1996.

[84] N. Radić and B. Šantić, “Optical cross section for the EL2 → EL2* metastable transformation” Phys. Rev. B, vol. 51, pp. 11 117-11 119, Apr. 1995.

[85] C. G. Van de Walle, “Band lineups and deformation potentials in the model-solid theory” Phys. Rev. B, pp. 1871-1883, Jan. 1989.

[86] M. F. Pereira, Jr., “Analytical solutions for the optical absorption of semiconductor superlattises” Phys. Rev. B, vol. 52, pp. 1978-1983, Jul. 1995.

[87] H. A. Haus, “Theory of Mode Locking with a Slow Saturable Absorber” IEEE J. Quantum Electron., vol. QE-11, pp.736-746, Sep. 1975.

[88] H. A. Haus, “Theory of Mode Locking with a Slow Saturable Absorber,” J. Appl. Phys., vol. 46, pp. 3049-3058, July 1975.

[89] A. Girndt, A. Knorr, M. Hormann and S. W. Koch, “Theory of coherent phenomena in pump-prbe excitation of semiconductor amplifiers” J. Appl. Phys., vol. 78, pp. 2946-2954, Sep. 1995.

[90] J. Mørk, A. Mecozzi and C. Hultgren, “Spectral Effects in short pulse pump-probe measurements” Appl. Phys. Lett., vol. 68, pp. 449-451, Jan. 1996.

[91] A. Girndt, A. Knorr, M. Hofmann, and S. W. Koch, “Theoretical analysis of ultrafast pump-probe experiments semiconductor amplifiers” Appl. Phys. Lett., vol. 65, pp. 550-552, Jan. 1995.

[92] J. Mørk and A. Mecozzi, “Response function for gain and refractive index dynamic in active semiconductor waveguides” Appl. Phys. Lett., vol.65, pp.1736-1738, Oct. 1994.

[93] P. S. Cross and W. G. Oldham, “Theory of Optical-Gain Measurements,” IEEE J. Quantum Electron., vol. QE-11, pp. 190-197, May 1975.

[94] R. A. Indik, R. Binder, M. Mlejnek, J. V. Moloney, S. Hughes, A. Knorr and S. W. Koch, “Role of plasma cooling, heating, and memory effects in subpicosecond pulse propagation in semiconductor amplifiers” Phys. Rev. A, vol. 53, pp. 3614-3620, May 1996.

[95] A. A. Bernussi, H. Temkin, D. L. Coblentz and R. A. Logan, “Gain Nonlinearity and Its Temperature Dependence in Bulk and Quantum-Well Quaternary Lasers” IEEE Photon. Technol. Lett. vol. 7, pp. 348-350, Apr. 1995.

[96] J.-N. Fehr, M.-A. Dupertuis, T. P. Hessler, L. Kappei, D. Marti, F. Salleras, M. S. Nomura, B. Deveaud, J.-y. Emerry and B. Dagens, “Hot Phonons and Auger Related Carrier Heating in Semiconductor Optical Amplifiers” IEEE J. Quantum Electron., vol. 38, pp. 674-681, Jun. 2002.

[97] J.-N. Fehr, M.-A. Dupertuis, T. P. Hessler, L. Kappei, D. Marti, P. E. Selbmann and B. Deveaud, "Direct observation of longitudinal spatial hole burning in semiconductor optical amplifiers with injection" Appl. Phys. Lett., vol. 78, pp. 4079-4081, Jun. 2001.

[99] F. Ginovart and J. C. Simon, "Effects of semiconductor optical amplifier length on gain dynamics" Workshop on Optical Signal Processing, pp. 93-95, Nov. 2001.

[100] H.-J. Wünschie, "Wave competition in a very long SOA" Workshop on Optical Signal Processing, pp. 96-98, Nov. 2001.

[101] E. A. Patent, J. J. G. M. van der Tol, N. Calabretta, N. Chalabretta and Y, Liu, "Compensation of the pattern effect in SOAs" Workshop on Optical Signal Processing, pp. 99-101, Nov. 2001.

[102] J. L. Pleumeekers, M-A. Dupertuis, T. Hessler, P. E. Selbmann, S. Haacke and B. Deveaud, "Longitudinal Spatial Hole Burning and Associated Nonlinear Gain in Gain-Clamped Semiconductor Optical Amplifiers" IEEE J. Quantum Electon., vol. 34, pp. 879-886, May 1998.

[103] P. E. Selbmann, T. P. Hessler, J. L. Pleumeekers, M.-A. Dupertuis, B. Deveaud, B. Dagens and J.-Y. Emery, "Observation of dark-pulse formation in gain-clamped semiconductor optical amplifiers by cross-gain modulation" Appl. Phys. Lett., vol. 75, pp. 3760-3762, Dec. 1999.

[104] J.-I. Shim, M. Yamaguchi, P. Delansay and M. Kitamura, "Refractive Index and Loss Changes Produced by Current Injection In InGaAs(P)-InGaAsP Multiple Quantum-Well (MQW) Waveguides," IEEE J. Selected Topics in Quantum Electron. vol. 1, pp.408-415, Jun. 1995.

[105] A. C. Bordonalli, C. Walton and A. J. Seeds, "High-Performance Phase Locking of Wide Linewidth Semiconductor Lasers by Combined Use of Optical Injection Locking and Optical Phase-Lock Loop" J. Lightwave Technol., vol. 17, pp. 328-342, Feb. 1999.

[106] S. Nogiwa, Y. Kawaguchi, H. Ohta and Y. Endo, "Generation of gain-switched optical pulses with very low timing jitter by using external CW-light injection seeding" Electron. Lett. vol. 36, pp. 1-2, Feb. 2000.

[107] K. L. Hall and K. A. Rauschenbach, "100-Gbit/s bitwise logic," Opt. Lett., vol. 23, pp. 1271-1273, Aug. 1998.

[108] R. J. Mannning, I. D. Phillips, A. D. Ellis, A. E. Kelly, A. J. Poustie and K. J. Blow, "All-optical clock division at 40GHz using semiconductor optical amplifier based nonlinear interferometer" Electron. Lett., vol. 35, pp. 827-829, May 1999.

[109] N. S. Patel, K. L. Hall and K. A. Rauschenbach, "40-Gbit/s cascadable all-optical logic with an ultrafast nonlinear interferometer" Opt. Lett., vol. 21, pp. 1466-1468, Sep. 1996.

[110] N. S. Patel, K. A. Rauschenbach and K. L. Hall, "40-Gbit/s Demultiplexing Using an Ultrafast Nonlinear Interferometer (UNI)" IEEE Photon. Technol. Lett., vol.8 pp. 1695-1697, Dec. 1996.

[111] N. S. Patel, K. L. Hall and K. A. Rauschenbach, "Interferometric all-optical switches for ultrafast signal processing" Appl. Opt. Vol. 37, pp. 2831-2841, May 1998.

[112] N.S. Bergano, F.W. Kerfoot, and C.R. Davidson, “Margin measurements in optical amplifier systems” IEEE Photonics Technol. Lett., vol.5, no.3, pp.304-306, Mar. 1993.

[113] A. Mecozzi and J. M. Wiesenfeld, “Semiconductor Optical Amplifiers” Opt. & Photon. News, pp. 36-42, Mar. 2001.

[114] P. Öhelén and E. Berglind, “BER caused by jitter and amplitude noise in limiting optoelectronic repeaters with excess bandwidth” IEE Proc.-Optoelectron., vol. 145, pp. 147-150, Jun. 1998.

[115] A. Tomlinson, C. Michie, T. Kelly and I. Andonovic, “Semiconductor Optical Amplifiers as Pre-Amplifiers and Boosters” Workshop on Optical Signal Processing, pp. 87-92, Nov. 2001.

[116] C. K. Madsen and G. Lenz, “Optical All-Pass Filters for Phase Response Design with Applications for Dispersion Compensation” IEEE Photon. Technol. Lett., vol. 10, 994-996, July 1998.

[117] M. Kauer, J. R. A. Cleaver, J. J. Baumberg and A. P. Heberle, “Femtosecond dynamics in semiconductor lasers: Dark pulse formation” Appl. Phys. Lett., pp. 1626-1628, Mar. 1998.

[118] R. O. Miles, M. A. Dupertuis, F. K. Reinhart and P. M. Brosson, “Gain measurements in InGaAsP multiquantum-well broad-area lasers” IEE Proceedings-J, vol. 139, pp. 33-38, Feb. 1992.

[119] P. A. Morton, D. A. Ackerman, G. E. Shtengel, R. F. Kazarinv, M. S. Hybertsen, T. Tanbun-Ek, R. A. Logan and A. M. Sergent, “Gain Characteristics of 1.55-μm Hight-Speed Multiple-Quantum-Well Lasers” IEEE Photon. Technol. Lett., vol. 7, pp. 833-835, Aug. 1995.

[120] P. Rees and P. Blood, “Derivation of Gain Spectra pf Laser Diodes from Spontaneous Emission Measurements” IEEE J. Quantum Electron., vol. 31, pp. 1047-1050, Jun 1995.

[121] D. T. Cassidy, “Technique for measurement of the gain spectra of semiconductor diode lasers” J. Appl. Phys. vol. 56, pp. 3096-3099, Dec. 1984.

[122] E. A. Swanson and S. R. Chinn, “23-GHz and 123-GHz Soliton Pulse Generation Using Two CW Lasers and Standard Single-Mode Fiber” IEEE Photon. Technol. Lett., vol. 6, pp. 796-798, July 1994.

[123] G. Toptchiyski, S. Randel, K. Petermann, C. Schubert, J. Berger and H. G. Weber, “Comparison of switching windows of an all-optical 160Gbit/s demultiplexer with base data rates of 10Gbit/s and 40Gbit/s” Conference Proceedings of Optical Fiber Communication Conference (OFC), MB5, Mar. 2001.

[124] C. Walton, A. C. Bordonalli and A. J. Seeds, “High-Performance Heterodyne Optical Injection Phase-Lock Loop Using Wide Linewidth Semiconductor Lasers” IEEE Photon. Technol. Lett., vol. 10, pp.427-429, Mar. 1998.

[125] K. I. Kang, T. G. Chang, I. Glesk and P. R. Pricnal, “Nonlinear-index-of-refraction measurement in a resonant region by the use of a fiber Mach-Zehnder Interferometer,” Appl. Opt.,

vol. 35, pp.1485-1488, Mar. 1996.
[126] X. Wang, H. Yokoyama and T. Shimizu, “Synchronized Harmonic Frequency Mode-Locking with Laser Diodes through Optical Pulse Train Injection” IEEE Photon. Technol. Lett., vol. 8, pp. 617-619, May 1996.
[127] A. J. Poustie, K. J. Blow and R. J. Manning, “Storage threshold and amplitude restoration in an all-optical regenerative memory,” Opt. Communications, 146, pp. 262-267, Jan. 1998.
[128] T. Watanabe, N. Sakaida, H. Yasaka, F. Kano and M. Koga, “Transmission Performance of Chirp-Controlled Signal by Using Semiconductor Optical Amplifier” J. Lightwave Technol., vol. 18, pp.1069-1077, Aug. 2000.
[129] A. K. Srivastava, Y. Sun, J. W. Sulhoff, K. Kantor and C. Wolf, “Cascaded semiconductor optical amplifiers for transmission of 32 DWDM channels over 315km” Conference Proceedings of Optical Fiber Communication Conference (OFC), WM32, Mar. 2000.
[130] A. Bogoni, L. Poti, A. Bizzi, M. Scaffardi and A. Reale, “Novel extended SOAs model for applications in very high-speed systems and its experimental validation” IEEE Photon. Technol. Lett., vol. 14, pp. 905-907, Jul. 2002.
[131] S. V. Chernikov, J. R. Taylor, P. V. Mamyshev and E. M. Dianov, “Generation of Soliton Pulse Train in Optical Fibre Using Two CW Singlemode Diode Lasers” Electron. Lett., vol. 28, pp. 931-932, May 1992.
[132] S.V. Chernikov, D. J. Richardson, R. I. Laming, E. M. Dianov and D. N. Payne, “70 Gbit/s Fibre Based Source of Fundamental Solitons at 1550nm” Electron. Lett, vol. 28, pp. 1210-1212, June 1992.
[133] C. Schubert, S Diez, J. Berger, R. Ludwig, U. Feiste, H. G. Weber, G. Toptchiski, K. Petermann and V. Krajinovic, “160-Gb/s all-optical demultiplexing using a gain-transparent ultrafast- nonlinear Interferometer (GT-UNI)” IEEE Photon. Technol. Lett., vol. 13, pp. 475-477, May. 2001.

List of the related works by the authors

<Paper>

M. Tsurusawa, M. Usami and Y. Matsushima, ”New Method for Reduction of Carrier Lifetime in Semiconductor Optical Amplifier using Assist Light”, Japanese Journal of Applied Physics, Vol.38 pp.1265-1268, Feb. 1999.

M. Tsurusawa, M. Usami and Y. Matsushima, “Demonstration of Optical Noise Reduction Using Nonlinear Absorption in a Semiconductor Laser Amplifier”, IEEE Journal of Selected Topics in Quantum Electronics, Vol.5 No.3 pp.861-865, Jun. 1999.

M. Tsurusawa, K. Nishimura and M. Usami, ”First Demonstration of Simultaneous Demultiplexing from 40 Gbit/s into Two Channels of 20 Gbit/s by SOA-based All-Optical Polarization Switch”, IEE Electronics Letters, Vol.37 No.23, pp.1398-1399, Nov. 2001.

M. Tsurusawa, K. Nishimura and M. Usami, “First Demonstration of Pattern Effect Reduction in 40 Gb/s Semiconductor Optical Amplifier Based All-Optical Switch Utilizing Transparent CW Assist Light”, Japanese Journal of Applied Physics, Vol.41 pp.1199-1202, Feb. 2002.

M. Usami, M. Tsurusawa and Y. Matsushima, “Novel Mechanism for Reducing Recovery Time of Optical Nonlinearity in Semiconductor Laser Amplifier Using Assist Light”, Applied Physics Letters, vol.72,21 2657～2659, May 1997.

<International Conference>

M. Tsurusawa, M. Usami and Y. Matsushima, “New Method for Reduction of Carrier Lifetime in Semiconductor Optical Amplifier by using Assist Light”, International Conference on Indium Phosphide and Related Materials (IPRM'98), May, 1998.

M. Tsurusawa, M. Usami and Y. Matsushima, “Optimum Wavelength of Assist Light for Efficient Reduction of Carrier Lifetime in Semiconductor Optical Amplifier”, Optoelectronics and Communications Conference (OECC'98), Jul. 1998.

M. Tsurusawa, M. Usami and Y. Matsushima, “Demonstration of Optical Noise Reduction using

Nonlinear Absorption in Semiconductor Laser Amplifier", 16th IEEE International Semiconductor Laser Conference, Oct. 1998.

M. Tsurusawa, M. Usami and Y. Matsushima, "Enhancement of Signal to Noise Ratio in Transmission Performance by Nonlinear Absorption in Semiconductor Waveguide", Optoelectronics and Communications Conference (OECC'00), Jul. 2000.

M. Tsurusawa, M. Usami and Y. Matsushima, "Novel Scheme for Reducing the Pattern Effect in 40 Gbps SOA based All-optical Switch Utilizing Transparent CW Assist Light", International Conference on Indium Phosphide and Related Materials (IPRM'01), May, 2001.

M. Tsurusawa, K. Nishimura and M. Usami, "First Demonstration or Simultaneous Demultiplexing from 80Gb/s to 2x40Gb/s by SOA-Based All-Optical Polarization Switch", European Conference on Optical Communication (ECOC '01), Sep. 2001.

M. Tsurusawa, K. Nishimura and M. Usami, "Distinct regeneration capability of 40Gbit/s signal impaired with amplitude noise and timing jitter using SOA-based all-optical polarization discriminated switch", The Optical Fiber Communication Conference (OFC '02), Mar. 2001.

M. Tsurusawa, K. Nishimura and M. Usami, "80Gbit/s Wavelength Conversion using SOA-based All-optical Polarization Discreminated Switch", Optoelectronics and Communications Conference (OECC'02), Jul. 2002.

M. Tsurusawa, K. Nishimura and M. Usami, "Bit-rate Tunable All-optical Regeneration by SOA-based Polarization Discriminated Switch using Variable Differential Group Delay Generator", European Conference on Optical Communication (ECOC '02), Sep. 2002.

M. Tsurusawa, K. Nishimura and M. Usami, "Operation margin of all-optical regenerator at 40 Gbit/s by SOA-based polarization discriminated switch", The Optical Fiber Communication Conference (OFC '03), Mar. 2003.